JMeXFRI

Journal of the Mexican Federation of Radiology and Imaging

J Mex Fed Radiol Imaging

Volume 1. Number 1, January-March 2022

ISSN: 2696-8444

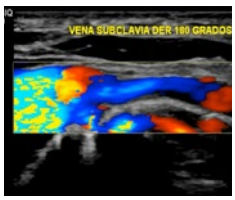

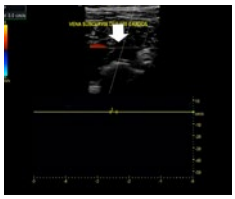

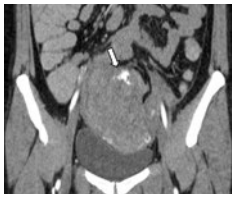

EDITORIAL
Science, publication, and the arc of radiology

IN-DEPTH REVIEW
Pulmonary artery thromboembolism and beyond

FULL RESEARCH ARTICLE
Mexican radiologists' and referring clinicians' preference for a standardized structured radiology report: qualities and content

FULL RESEARCH ARTICLE
Diagnostic criteria of ultrasound duplex doppler for venous thoracic outlet syndrome: fifteen years' experience

FULL RESEARCH ARTICLE
Image optimization of abdominal and pelvic multislice computed tomography with oral mannitol contrast

FULL RESEARCH ARTICLE
Ultrafast brain magnetic resonance imaging in hyperacute and acute ischemic stroke: diagnostic accuracy and interobserver concordance

BRIEF RESEARCH ARTICLE
Decreased ^{18}F-FDG PET/CT uptake in the gastrointestinal tract with oral hyoscine-N-butyl bromide

CASE REPORT
Usefulness of computed tomography in complicated femoral Littre hernia: case report and literature review

IMAGES IN RADIOLOGY
Ultrasound and computed tomography: epiploic appendagitis

Official Journal of the

FEDERACIÓN MEXICANA DE RADIOLOGÍA E IMAGEN, A.C

PERMANYER
www.permanyer.com

WWW.JMeXFRI.COM

Carestream

GE Healthcare

BRACCO
LIFE FROM INSIDE

PHILIPS

SIEMENS
Healthineers

esaote

AGFA HealthCare

TESA | Canon
CANON MEDICAL SYSTEMS
OFFICIAL DISTRIBUTOR

KONICA MINOLTA
Latino América

EYMSA
ELECTRONICA Y MEDICINA, S.A.

mindray
healthcare within reach

LAICO®

FUJIFILM
Value from Innovation

Dinteligencia
DISPOSITIVOS DE INTELIGENCIA MÉDICA

BARCO

ARSA
ASESORES EN RADIACIONES S.A.

Contrastes & Equipos
EXPERIENCIA A SU SERVICIO

ecodsa
grupo

Carestream


PHILIPS


esaote


SIEMENS
Healthineers


AGFA
Agfa
HealthCare


TESA
Canon
CANON MEDICAL SYSTEMS
OFFICIAL DISTRIBUTOR


KONICA MINOLTA
Latino América


EYMSA
ELECTRONICA Y MEDICINA, S.A.


mindray
healthcare within reach


LAICO


FUJIFILM
Value from Innovation


Dinteligencia


BARCO


ARSA
ASESORES EN RADIACIONES S.A.


Contrastes
& Equipos
EXPERIENCIA A SU SERVICIO


ecodsa
grupo

JMeXFRI

Journal of the Mexican Federation of Radiology and Imaging

J Mex Fed Radiol Imaging

Volume 1. Number 1, January-March 2022

ISSN: 2696-8444

online Submission Manuscript

Original papers should be deposited in their electronic version through the following URL:

https://publisher.jmexfri.permanyer.com

PERMANYER
www.permanyer.com

Permanyer
Mallorca, 310 – Barcelona (Cataluña), España
permanyer@permanyer.com

Permanyer México
Temístocles, 315
Col. Polanco, Del. Miguel Hidalgo
11560 Ciudad de México
Tel.: +52 55 2728 5183
mexico@permanyer.com

www.permanyer.com

ISSN: 2696-8444
Ref.: 6296DX201

JMeXFRI

Journal of the Mexican Federation of Radiology and Imaging

EDITORIAL

Science, publication, and the arc of radiology

Umar Mahmood[1,2]*

[1]*Department of Radiology, Massachusetts General Hospital;* [2]*School of Medicine, Harvard Medical School. Boston, Massachusetts, United States of America*

It is truly a great honor for me to share my thoughts in the inaugural issue of the *Journal of the Mexican Federation of Radiology and Imaging* (*JMeXFRI*) about science, the connection of knowledge through publication, and our field of radiology. My deep friendship with so many colleagues and leaders of the *Federación Mexicana de Radiología e Imagen* (FMRI) spans, in some cases, multiple decades, and reflects many in-depth conversations, the sharing of ideas, our vision on how to best help our patients, and of course the happiness we have when we spend time together. So, it is especially meaningful for me to share your joy in launching the JMeXFRI.

Our field of radiology spans more than 125 years of innovation, insight, and understanding. That creativity by radiologists has taken place millions of times everywhere around the globe. This arc has led us to where our best practices are to date, reflecting the integration of all cumulative knowledge. Of course, the arc does not end here but continues to the future to provide the best care for the next generation of patients. Each of us can reflect on where we were a decade ago and two decades ago, and the incredible progress that has been made in radiology during our careers. The realization of the incredible rate of advancement in how we practice crystalizes when we benchmark the field compared to how we acquired and interpreted scans in our recent past. This constant movement forward is like an encompassing, fast-moving wave pushing our ability to identify and characterize disease. I want to frame some of the layers of creativity that define and drive our field.

Numerous fundamental advancements have created large sections of radiology, and the field of imaging has been quick to utilize these insights to help patients. Our ability to see inside the body has been built on tens of thousands of discoveries and breakthrough inventions, spanning from Wilhelm Röntgen's discovery of x-rays in 1895 to the discovery of nuclear magnetic resonance in the 1940s by Edward Purcell and Felix Bloch to the first human CT scan in 1971 by Godfrey Hounsfield to the work in the 1970s by Paul Lauterbur and Peter Mansfield making MRI possible, to the advancements of artificial intelligence today, among an endless list of creativity across and beyond the electromagnetic spectrum. These insights have been multiplied by thousands of physicians and scientists who have given us the ability to acquire human images in practice. The developed imaging systems have led tens of thousands of radiologists and other physicians over the years to create knowledge on how best to characterize normal human anatomy and physiological processes and to develop an understanding of how pathophysiology is revealed using all of our imaging and interventional technology. Numerous other radiologists and scientists have built data on how best to use this understanding to provide the best care for our patient populations. Many of these insights are globally applicable; however, populations vary across the globe regarding health risks, environmental exposures, and resources brought to bear to screen and treat disease.

It takes all of us to contribute to the global development of radiology to make sure the arc of innovation and understanding continues. None of the fundamental

Corresponding author:
*Umar Mahmood
E.mail: umahmood@mgh.harvard.edu

Received for publication: 12-11-2021
Approved for publication: 15-11-2021
DOI: 10.24875/JMEXFRI.M21000004

Available online: 31-03-2022
J Mex Fed Radiol Imaging. 2022;1(1):1-2
www.JMeXFRI.com

discoveries would help the patients we are taking care of today without hundreds of thousands of people doing their part in understanding imaging, understanding disease, and being willing to spend the time to share their insights. Publications such as the *JMeXFRI* are vital to share techniques on how to best acquire an image to highlight specific cancer, data on how CT scan findings may adjust our best estimates of heart attack risk in individual patients, and the creation of an educational framework to improve the interpretation of images in patients with COVID. For each article published, hundreds or thousands of readers gain their own insights, making it easier for them to interpret patients' images or put findings into context. Other readers gain insights into their areas of research or education, and the published articles will help build and improve their work. The *JMeXFRI* has the opportunity to help radiologists throughout Mexico, the region, and the world improve their image interpretations and radiologists and scientists everywhere to build on the work the Journal publishes.

In addition to the broad areas related to current diagnostic and interventional approaches, the coming years will bring an array of new areas of growth in our field. These growth areas include technologies such as artificial intelligence and approaches such as precision medicine, along with a growing understanding of the need for all of us to help address disparities in care for underserved populations and the challenges radiologists face as the number and complexity of images we are each asked to interpret, continues to grow. I know that many radiologists from the region and around the world will rely on the insights and opinions of the *JMeXFRI* authors to help better understand the imaging and disease challenges of today and the future. I personally look forward to reading the *JMeXFRI* in the coming years, knowing that the field is in good hands.

JMeXFRI

Journal of the Mexican Federation of Radiology and Imaging

Check for updates

IN-DEPTH REVIEW

Pulmonary artery thromboembolism and beyond

Felipe Aluja-Jaramillo[1,a] and Fernando R. Gutierrez[2]*

[1]Radiology Department, Hospital Universitario San Ignacio, Pontificia Universidad Javeriana, Bogota, Colombia; [2]Cardiothoracic Imaging Section, Radiology Department Mallinckrodt Institute of Radiology, Washington University, St. Louis, Missouri, United States of America

[a]0000-0002-3093-2509

ABSTRACT

Pulmonary embolism (PE) is the third leading cause of cardiovascular disease. Although diagnosis has increased with the advent of multidetector computed tomography, morbidity and mortality have not decreased. The clinical diagnosis of PE remains controversial; therefore, diagnostic imaging plays a key role. Chest radiography continues to be the initial evaluation method. Computed tomography pulmonary angiography (CTPA) is the gold standard, and magnetic resonance imaging can be used in specific cases. Although PE is diagnosed by visualizing filling defects in the pulmonary arteries, associated findings in the lung parenchyma and heart help establish the diagnosis and its complications. We must consider that PE is not always of vascular origin and must be aware of non-vascular causes of PE in our differential diagnoses.

Keywords: *Pulmonary embolism. Multidetector computed tomography. Pulmonary artery. Pulmonary circulation. CTPA.*

INTRODUCTION

Pulmonary embolism (PE) is a filling defect of the pulmonary arteries caused by soft tissue density material, usually thrombi that originate from the veins in the legs[1]. It is considered the third cause of cardiovascular disease[2,3], and although the diagnosis of PE has been increasing, mortality has not decreased[4]. It is characterized by considerable mortality and morbidity with a reported incidence of approximately 1 per 1000 patients in the United States[1] and 60 to 70 per 100,000 inhabitants in Europe[5]. In untreated patients, mortality reaches up to 30%[1,6], while in treated patients, it is approximately 8%[5,6], with a reported in-hospital mortality between 5 and 10%[3]. In general, mortality has been increasing in recent years[2]. Furthermore, the development of pulmonary hypertension due to chronic thromboembolic disease has increased its morbidity and mortality[7]. The risk factor reported for the development of PE is venous thromboembolism (VTE)[5].

The clinical diagnosis of PE remains controversial in large part due to its varied clinical presentation with chest pain, dyspnea, hemoptysis, and even fever[3]. Clinical classifications have been used for risk stratification (Wells Classification or Genoa Score) in suspected PE, with patients stratified as low, moderate, and high probability with a prevalence of 3%, 25%, and 78%, respectively[3,8,9].

IMAGING MODALITIES IN SUSPECTED PULMONARY EMBOLISM

Given these considerations, diagnostic imaging is fundamental in patients with PE. Computed tomography pulmonary angiography (CPTA) is currently considered the imaging tool of choice for diagnosis[10].

Chest X-ray

The chest X-ray is considered the initial diagnostic method. It is key in excluding other causes of PE such

Corresponding author:
*Felipe Aluja-Jaramillo
E-mail: falujaj@husi.org.co

Received for publication: 05-10-2021
Approved for publication: 11-11-2021
DOI: 10.24875/JMEXFRI.M21000006

Available online: 31-03-2022
J Mex Fed Radiol Imaging. 2022;1(1):3-12
www.JMeXFRI.com

as pneumonia, pulmonary edema, pleural or pericardial effusion, acute aortic disease, or even pneumothorax[1,9,11]. Although chest radiography is believed to be normal in most PE patients, the PIOPED (Prospective Investigation of Pulmonary Embolism Diagnosis) study found that only 12% of radiographs were reported normal[12]. The most frequent findings were cardiomegaly (29%), pleural effusion, hemidiaphragm elevation, and pulmonary opacities[12].

Classic signs may still be useful during the evaluation of a patient with PE. The following are some of these signs with their corresponding historical perspectives.

– *"Hampton´s Hump"*

Described in 1904 by Hampton and Castleman, it is a subpleural or peripheral wedge-shaped opacity with a pleural base and an apex towards the pulmonary hilum that represents an area of lung infarction (Figure 1)[1,9]. It has a sensitivity of 22%, a specificity of 82%, a positive predictive value (PPV) of 28%, and a negative predictive value (NPV) of 76%[9].

– *Westermark sign*

These are radiolucent areas in the lung parenchyma that correspond to zones of oligemia (Figure 1)[1,9]. It has a sensitivity of 14%, a specificity of 92%, PPV of 38%, and an NPV of 76%[9].

– *Fleischner's sign*

Described in 1962 by Fleischner, it is a prominent central pulmonary artery that may be secondary to a thrombus that dilates the vascular structure or the result of pulmonary arterial hypertension (Figure 1)[1,9].

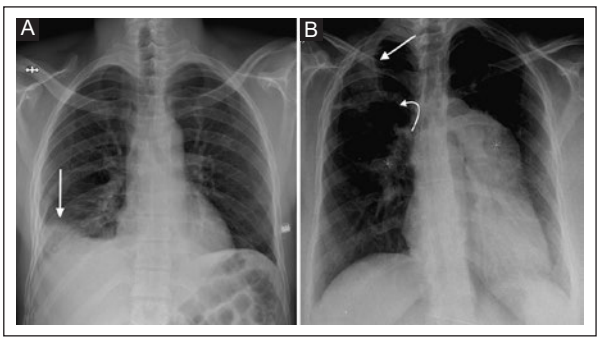

Figure 1. A: a 42-year-old female patient with a diagnosis of pulmonary embolism. Chest X-ray, posteroanterior view. A wedge-shaped opacity is observed with an apex towards the pulmonary hilum in the right basal location corresponding to Hampton's hump with slight volume loss of the right lower lobe and obliteration of the costophrenic angle on this side (arrow). **B:** 56-year-old female patient with a diagnosis of pulmonary embolism. Chest X-ray, posteroanterior projection. A wedge-shaped opacity is observed with apex towards the pulmonary hilum located in the right upper lobe corresponding to Hampton's hump (arrow). Likewise, there is prominence of the pulmonary arteries representing the Fleischner sign (asterisk) and some areas of lower density or radiolucency of the parenchyma around the opacity and in the upper right lobe that may correspond to areas of oligemia representing the Westermark sign (curved arrow).

Magnetic resonance angiography

The PIOPED III study concluded that magnetic resonance angiography had limitations in image interpretation because it is technically inadequate. It should be considered an option in institutions where it is performed routinely and only in patients in which other imaging methods are contraindicated[13]. Magnetic resonance angiography has a sensitivity of 79% for detecting thrombi in the central pulmonary arteries or for lobar thrombi[13]. Imaging findings are similar to those reported in CT angiography of pulmonary vessels with filling defects of the pulmonary arteries or their branches (Figure 2)[1].

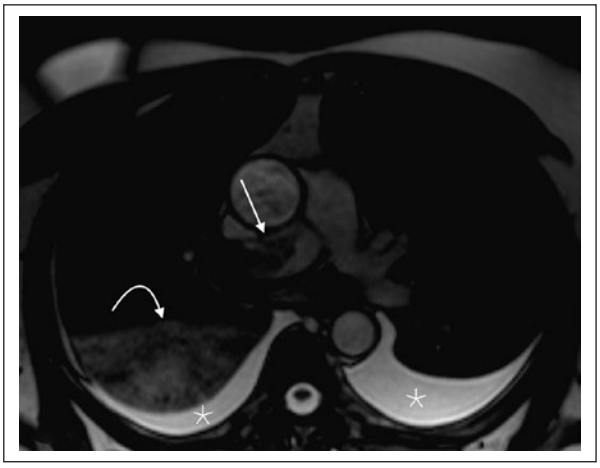

Figure 2. A Male patient with a history of pulmonary embolism. Magnetic resonance imaging, axial image in T2-weighted sequence. An opacification defect is observed in the right pulmonary artery (arrow) with acute angles to the wall of the vessel, conditioning its dilation in relation to acute pulmonary embolism (arrow). There are bilateral pleural effusions (asterisks) and a hyperintense area in the right lower lobe (curved arrow) related to the area of edema.

Computed tomography pulmonary angiography

The first diagnosis of PE with CTPA was made incidentally by Sinner in 1978[1]. The use of this technique has increased in recent years[2], allowing the detection of increasingly smaller subsegmental pulmonary arteries, and increasing its sensitivity for diagnosis[14]. Its increased use has been reflected in the increase

in diagnosis of subsegmental pulmonary embolism (SSPE)[14]. It is currently considered the gold standard for this entity with a sensitivity of 83% and a specificity of 96% according to the PIOPED II study and an NPV of 99%[1,11,15,16]. Due to its relevance for diagnosis, we will focus on the findings of this imaging modality. Other incidental findings can be found in CT scans allowing an alternate diagnosis[17].

The ideal protocol will depend on the available equipment. The greater the number of detectors (64 or more), the shorter the breath-hold periods, improving patient comfort and avoiding motion artifacts. However, the quality of the study does not depend exclusively on this factor. In general, the images must be acquired in deep inspiration, preferably in the caudocranial direction, to avoid motion artifacts in the lower lobes, especially in patients who cannot maintain the necessary periods of apnea[18,19]. The possibility of synchronizing a study with the heartbeat will benefit image quality, avoid motion artifacts, and allow adequate assessment of the heart chambers[19]. A minimum pulmonary artery density of 93 HU and 211 HU are necessary for diagnosing acute and chronic PE, respectively[18,19]. Changing the windows to adjust the Hounsfield units allows identifying vascular thrombi and non-vascular lesions of the pulmonary arteries; thus, it is an indispensable tool in differential diagnosis.

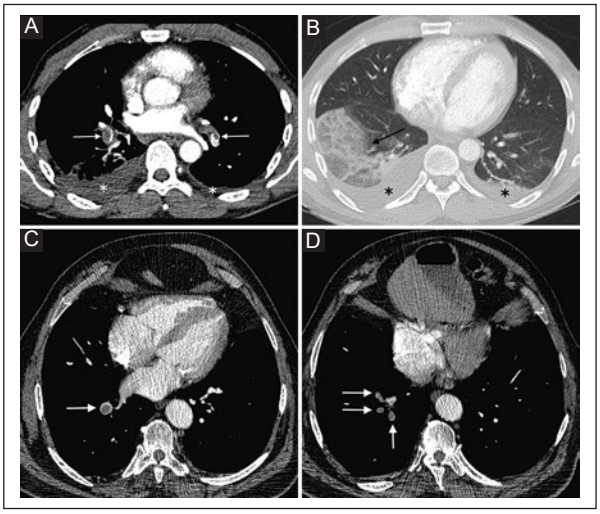

Figure 3. A 48-year-old male patient. **A:** CTPA, mediastinal window. A central filling defect occupying the lumen of the artery of the right lower lobe is observed, configuring the "polo mint sign", with proximal dilation, in relation to an episode of acute pulmonary embolism (arrow). There is a similar defect in the pulmonary artery of the left lower lobe (arrow). **B:** CTPA, lung window. A "ground glass" area in the lower right lobe that may correspond to an area of hemorrhage or edema (arrow). There are also bilateral pleural effusions (asterisk). A 73-year-old male patient, **C-D:** CTPA, axial image, a central filling defect is observed occupying the lumen of the artery of the right lower lobe and the segmental branches, configuring the "polo mint sign", with proximal dilatation, as a consequence of an episode of acute pulmonary embolism (arrow). Note the difference in caliber with the contralateral pulmonary arteries.

CTPA: Computed tomography pulmonary angiography.

THROMBOTIC OR VASCULAR PULMONARY EMBOLISM

Although the diagnosis of PE is made by visualizing the pulmonary arteries, additional findings in the lung parenchyma and heart must be evaluated for appropriate scan interpretation, either in the acute or chronic context.

ACUTE PULMONARY EMBOLISM (APE)

Evaluation of the pulmonary arteries

A low-attenuation opacification defect partially or completely occupying the lumen of the pulmonary arteries establishes the diagnosis of PE. It is common to find dilatation of the embolized pulmonary artery more evident in subsegmental or small-caliber arteries[20].

When the opacification defect partially occupies the center of the lumen of the vessel with its low-attenuation appearance surrounded by a halo of contrast medium, it forms a "ring," also known as the "polo mint sign" (Figure 3). This same sign in the longitudinal plane of the vessel results in the "railway track" sign (Figure 4)[20]. Associated with the filling defect, we can also find an increase in the caliber of the occluded vessel that is more evident in small-caliber pulmonary arteries[20].

Lung parenchyma assessment

The most frequently found pulmonary parenchyma alteration in patients with acute PE corresponds to pulmonary infarction[20]. Although the lung has systemic circulation (through the bronchial arteries) and pulmonary circulation (through the pulmonary arteries) that are anastomosed by capillaries, it is not always possible to protect the parenchyma from an infarct (Figure 4)[21]. This alteration is more frequent in peripheral embolisms than central ones[21]. It is represented as a subpleural opacity with a "wedge-shaped" morphology, whose base is pleural with an apex towards the pulmonary hilum or the vessel occluded by the thrombus. The central portion may be more hypodense and usually does not enhance with contrast media[20]. It is not frequent to find an air bronchogram,

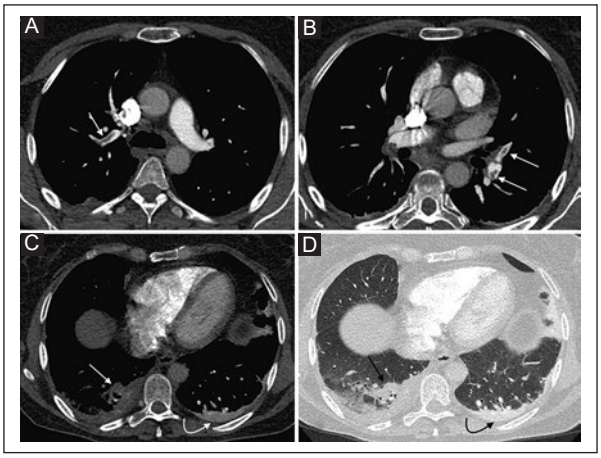

Figure 4. A 58-year-old female patient with chest pain, dyspnea, and fever. **A-B:** CTPA, axial image. A central defect occupying the lumen of the artery of the right upper lobe and the left lower lobe is observed that, due to its longitudinal disposition, configures the lane or double lane sign, with proximal dilation, related to an episode of acute pulmonary embolism (arrow). **C:** CTPA, axial image, mediastinal window. **D:** lung window. Wedge morphology opacity is evidenced in the lower right lobe whose base is pleural and its apex points towards the central region, not enhancing with contrast medium, corresponds to a pulmonary infarct zone (white arrow in **C** and black arrow in **D**). There is opacity with a volume loss in the left lower lobe that demonstrates contrast medium enhancement associated with an area of atelectasis (white curved arrow in **C** and black arrow in **D**).

CTPA: Computed tomography pulmonary angiography.

Figure 5. A 61-year-old female patient. **A-B:** CTPA, axial image, shows prominence of the pulmonary artery due to pulmonary arterial hypertension. Opacification defect with soft tissue-density material in the main pulmonary arteries and branches of the lower lobes in association with acute pulmonary embolism (arrow). **C:** CTPA, axial image, at the level of the heart showing dilation of the right heart chambers with straightening of the interventricular septum and alteration of the RV/LV ratio. **D:** axial section in the upper abdomen where we can see contrast medium reflux into the suprahepatic veins (arrows). These findings are suggestive of increased right heart chamber pressures.

CTPA: Computed tomography pulmonary angiography; RV/LV ratio: right ventricle/left ventricle index.

which is key for the differential diagnosis[20,22,23]. Infarct areas can cavitate after a few weeks[22]. The "reverse halo" sign has been described in 18% of pulmonary infarcts[24].

Up to 50% of patients show some degree of lung volume loss, usually represented as an elevation of the hemidiaphragm in the first 24 hours after the onset of symptoms[22]. Areas of atelectasis have been described in up to 35% of patients and are considered the most frequent finding on chest radiography[22]. Likewise, consolidation due to areas of edema or hemorrhage can also be found but is not necessarily associated with pulmonary infarcts (Figure 3)[22]. Pleural effusions are found in 35% to 55% of patients with PE, bearing in mind that the laterality of PE and pleural effusions are not related (Figure 3)[22,25].

Heart assessment

PE increases the resistance of the pulmonary circulation and, therefore, right ventricle pressures that can be identified on CT when 30% of the pulmonary vasculature is occluded[11,26]. The progressive elevation of pressure in the pulmonary circulation translates into compensatory dilation of the right ventricle, increasing intramural pressure and decreasing blood flow to the coronary arteries with ischemic changes, resulting in decreased right ventricular contractility[11]. We must understand that the interventricular septum tends to arch towards the left ventricle under normal conditions[27]. All these changes in chamber pressure dynamics produce rectification of the interventricular septum that reduces left ventricle filling and decreases cardiac output[11,28]. An increase in the ratio between the right ventricle and the left ventricle (RV/LV) greater than 0.9 is associated with an increase in short-term risk of death of 2.8 to 7.4 times, and right ventricular dysfunction evaluated by echocardiography is associated with an increase in this same indicator up to 2.4 times (Figure 5)[11]. Signs such as the presence of contrast medium reflux into the inferior vena cava and dilation of the azygos vein have been considered by some authors as indirect signs of increased right-sided cavity pressure (Figure 5)[1,27].

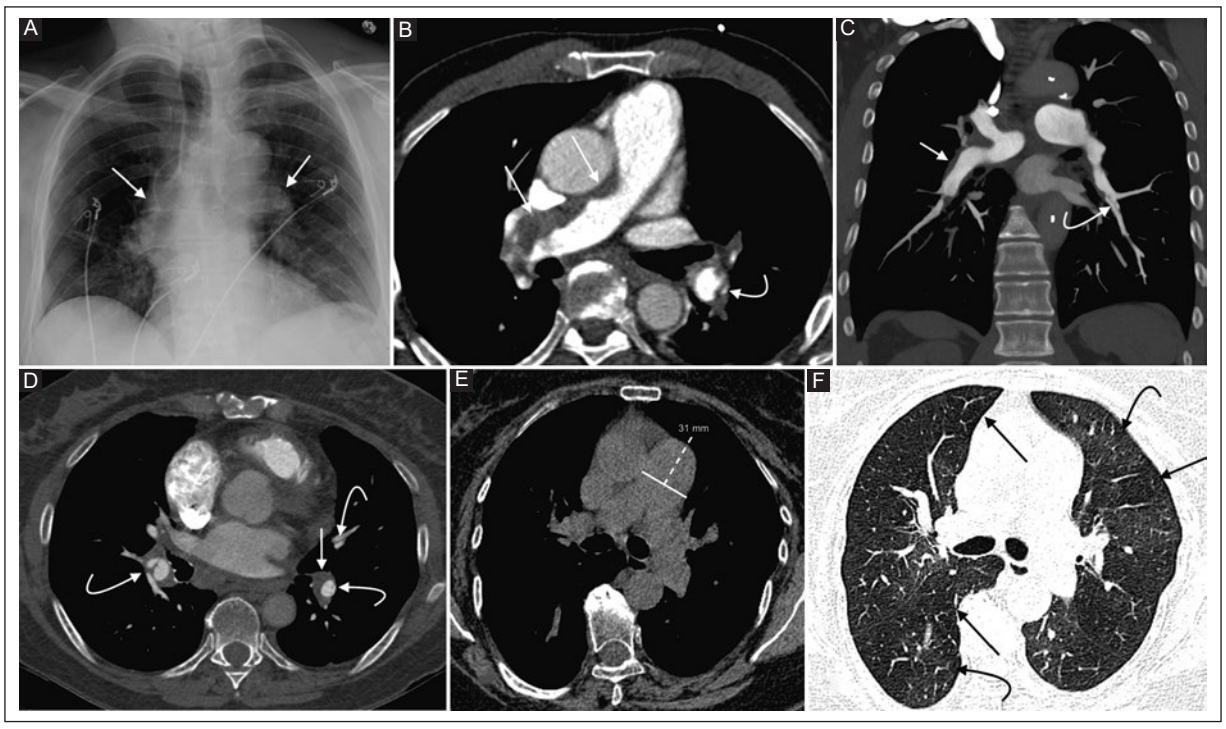

Figure 6. A 77-year-old male patient. **A:** portable chest radiograph, anteroposterior view. Prominence of the pulmonary artery (arrow) and its branches as signs of pulmonary arterial hypertension. **B:** CTPA, axial image, and **C:** coronal reconstruction in maximum intensity projection. Dilation of the main pulmonary artery due to pulmonary arterial hypertension. Filling defect towards the wall of the right pulmonary artery with smooth contours and forming an obtuse angle with the vessel wall (arrow). There are some bands inside the artery of the left lower lobe; both findings are related to chronic pulmonary embolism (curved arrow). **D:** a 66-year-old female patient. CTPA, axial image. Partial filling defect in the lumen of the pulmonary artery of the right lower lobe and other thinner ones in segmental branches of the lower lobes related to chronic pulmonary embolism (curved arrow). There is also thickening of the pulmonary artery wall of the left lower lobe (arrow). **E:** a 59-year-old female patient with episodes of recurrent pulmonary embolism. Non-enhanced chest CT, axial section in the mediastinal window showing dilation of the main pulmonary artery due to pulmonary arterial hypertension. **F:** non-enhanced chest CT, axial image in the lung window. There are geographically arranged "ground glass" areas, with areas of hyperemia (increased attenuation) (curved arrow) and oligemia (less attenuation) (arrow). Findings related to CTEPH.

CTPA: Computed tomography pulmonary angiography; CT: Computed tomography; CTEPH: Chronic thromboembolic pulmonary hypertension.

CHRONIC PULMONARY EMBOLISM (CPE)

Evaluation of the pulmonary arteries

The presence of peripheral filling defects that occupy the branches of the pulmonary arteries with smooth contours and forming an obtuse angle with the vessel wall should lead to suspect CPE[18]. In some cases, it is observed as a thickening of the pulmonary artery wall with a decrease in the caliber that shows vessel recanalization[18]. A flap-like band in the vessel lumen also suggests CPE[18]. These thrombi or areas of wall thickening, in some cases, can be evidenced from non-enhanced images by modifying the window, especially when they are markedly hypodense (Figure 6). We can find variable chronic thrombi enhancement usually associated with the development of collateral circulation during the recanalization process. This finding can be a confounding factor if this characteristic is unknown[29]. We must remember that an opacification defect with a morphology similar to APE can be observed up to 3 months after the initial episode[18].

Assessment of the lung parenchyma and heart

When we find perfusion mosaic and/or hypertrophy of the right ventricle with an increase in the caliber of the main pulmonary artery, we must consider chronic thromboembolic pulmonary hypertension (CTEPH)[11,30].

The perfusion mosaic corresponds to differences between lung vascularization and areas of hyperemia (high attenuation) and oligemia (low attenuation)[31]. In the specific context of CTEPH, it has been reported that between 77% and 100% of patients demonstrate perfusion mosaic changes which have a predominantly segmental or subsegmental distribution (Figure 6)[30].

Subpleural opacities are manifestations of an area of scarring in the lung parenchyma in the chronic context[30]. They can be found in up to 87% of patients with CTEPH[30,32]. Hypertrophy of the bronchial arteries is a finding that can also be found in up to 77% of CTEPH cases and even in acute episodes of PE, especially when there is proximal obstruction of the pulmonary arteries[30].

NON-THROMBOTIC OR NON-VASCULAR PULMONARY EMBOLISM

The presence of soft tissue-dense material within the lumen of the pulmonary arteries is not unique to PE. Embolization of tissue (tumor) fragments, infectious material (septic emboli), or foreign bodies[33] can occur. Authors such as Unal et al.[34] in their non-vascular PE articles describe entities such as fatty embolism, amniotic fluid embolism, or septic embolism. We will not consider these entities in this review since they do not impact pulmonary artery opacification.

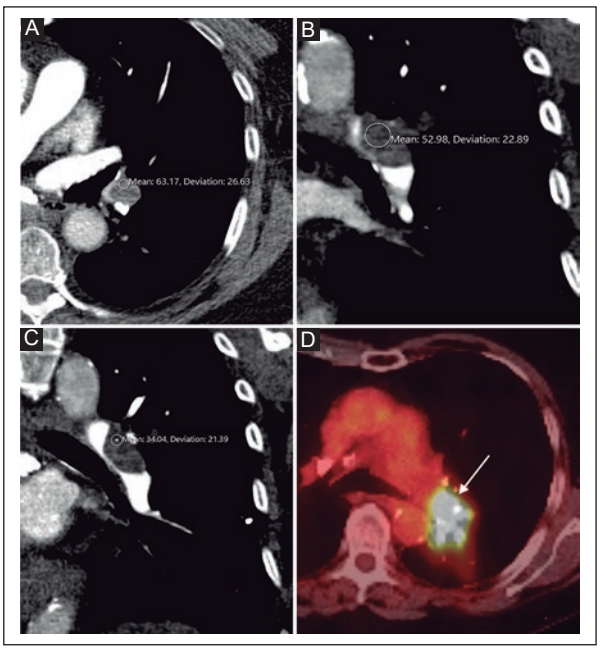

Figure 7. A male patient with pulmonary artery opacification defect. **A:** CTPA, axial image. **B-C:** coronal reconstruction. There is a partial opacification defect occupying the pulmonary artery of the left lower lobe, predominantly hypodense, with lobulated contours and enhancement during the administration of contrast medium. **D:** ^{18}FDG-PET/CT demonstrating marked tracer uptake (arrow). This finding corresponds to a pulmonary sarcoma.

CTPA: computed tomography pulmonary angiography; FDG-^{18}FDG-PET/CT: Fluorodeoxyglucose positron emission tomography/computed tomography.

NEOPLASIA AND PULMONARY EMBOLISM

One of the main imitators of PE is tumor embolisms or primary tumors of the pulmonary arteries. The latter can be seen in pulmonary artery sarcoma, which usually originates near the pulmonary valve, occupying and widening the vessel lumen, simulating a thrombus.[30] The differential diagnosis can be established by identifying lobulated margins of the lesion and the presence of heterogeneous enhancement within the mass (Figure 7)[11].

Gross tumor pulmonary embolism has been described in several types of tumors, including hepatocellular carcinoma, renal cell carcinoma, breast cancer, and even osteosarcomas, in these cases, secondary to an invasion of the iliac veins and the inferior vena cava[34,35]. On CTPA, a filling defect of the pulmonary vessels with soft tissue density is observed[34]. There may be contrast enhancement, especially in chronic appearing thrombi[34]. In both cases, positron emission tomography/computed tomography (PET/CT) may be beneficial to establish the diagnosis[34]. We must also consider the extension or local invasion of the pulmonary arteries by neoplasms involving the lung parenchyma, which can condition tumor thrombosis within the affected vessel.

IATROGENIC, TRAUMATIC, AND OTHERS

PE related with iatrogenic conditions are frequently caused by the injection of polymethylmethacrylate (known as cement) for vertebroplasties in the management of vertebral fractures[34]. It is common to find material leaks along the injection sites, the prevertebral tissues, the spinal canal, intervertebral spaces, or the epidural veins; it has even been described in the metameric arteries[34,36]. It has a reported incidence that varies between 2.1% and 23%, with an increased risk in those patients with compression fractures secondary to osteoporosis and can be related to

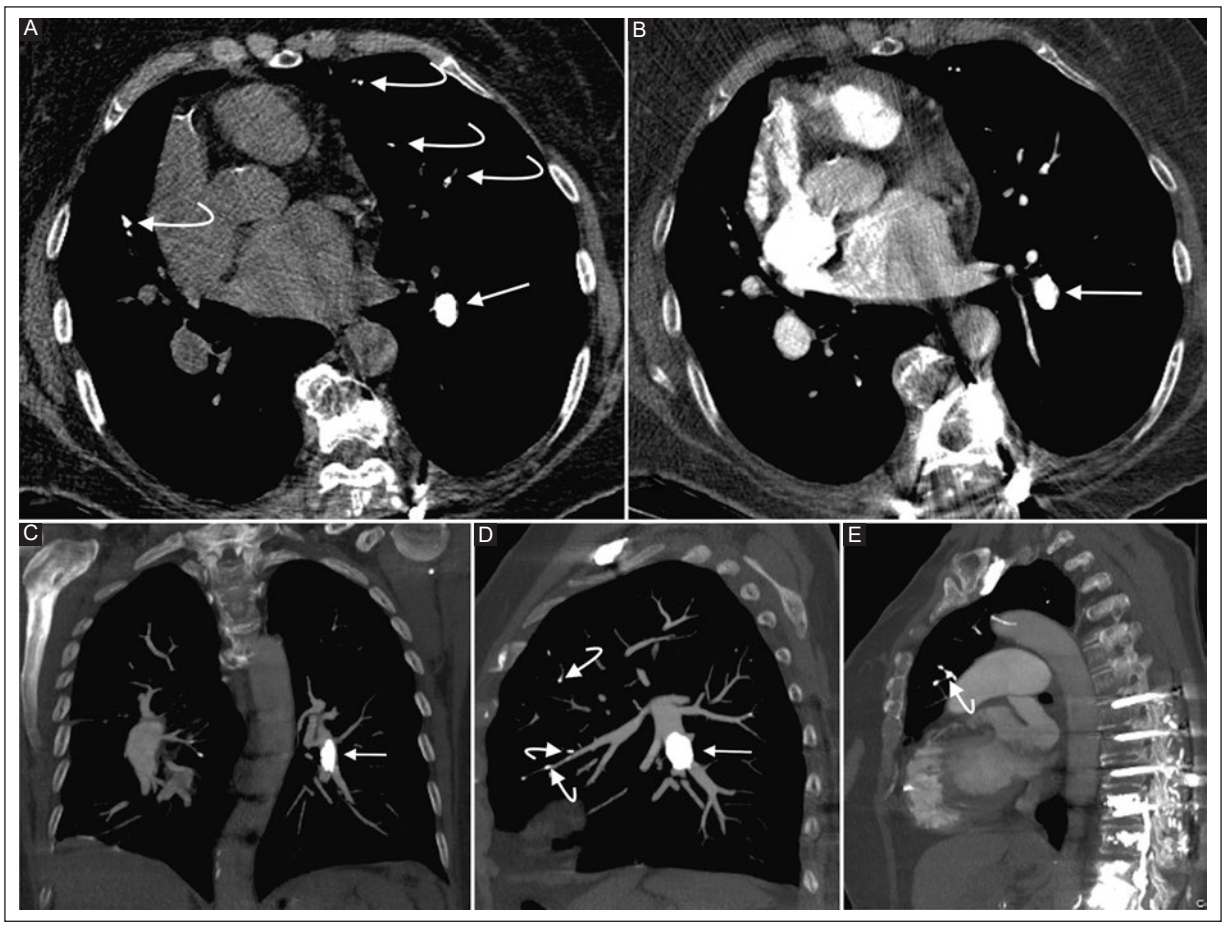

Figure 8. An 88-year-old female patient with a history of vertebroplasty and fixation with osteosynthesis of the dorsolumbar spine. **A:** non-enhanced chest CT, axial image. **B:** CTPA, axial image. **C:** coronal reconstruction. **D-E:** sagittal reconstruction. A hyperdense image is observed occupying the entire pulmonary artery lumen of the left lower lobe (arrow) and some additional images in subsegmental branches in the middle lobe and lingula (curved arrow). Post-surgical changes of the dorsal spine with osteosynthesis material and vertebroplasty changes with hyperdense material in the vertebral bodies and some lumbar veins.

CT: computed tomography; CTPA: computed tomography pulmonary angiography.

vertebroplasty techniques[34,37,38]. Neither the number of vertebral bodies treated, the vertebral level treated, nor the volume of material injected is related to the risk of embolism[34,37,38]. Laredo et al.[36] demonstrated that the presence of cortical destruction of the vertebral body, vascularized lesions, or severe collapse of the vertebral body are factors that increase the risk of embolism. Radiopaque and branched linear areas can be identified in CT, while hyperdense, branched opacification defects are observed in CTPA, especially in the segmental and subsegmental branches (Figure 8).

There is also the possibility of embolism of fragments of medical devices, especially parts of central catheters, inferior vena cava filters, endovascular stents, guidewires, and catheter sleeves that can occlude the pulmonary arteries (Figure 9)[34,39,40]. It is important to properly modify the study windows when considering device or foreign body embolization to allow optimal visualization and identification (Figure 9).

Embolisms of other materials or substances such as talc, mercury, silicone, and hyaluronic acid have been described[34]. Even more striking, embolism of metal fragments from firearm projectiles causing penetrating wounds has been described[34,39,40].

Air embolism is an entity that can occur during intravenous administration of contrast medium and after episodes of trauma, iatrogenesis, surgery, diving accidents, or even during the manipulation of a central venous catheter[33,34,41,42]. Between 300 and 500 ml are necessary to achieve a lethal dose that conditions a

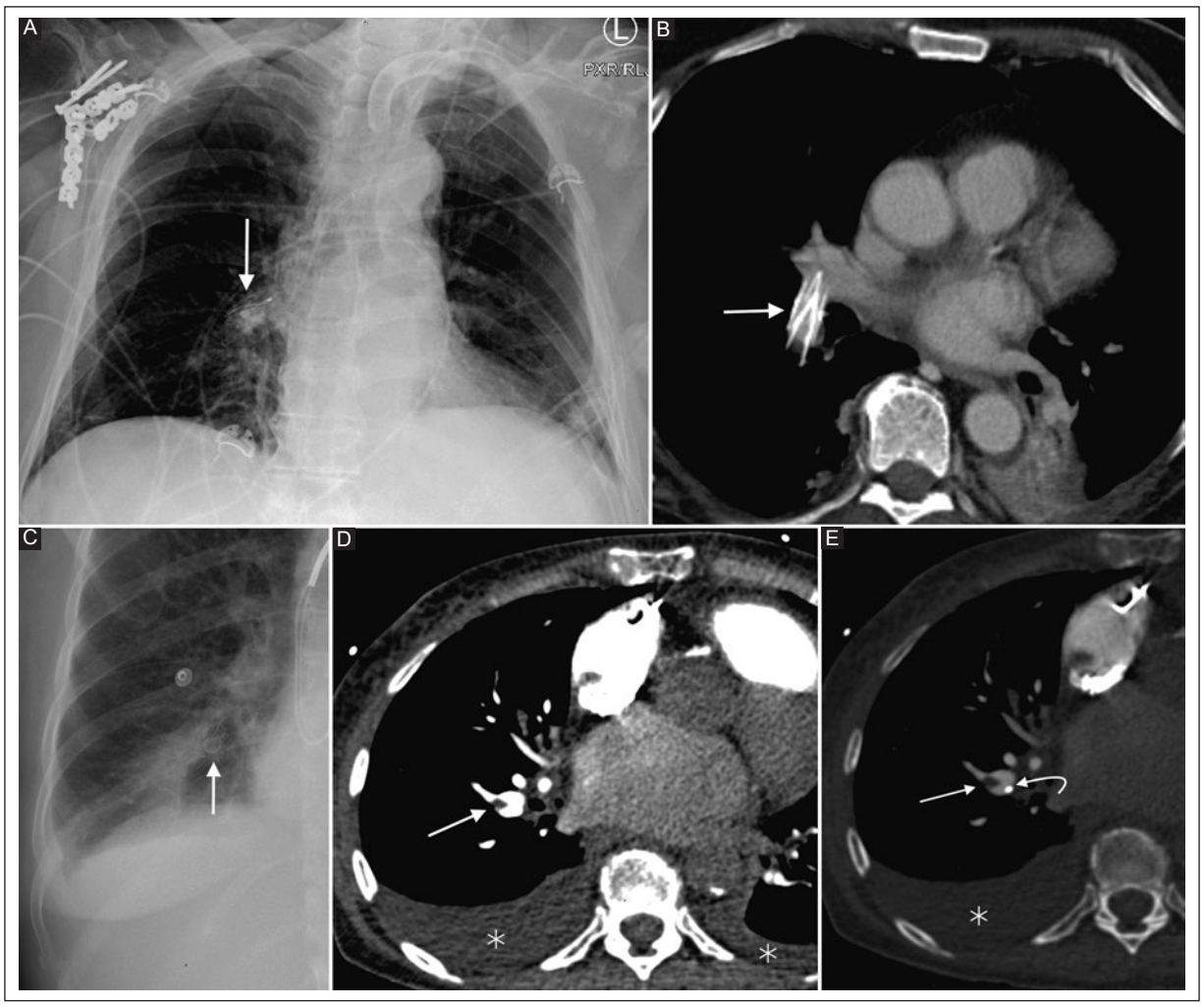

Figure 9. Female patient with a history of multiple episodes of pulmonary embolism. **A:** chest radiograph, anteroposterior view. A radiopaque object is observed, with a mesh appearance, occupying the interlobar artery corresponding to a medical device embolized to the pulmonary circulation (inferior vena cava filter) (arrow). **B:** CTPA, axial image. An inferior vena cava filter is identified in the interlobar artery (arrow). **C:** patient with chest pain, chest X-ray, posteroanterior view focused on the right lower lobe. A radiopaque loop-shaped foreign object is seen projected in the right lower lobe (arrow); **D-E:** CTPA, axial image. Opacification defect partially occupying the right lower lobe artery in relation to pulmonary embolism (arrow). By modifying the window, a radiopaque image is identified inside the pulmonary artery lumen for the left lower lobe in relation to the catheter fragment (curved arrow). Bilateral pleural effusions (asterisks).

CTPA: computed tomography pulmonary angiography.

pulmonary artery obstruction resulting in pulmonary edema and cardiovascular dysfunction with pulmonary hypertension[34].

PITFALLS, ARTIFACTS, AND MIMICKERS OF PULMONARY EMBOLISM

Perihilar lymph nodes can be confused with PE, although this confusion can be avoided with a detailed evaluation and fine reconstruction (Figure 10)[20]. Due to the path of the pulmonary veins or even the bronchi that show hypodense content, they can be confused with opacification defects in a pulmonary artery, which is why it is essential to follow the structure of interest in detail to its proximal origin[20].

The main imitator of the diagnosis of thrombotic or vascular PE is the mixture of contrast medium with the blood flow, which can produce a heterogeneous appearance in the lumen of the pulmonary arteries that can simulate an opacification defect of the vessel, which should not be confused with PE (Figure 10)[11]. This artifact is more frequent when a deep inspiration

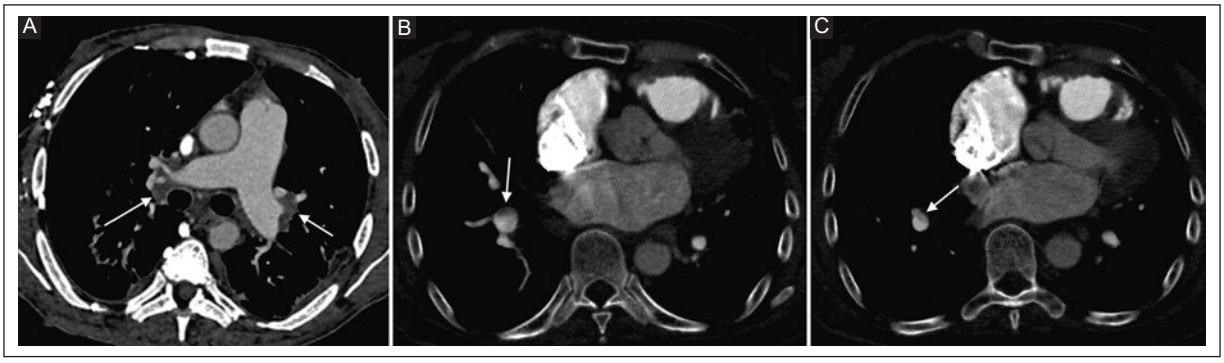

Figure 10. A: an 81-year-old male patient with dyspnea. CTPA shows adequate opacification of the pulmonary arteries with no evidence suggesting pulmonary embolism. There are hilar lymph nodes that reduce the caliber of the pulmonary arteries, which due to their location, can be confused with chronic pulmonary embolism (arrow). **B-C:** a 71-year-old female patient with chest pain. CTPA, axial section. The heterogeneous appearance of the interlobar artery lumen, especially in its anterior aspect corresponds to a flow artifact simulating a pulmonary embolism (arrow).
CTPA: computed tomography pulmonary angiography.

is taken immediately before acquisition. This problem can be corrected by carrying out the study during a sustained continuous inspiration, after which the contrast medium is injected to avoid a Valsalva maneuver[20]. A similar artifact can be found in the segmental or subsegmental arteries secondary to slow flow produced by increased vascular resistance in areas of consolidation or atelectasis[18]. The artifact generated by movement can generate a "double wall" or "double contour" image that can create the illusion of an opacification defect[43].

CONCLUSION

PE continues to be a frequent medical entity with high morbidity and mortality. Diagnostic images play a fundamental role in its diagnosis. We must know the characteristics of PE on the chest X-ray, in which we can suspect this entity until CTPA can be obtained to establish a definitive diagnosis. In addition, we must be familiar with the non-thrombotic causes of PE to enhance diagnosis and improve patient survival in these entities.

Funding

All authors declare that they have no funding.

Conflicts of interest

All authors declare that they have no conflicts of interest.

Ethical disclosures

Protection of human and animal subjects. The authors declare that no experiments were performed on humans or animals for this study.

Confidentiality of data. The authors declare that no patient data appear in this article.

Right to privacy and informed consent. The authors declare that no patient data appear in this article.

REFERENCES

1. Yazdani M, Lau CT, Lempel JK, Yadav R, El-Sherief AH, Azok JT, et al. Historical Evolution of Imaging Techniques for the Evaluation of Pulmonary Embolism. RadioGraphics. 2015;35(4):1245-1262. doi: 10.1148/rg.2015140280.
2. Martin KA, Molsberry R, Cuttica MJ, Desai KR, Schimmel DR, Khan SS. Time Trends in Pulmonary Embolism Mortality Rates in the United States, 1999 to 2018. J Am Heart Assoc. 2020;9(17):e016784. doi: 10.1161/JAHA.120.016784.
3. Wells PS, Rodger M. Diagnosis of pulmonary embolism: when is imaging needed? Clin Chest Med. 2003;24(1):13-28. doi:10.1016/s0272-5231(02)00052-7.
4. Burge AJ, Freeman KD, Klapper PJ, Haramati LB. Increased diagnosis of pulmonary embolism without a corresponding decline in mortality during the CT era. Clin Radiol. 2008;63(4):381-386. doi: 10.1016/j.crad.2007.10.004.
5. Bělohlávek J, Dytrych V, Linhart A. Pulmonary embolism, part I: Epidemiology, risk factors and risk stratification, pathophysiology, clinical presentation, diagnosis and nonthrombotic pulmonary embolism. Exp Clin Cardiol. 2013;18(2):129-138.
6. Daftary A, Gregory M, Daftary A, Seibyl JP, Saluja S. Chest radiograph as a triage tool in the imaging-based diagnosis of pulmonary embolism. AJR Am J Roentgenol. 2005;185(1):132-134. doi: 10.2214/ajr.185.1.01850132.
7. Pengo V, Lensing AW, Prins MH, Marchiori A, Davidson BL, Tiozzo F, et al. Thromboembolic Pulmonary Hypertension Study Group. Incidence of chronic thromboembolic pulmonary hypertension after pulmonary embolism. N Engl J Med. 2004;350(22):2257-2264. doi: 10.1056/NEJMoa032274.
8. Wells PS, Anderson DR, Rodger M, Stiell I, Dreyer JF, Barnes D, et al. Excluding pulmonary embolism at the bedside without diagnostic imaging: management of patients with suspected pulmonary embolism presenting to the emergency department by using a simple clinical model and d-dimer. Ann Intern Med. 2001;135(2):98-107. doi: 10.7326/0003-4819-135-2-200107170-00010.
9. Moore AJE, Wachsmann J, Chamarthy MR, Panjikaran L, Tanabe Y, Rajiah P. Imaging of acute pulmonary embolism: an update. Cardiovasc Diagn Ther. 2018;8(3):225-243. doi: 10.21037/cdt.2017.12.01.

10. Expert Panels on Cardiac and Thoracic Imaging: Kirsch J, Brown RKJ, Henry TS, Javidan-Nejad C, Jokerst C, Julsrud PR, et al. ACR Appropriateness Criteria® Acute Chest Pain-Suspected Pulmonary Embolism. J Am Coll Radiol. 2017;14(5S): S2-S12. doi: 10.1016/j.jacr.2017.02.027.
11. Sista AK, Kuo WT, Schiebler M, Madoff DC. Stratification, Imaging, and Management of Acute Massive and Sub massive Pulmonary Embolism. Radiology. 2017;284(1):5-24. doi: 10.1148/radiol.2017151978.
12. Kluetz PG, White CS. Acute pulmonary embolism: imaging in the emergency department. Radiol Clin North Am. 2006;44(2):259-271. doi: 10.1016/j.rcl.2005.10.004.
13. Stein PD, Chenevert TL, Fowler SE, Goodman LR, Gottschalk A, Hales CA, et al. PIOPED III (Prospective Investigation of Pulmonary Embolism Diagnosis III) Investigators. Gadolinium-enhanced magnetic resonance angiography for pulmonary embolism: a multicenter prospective study (PIOPED III). Ann Intern Med. 2010;152(7):434-443, W142-3. doi: 10.7326/0003-4819-152-7-201004060-00008.
14. Baumgartner C, Tritschler T. Clinical significance of subsegmental pulmonary embolism: An ongoing controversy. Res Pract Thromb Haemost. 2020; 5(1):14-16. doi: 10.1002/rth2.12464.
15. Roshkovan L, Litt H. State-of-the-Art Imaging for the Evaluation of Pulmonary Embolism. Curr Treat Options Cardiovasc Med. 2018;20(9):71. doi: 10.1007/s11936-018-0671-6.
16. Hunsaker AR, Lu MT, Goldhaber SZ, Rybicki FJ. Imaging in acute pulmonary embolism with special clinical scenarios. Circ Cardiovasc Imaging. 2010;3(4):491-500. doi: 10.1161/CIRCIMAGING.109.855981.
17. Remy-Jardin M, Pistolesi M, Goodman LR, Gefter WB, Gottschalk A, Mayo JR, et al. Management of suspected acute pulmonary embolism in the era of CT angiography: a statement from the Fleischner Society. Radiology. 2007;245(2):315-329. doi: 10.1148/radiol.2452070397.
18. Wittram C. How I do it: CT pulmonary angiography. AJR Am J Roentgenol. 2007;188(5):1255-1261. doi: 10.2214/AJR.06.1104.
19. Hartmann IJ, Wittenberg R, Schaefer-Prokop C. Imaging of acute pulmonary embolism using multi-detector CT angiography: an update on imaging technique and interpretation. Eur J Radiol. 2010;74(1):40-49. doi: 10.1016/j.ejrad.2010.02.007.
20. Kuriakose J, Patel S. Acute pulmonary embolism. Radiol Clin North Am. 2010;48(1):31-50. doi: 10.1016/j.rcl.2009.10.002.
21. Torres PPTES, Mançano AD, Zanetti G, Hochhegger B, Aurione ACV, Rabahi MF, et al. Multimodal indirect imaging signs of pulmonary embolism. Br J Radiol. 2020;93(1108):20190635. doi: 10.1259/bjr.20190635.
22. Coche E, Verschuren F, Hainaut P, Goncette L. Pulmonary embolism findings on chest radiographs and multislice spiral CT. Eur Radiol. 2004;14(7):1241-1248. doi: 10.1007/s00330-003-2203-2.
23. Shah AA, Davis SD, Gamsu G, Intriere L. Parenchymal and pleural findings in patients with and patients without acute pulmonary embolism detected at spiral CT. Radiology.1999;211(1):147-153. doi: 10.1148/radiology.211.1.r99ap03147.
24. Marchiori E, Nobre LF, Hochhegger B, Zanetti G. The reversed halo sign: Considerations in the context of the COVID-19 pandemic. Thromb Res. 2020; 195:228-230. doi: 10.1016/j.thromres.2020.08.001.
25. Coche EE, Müller NL, Kim KI, Wiggs BR, Mayo JR. Acute pulmonary embolism: ancillary findings at spiral CT. Radiology. 1998;207(3):753-758. doi: 10.1148/radiology.207.3.9609900.
26. McIntyre KM, Sasahara AA. The hemodynamic response to pulmonary embolism in patients without prior cardiopulmonary disease. Am J Cardiol. 1971;28(3):288-294. doi: 10.1016/0002-9149(71)90116-0.
27. Henzler T, Barraza JM Jr, Nance JW Jr, Costello P, Krissak R, Fink C, et al. CT imaging of acute pulmonary embolism. J Cardiovasc Comput Tomogr. 2011;5(1):3-11. doi: 10.1016/j.jcct.2010.10.001.
28. Piazza G, Goldhaber SZ. Management of submassive pulmonary embolism. Circulation. 2010;122(11):1124-1129. doi: 10.1161/CIRCULATIONAHA.110.961136.
29. De Luca F, Modolon C, Buia F, Attinà D, Fughelli P, Bacchi Reggiani ML, et al. Densitometric CT evaluation of acute and chronic thromboembolic filling defects of the pulmonary arteries before and after contrast injection. Radiol Med. 2012;117(6):979-991. doi: 10.1007/s11547-012-0828-4.
30. Aluja Jaramillo F, Gutierrez FR, Díaz Telli FG, Yevenes Aravena S, Javidan-Nejad C, Bhalla S. Approach to Pulmonary Hypertension: From CT to Clinical Diagnosis. RadioGraphics. 2018;38(2):357-373. doi: 10.1148/rg.2018170046.
31. Kligerman SJ, Henry T, Lin CT, Franks TJ, Galvin JR. Mosaic Attenuation: Etiology, Methods of Differentiation, and Pitfalls. RadioGraphics. 2015;35(5):1360-1380. doi: 10.1148/rg.2015140308.
32. Grosse C, Grosse A. CT findings in diseases associated with pulmonary hypertension: a current review. RadioGraphics. 2010;30(7):1753-1777.
33. Khashper A, Discepola F, Kosiuk J, Qanadli SD, Mesurolle B. Nonthrombotic pulmonary embolism. AJR. Am J Roentgenol. 2012;198(2):W152-159. doi: 10.2214/AJR.11.6407.
34. Unal E, Balci S, Atceken Z, Akpinar E, Ariyurek OM. Nonthrombotic Pulmonary Artery Embolism: Imaging Findings and Review of the Literature. Am J Roentgenol. 2017;208(3):505-516. doi: 10.2214/AJR.16.17326.
35. Lin WC, Lin CH, Chao YH, Lin HC, Chen PY, Wu HP, et al. Simultaneous pulmonary and inferior vena cava thromboembolism secondary to pelvic osteosarcoma. J Pediatr Hematol Oncol. 2013;35(8):e320-e322. doi: 10.1097/MPH.0b013e3182707a1a.
36. Laredo JD, Hamze B. Complications of percutaneous vertebroplasty and their prevention. Skeletal Radiol. 2004;33(9):493-505. doi: 10.1007/s00256-004-0776-8.
37. Kim YJ, Lee JW, Park KW, Yeom JS, Jeong HS, Park JM, et al. Pulmonary cement embolism after percutaneous vertebroplasty in osteoporotic vertebral compression fractures: incidence, characteristics, and risk factors. Radiology. 2009;251(1):250-259. doi: 10.1148/radiol.2511080854.
38. Venmans A, Lohle PN, van Rooij WJ, Verhaar HJ, Mali WP. Frequency and outcome of pulmonary polymethylmethacrylate embolism during percutaneous vertebroplasty. AJNR. Am J Neuroradiol. 2008;29(10):1983-1985. doi: 10.3174/ajnr.A1269.
39. Wolf F, Schernthaner RE, Dirisamer A, Schoder M, Funovics M, Kettenbach J, et al. Endovascular management of lost or misplaced intravascular objects: experiences of 12 years. Cardiovasc Intervent Radiol. 2008;31(3):563-568. doi: 10.1007/s00270-007-9201-8.
40. Gabelmann A, Kramer S, Gorich J. Percutaneous retrieval of lost or misplaced intravascular objects. AJR Am J Roentgenol. 2001;176(6):1509-1513. doi: 10.2214/ajr.176.6.1761509.
41. Groell R, Schaffler GJ, Rienmueller R, Kern R. Vascular air embolism: location, frequency, and cause on electron-beam CT studies of the chest. Radiology. 1997;202(2):459-462. doi: 10.1148/radiology.202.2.9015074.
42. Gordy S, Rowell S. Vascular air embolism. Int J Crit Illn Inj Sci. 2013;3(1):73-76. doi: 10.4103/2229-5151.109428.
43. Perrier A, Howarth N, Didier D, Loubeyre P, Unger PF, de Moerloose P, et al. Performance of helical computed tomography in unselected outpatients with suspected pulmonary embolism. Ann Intern Med.2001;135(2):88-97. doi: 10.7326/0003-4819-135-2-200107170-00008.

JMeXFRI

Journal of the Mexican Federation of Radiology and Imaging

Check for updates

FULL RESEARCH ARTICLE

Mexican radiologists' and referring clinicians' preference for a standardized structured radiology report: qualities and content

Carla Garcia-Moreno[a], E. Ricardo Jimenez-De La O, and Alejandro Herrera-Sanchez*

Radiology and Imaging Service, Angeles Lomas Hospital, Huixquilucan, State of Mexico. Mexico

[a]0000-0001-7551-4549

ABSTRACT

Introduction: *There is insufficient evidence regarding the preferences, qualities, and content of the ideal radiology report. This study aimed to 1) compare Mexican radiologists' and referring clinicians' preferences between a standardized structured radiology report and a prose report and 2) define the qualities and necessary content of a radiology report.* **Material and methods:** *This cross-sectional study included radiologists and referring clinicians. A two-section survey was used that first included 11 magnetic resonance imaging (MRI) reports with specific clinical scenarios for each specialty. Each clinical scenario was presented as a standardized structured report and a prose report, and the participants freely identified the qualities. The second section included eleven characteristics of a radiology report to select those considered necessary.* **Results:** *A total of 159 surveys were applied; 53 (75%) of 71 radiologists and 74 (84%) of 88 referring clinicians preferred the standardized structured radiology report, regardless of age, specialty, or years of professional practice. The most mentioned qualities of the standardized structured radiology report were organized, understandable, concise, easy to read, descriptive, and focused on the clinical setting. Participants considered the clinical indication of the study, a recommendation for additional testing, negative or normal findings, quality of the study, date of previous studies, administration of a contrast agent, and recommendation for evaluation by other specialties as necessary contents of the radiology report.* **Conclusion:** *This is the first report from Mexico showing that radiologists and referring clinicians prefer the standardized structured radiology report and its qualities and necessary contents were defined.*

Keywords: *Preference. Qualities. Standardized. Structured. Radiology. Reports.*

INTRODUCTION

The characteristics of a good radiology report are described by the 6 C's: clear, correct, confident, concise, complete, and consistent[1]. Free text or prose, structured, and standardized structured are the three types of radiology reports[2]. The most commonly used type is the prose report[3,4], which describes the radiology findings in free text with or without a conclusion. Inconsistency in nomenclature and disorganization in its structure and content are its disadvantages[5]. On the other hand, the structured report contains a paragraph for each organ or anatomical segment with a systematic sequence. In contrast, the standardized structured report contains a checklist based on diagnostic suspicion with predetermined text for normal findings. In structured and standardized structured reports, the radiologist describes only the abnormal findings and always includes a conclusion. The advantages of the standardized structured report are clarity and standardized language[2]. It has been reported that radiologists prefer the standardized structured report[2,6,7]. Referring clinicians prefer it because they believe it facilitates

Corresponding author:
*Carla Garcia-Moreno
E-mail: garmorcarla@gmail.com

Received for publication: 08-11-2021
Approved for publication: 23-11-2021
DOI: 10.24875/JMEXFRI.M21000001

Available online: 31-03-2022
J Mex Fed Radiol Imaging. 2022;1(1):13-22
www.JMeXFRI.com

communication, follow-up, and comparison with previous studies[2,8].

It is well known that it is difficult to reach a consensus on the characteristics and content of the ideal radiology report[8]. It is important for clinicians because it affects diagnostic and treatment decisions, and for radiologists, it is the best tool for communication with referring clinicians and patients[9]. Specific recommendations that have been suggested for the content of the radiology report include relevant information from the patient's medical history, findings from previous imaging studies, laboratory test results and pathology reports, and recommendations for complementary imaging studies and/or evaluation by another specialist if needed[2]. The Radiological Society of North America[5] and the European Society of Radiology[10] have proposed standards, guidelines, and procedures for the implementation of standardized structured reports in radiology centers[8]. Nevertheless, in Mexico, the preference of radiologists and referring clinicians regarding the different types of radiology reports and their quality and necessary content is unknown. This study aimed to 1) compare the preference of Mexican radiologists and referring clinicians for a standardized structured or a prose radiology report, and 2) define the qualities and necessary content of the radiology report.

MATERIAL AND METHODS

This cross-sectional study was conducted from November to December 2020 in the Magnetic Resonance Department of Angeles Lomas Hospital, Mexico state, México. Radiologists and referring clinicians with an active professional practice who agreed to participate in the survey to determine their preference for the type of radiology report, standardized structured or prose, were included. Referring clinicians who do not receive radiology reports in their practice, such as clinical pathologists, were not included. Incomplete data or repeated questionnaires were excluded. The institutional ethics and research committees approved the study, and participants provided written informed consent.

Participant characteristics

Mexican radiologists and referring clinicians from Mexico City, the states of Chihuahua, Nuevo Leon, Sinaloa, Zacatecas, and Mexico state were invited to participate by telephone. The participating specialties were cardiology, gastroenterology, gynecology and obstetrics, nuclear medicine, emergency medicine, neurosurgery, neurology, ophthalmology, otorhinolaryngology, pediatrics, radiology, urology, traumatology, and orthopedics. Participants were eligible regardless of years of professional practice. Only referring clinicians who receive magnetic resonance imaging (MRI) radiology reports were considered. The participants' age, specialty, and years of professional practice were recorded. All specialists were asked whether they were familiar with the standardized structured radiology report.

Structure of the questionnaire

A two-section questionnaire was used. The first section contained 11 examples of MRI reports with specific clinical scenarios for each specialty. The same clinical scenario was presented as a standardized structured report and a prose report. Radiologists and nuclear medicine physicians selected one example of a standardized structured report and one prose report from the 11 clinical specialties described above. Participants were recommended to choose the report with which they were more familiar. The radiology reports were taken from our center's picture archiving and communication system (PACS). Two examples of clinical scenarios from the specialties that most frequently request MRI studies are shown below.

Scenario 1: A gadolinium-enhanced brain MRI report of a multiple sclerosis case was selected for neurology specialists (Table 1). Participants were presented with an example of a standardized structured radiology report (1A) and a prose radiology report (1B).

Scenario 2: MRI findings of a case of degenerative joint disease of the knee were selected for the traumatology and orthopedics specialists (Table 2). Participants were presented with an example of a standardized structured radiology report (2A) and a prose radiology report (2B).

After analyzing the clinical scenarios, radiologists and referring clinicians were asked to define their preference for a particular type of report and to indicate which type of report they thought was the most comprehensive, and to describe in the free text the qualities of the chosen type of report that determined their preference.

The second section of the questionnaire included 11 characteristics from which participants could select those they considered necessary to complete the radiology report[6]: clinical indication, technique description, administration of contrast agent, study quality,

Table 1. Brain MRI of a patient with multiple sclerosis for the neurology specialists; standardized structured radiology report (scenario 1A), and prose radiology report (scenario 1B)

1A. Standardized structured radiology report
Brain MRI without and with 7.5 ml intravenous contrast: multiple sclerosis protocol. **Medical history**: A 50-year-old woman with demyelinating disease. **Technique**: brain imaging acquisition **Comparison**: A previous examination was performed on July 01, 2019. **Findings: new T2 hyperintense lesions** Periventricular: no Juxtacortical: present, one new lesion Infratentorial: present, one new lesion Optic nerve: no Cervicomedullary junction: no **Diffusion restriction**: Yes, lesion in the posterior arm of the right internal capsule. **Gadolinium-enhanced lesions:** present in the pons, posterior arm of the right capsule, and cervical spinal cord (C1-C2) **Total number of lesions:** 10 to 20 **Parenchymal atrophy:** no **Callosal atrophy:** no **Other:** lesions at C1-C2 and C3-C4 **Diagnostic impression:** multiple white matter lesions due to demyelinating disease with spatial spread.
1B. Prose radiology report
Cranial MRI in axial, coronal, and sagittal planes in T1, T2, FLAIR, and diffusion pulse sequences. Thin sections in MPR and Flair. Selective imaging at the optic nerve level. Administration of a paramagnetic contrast agent. A comparative study with a previous study from 01/07/2019. **Findings:** Hyperintense images were identified on FLAIR-type pulse sequences that involved the deep white matter of the semioval centers bilaterally and symmetrically. Generalized periventricular involvement mainly in the periphery of the left frontal horn, the callosal-septal junctions, and the inferior border of the corpus callosum. Two new lesions were identified: the first with the largest diameter of 8 x 6 x 14 mm in the posterior arm of the right internal capsule (with restricted signal intensity in diffusion) at the edge of the right brainstem and the second ventral to the pons measuring 8.5 x 8 x 8 mm. Extension of the process to the middle cerebellar peduncle and the right superior cerebellar peduncle. Thin sections performed in both orbits exclude signal intensity changes in the optic nerves without abnormal contrast uptake. In the sagittal section of the MPR pulse sequence, two additional previously visible images were observed in the high cervical spinal cord, toward its ventral region in C1-C2 with a diameter of 8.5 mm and another in C3-C4. After contrast administration, there was a significant enhancement in the new image detected at the pons and cervical spinal cord level of C1-C2. There was weak lesion enhancement in the posterior arm of the right internal capsule, the presence of mucosal thickening, and partial obliteration of the right sphenoid sinus. **Conclusion:** The images are consistent with a demyelinating process that affects the supra and infratentorial compartments and the cervical spinal cord. Two new lesions were detected in this study. One at the level of the posterior arm of the right internal capsule and another at the pons. Contrast enhancement of the two previously mentioned lesions and the lesion in the cervical spinal cord at C1-C2.

C: Cervical; MPR: Multiplanar; MRI: Magnetic Resonance Imaging; RSNA: RadReport.org, June 4, 202.

date of the previous study, relevant negative or normal findings, radiologist's recommendation to perform additional studies, recommendation of when to follow-up with imaging, radiologist's recommendation for referral to another specialty, other paraclinical studies, and therapeutic recommendations.

Statistical analysis

A sample size of 96 participants was calculated with a 95% confidence interval and a 10% margin of error. Measures of central tendency and dispersion were calculated. The X^2 Test of Goodness of Fit was calculated to define preference percentages. Knowledge of the standardized structured report, preference for type of report, most complete report, qualities, and content of the radiology report considered necessary by radiologists and referring clinicians were compared using the Chi-square test or Fisher's exact test. A p-value ≤ 0.05 was statistically significant. IBM-SPSS software (version 20.0. IBM Corp., Armonk, NY, USA) was used.

RESULTS

A total of 184 questionnaires were completed. Twenty-five were excluded because of incomplete information or duplicated formats. A total of 159 questionnaires from 71 (44.7%) radiologists and 88 (55.3%)

Table 2. Knee MRI of a patient with degenerative joint disease for traumatology and orthopedics specialists: Standardized structured radiology report (scenario 2A) and prose radiology report (scenario 2B)

2A. Standardized structured radiology report

MRI of the left knee
Long TR images were acquired in the coronal, sagittal, and axial planes.
Clinical information: A 40-year-old man with post-traumatic left knee pain.
Comparison: None.
Findings:
MENISCUS
Medial meniscus: hyperintense linear images extending from the capsule periphery toward the meniscus body, with no connection to the joint surfaces.
Lateral meniscus: intact.
LEFT
Cruciate ligaments: edema and disruption of the fibers of the posterolateral bundle of the anterior cruciate ligament. Anteromedial bundle and posterior cruciate ligament intact.
Medial collateral ligament: superficial and deep components intact. No periligamentous edema.
Lateral collateral ligament: intact.
Posterolateral corner structures: intact
EXTENSION MECHANISM
Distal quadriceps and patellar tendon intact. Patella is in a normal position in the femoral groove. No disruption of the retinaculum.
LIQUID
Minimal increase in synovial fluid in the mid-knee and retropatella. No Baker's cysts.
BONES AND JOINT STRUCTURES
Bone: No fractures, no stress reaction, no bone lesions.
Patellofemoral compartment: 5.0 mm thickening of the joint cartilage and superficial fibrillation. Uncomplicated retropatellar synovitis and medial plica.
Medial compartment: Tibiofemoral hyaline cartilage thickening and superficial fibrillation.
Lateral compartment: Tibiofemoral hyaline cartilage thickening and superficial fibrillation.
Diagnostic impression:
1. Medial meniscus with grade 2 mucinous degeneration.
2. Partial tear of the anterior cruciate ligament due to rupture of the posterolateral bundle.
3. Patella and tibiofemoral grade 1 chondromalacia.

2B. Prose radiology report

MRI of the left knee
Technique: pd_tse_fs coronal and sagittal, t2_me3d_we sagittal, pd_tse axial, sagittal, t2_tse_coronal, coronal oblique and t2_me2d_fs axial sequences were used.
Findings:
Both menisci were assessed with normal morphology and volume; in the medial meniscus, I detected hyperintense linear images extending from the capsular periphery toward the meniscus body without showing communication with the articular surfaces. These findings correspond to a **grade 2 mucinous degeneration.**
The patellar **tendon**, quadriceps **tendon**, and **collateral ligaments** maintain their normal tension, direction, and attachment.
The anterior cruciate ligament is thickened. There is signal enhancement associated with **edema** at the level of the posterolateral bundle. Fibrillar disruption was seen in the coronal oblique images toward the femoral attachment. This finding should be clinically correlated—the posterior cruciate ligament with normal course and attachments.
I detect a discrete increase in synovial fluid in the midline of the joint and retropatella.
5. A patellar index (Insall-Salvati) of 1.0 (normal situation) was noted on sagittal images.
I found congruence of the patellofemoral joint surfaces on the axial images, and the trochlear angle was evaluated as 142°. The articular cartilage of the patella and trochlea femoris shows diffuse thickening of up to 5 mm, and there are areas of superficial fibrils and edema. These findings are consistent with **grade 1 chondromalacia;** retropatellar **synovitis** and uncomplicated medial **plica** data were observed. The **retinacula were** intact and showed a normal homogeneous hypointense signal. I find adequate congruency in the tibiofemoral articular surfaces. Diffuse thickening of the articular cartilage greater than 4 mm, increased free intrachondral water, and superficial fibrillation was observed in the lateral loading axis. In the **medial loading axis**, the joint cartilage measured 3.4 mm on the femoral surface and 1.2 mm on the tibial surface; superficial fibrillar areas and edema were observed. These findings are consistent with **chondromalacia.**
8. Using the fat displacement technique, I note an increase in fluid in the subcutaneous tissue of the pre-and infrapatellar regions.
The **cortical** and **medullary** tibiofemoral **bone** showed no signal changes.

MRI: Magnetic Resonance Imaging; RSNA: RadReport.org, June 4, 2021.

Table 3. Specialties of surveyed physicians who participated in the evaluation of standardized structured radiology and prose reports

Description	n = 159 (%)
Radiology	71 (44.7)
Gynecology and obstetrics	16 (10.1)
Traumatology and orthopedics	16 (10.1)
Otorhinolaryngology	12 (7.5)
Neurology	10 (6.3)
Gastroenterology	8 (5.0)
Neurosurgery	6 (3.8)
Cardiology	6 (3.8)
Pediatrics	5 (3.1)
Ophthalmology	3 (1.9)
Urology	3 (1.9)
Emergency medicine	2 (1.3)
Nuclear medicine	1 (0.6)

referring clinicians were analyzed. The mean age of the participating physicians was 45 ± 10 (30 to 77) years, and the mean length of professional practice was 14 ± 11 (1 to 46) years. The specialties of the participants are described in Table 3.

Previous knowledge of the standardized structured radiology report was significantly higher among radiologists (n = 63, 88.7%) ($p < 0.001$) than referring clinicians (n = 45, 51.1%) (Table 4). After reading the radiology reports, the preference for the standardized structured report compared to a prose was significantly higher report among radiologists (n = 53, 74.6%) ($p < 0.001$) and referring clinicians (n = 74, 84.1%) ($p<0.001$). A similar result was observed when evaluating its content ($p < 0.001$). The standardized structured radiology report was preferred regardless of the participant's age (Figure 1) and specialty (Figure 2). The association between the years of professional practice of radiologists and referring clinicians in relation to the preferred type of radiology report is shown in Table 5. Regardless of the years of professional practice, a significant difference was found in the preference for the standardized structured report over the prose report in 127 (79.9%) compared to 32 (20.1%), respectively ($p < 0.001$).

The qualities of the standardized structured report and prose radiology report defined by the radiologists and referring clinicians are shown in Table 6. Of the159 participants who indicated one or more qualities, a total of 204 responses were received: 128 respondents indicated 162 qualities of the standardized structured report, and 31 participants who preferred the prose report indicated 42 qualities.

The qualities most frequently mentioned by radiologists and referring clinicians of the standardized structured radiology report were: organized, understandable, concise, easy to read, descriptive, and focused on the clinical setting. Those qualities attributed to the prose radiology report were: descriptive, concise, understandable, and easy to read. The necessary content of the radiology report was comparable between radiologists and referring clinicians (Figure 3); the most important were: clinical indication for the study, recommendation for additional testing, negative or normal findings, quality of the study, date of previous studies, administration of a contrast agent, and recommendation for evaluation by other specialties. In addition, radiologists suggested that the radiology report include the study technique description, recommendations for radiological and therapeutic follow-up, and other paraclinical studies.

DISCUSSION

In our study, the preference of Mexican radiologists and referring clinicians for the standardized structured radiology report was significant, regardless of age, specialty, and years of professional practice. The most important qualities of the standardized structured report were: organized, understandable, concise, easy to read, descriptive, and focused on the clinical setting. Radiologists and referring clinicians considered the following elements necessary for the content of the radiology report: clinical indication for the study, recommendation for additional testing, negative or normal findings, quality of the study, date of previous studies, administration of a contrast agent, and recommendation for evaluation by other specialties. This is the first report from Mexico showing that radiologists and referring clinicians prefer the standardized structured radiology report.

Previous studies have investigated preferences for the type of radiology reporting[6-8,11,12]. In a binational European study, Bosmans et al.[13] informed that 592 (84.5%) of 701 referring clinicians and 88 (65.7%) of 134 radiologists preferred standardized structured radiologic reporting of complex imaging studies (e.g., ultrasound, CT, or MRI). On the other hand, 394 (56%) of 704 referring clinicians and 97 (73%) of 133 radiologists

Table 4. Knowledge and preference for the type of radiology report among radiologists and referring clinicians

Description	Radiologists, (n = 71)	Referring Clinicians, (n = 88)	Total, (n = 159)
	n (%)	n (%)	n (%)
Previous knowledge of standardized structured radiology report:			
Yes	63 (88.7)	45 (51.1)	108 (69.7)
No	8 (11.3)	43 (48.9)	51 (32.1)
	p<0.001	p = 0.831	
Preference for type of radiology report:			
Standardized structured	53 (74.6)	74 (84.1)	127 (79.9)
Prose	18 (25.4)	14 (15.9)	32 (20.1)
	p<0.001	p<0.001	
The radiology report is more complete in terms of content:			
Standardized structured	52 (73.2)	73 (83.0)	125 (78.6)
Prose	19 (26.8)	15 (17.0)	34 (21.4)
	p<0.001	p<0.001	

The X^2 Test of Goodness of Fit was calculated to define preference percentages.

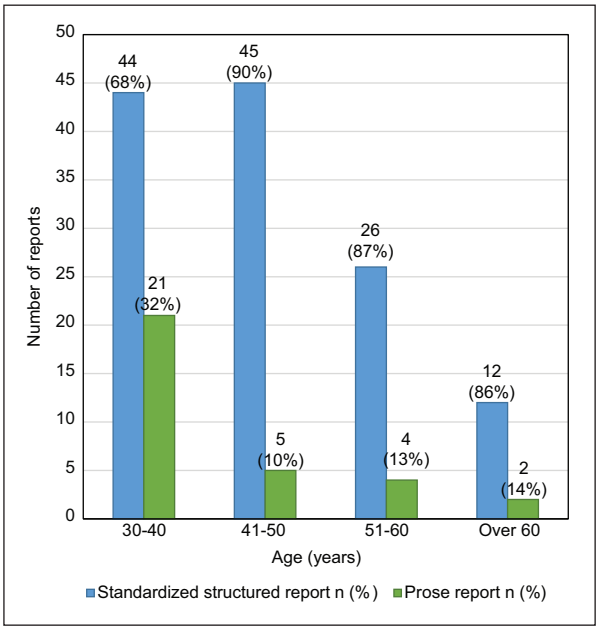

Figure 1. Age of radiologists and referring clinicians and association with the type of radiology report preferred. The standardized structured radiology report was preferred regardless of the participant's age.

rejected prose reporting; some study participants gave no response. In another study, in a Canadian College Hospital, 16 (64%) of 25 radiologists and 73 (86%) of 89 referring clinicians expressed a preference for the standardized structured report in three ultrasound scenarios (normal, benign, or malignant disease), whereas 5 (20%) of 25 radiologists preferred a prose report; four expressed no preference. On the other hand, only 10 (11%) of 89 referring clinicians chose the prose report; two expressed no preference[6]. These results are comparable to our study in which 53 (74.6%) of 71 radiologists and 74 (84.1%) of 88 referring clinicians preferred the standardized structured radiology report, in contrast with 18 (25.4%) and 14 (15.9%) who preferred the prose report ($p < 0.001$). Our results on the preference for standardized structured radiology reports by Mexican radiologists and referring clinicians could motivate their implementation in daily practice.

There are few studies in which radiologists and referring clinicians were asked about their opinions on the qualities of the radiology report[6-8,12]. The radiology report is considered a personal reflection of radiologists' attitudes, perceptions, and skills[14]. In our study, the main qualities of the standardized structured radiology report identified by radiologists and referring clinicians are comparable to those described in the literature in terms of clarity and better content with a complete and detailed description of imaging findings that can be communicated to referring clinicians. These characteristics reduce the possibility of errors and improve quality and patient care[6,12,15,16]. In addition, the appearance and completeness of the standardized structured radiology report are independent of the clinical setting[6]. This finding contrasts with the variability from brief to extensive information on normal findings that prose

Table 5. Association between years of professional practice in the specialty of radiologists and referring clinicians, and type of radiology report preferred

Professional practice (Years)	Radiologists and referring clinicians (n = 159)	Preference for standardized structured report (n = 127) (%)	Preference for prose report (n = 32) (%)
1 - 10	69	48 (37.8)	21 (65.6)
11 - 20	47	42 (33.1)	5 (15.6)
21 - 30	29	25 (19.7)	4 (12.5)
31 - 40	11	9 (7.1)	2 (6.3)
> 40	3	3 (2.4)	0 (0.0)

Chi-square to 2 × 2 contingency tables: $p < 0.001$..

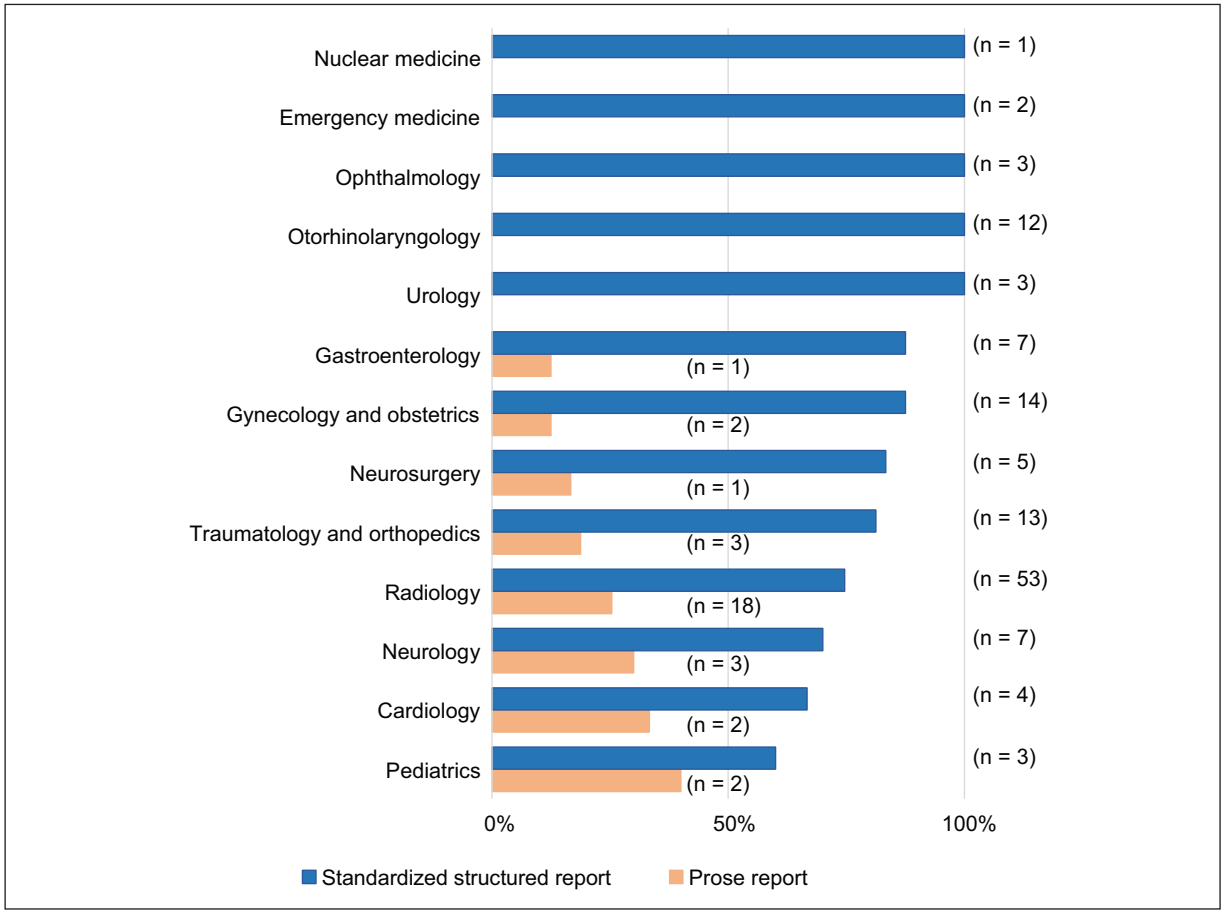

Figure 2. Preferred type of radiology report by radiologists and referring clinicians according to their medical specialty. The standardized structured radiology report was preferred regardless of the participant's specialty.

report contains[17] with inconsistencies that can confuse referring clinicians[6,10,11,18] because it lacks structure and can be difficult to identify and compare specific details of previous radiology reports[18,19]. In our study, the qualities of the standardized structured radiology report were that it was organized, understandable, concise, easy to read, descriptive, and focused on the clinical setting to achieve the balance of a brief but sufficiently clear report that includes abnormal findings in a structured checklist. This structure represents a "trade-off"

Table 6. Qualities of the standardized structured report and the prose report, as defined by radiologists and referring clinicians, according to the preference for each report type

Description	Standardized structured radiology report (n = 162) (%)	Prose radiology report (n = 42) (%)
Organized	41 (25.3)	1 (2.4)
Understandable	41 (25.3)	10 (23.8)
Concise	19 (11.7)	10 (34.5)
Easy to read	19 (11.7)	5 (20.8)
Descriptive	17 (10.5)	12 (41.4)
Focused on the clinical setting	10 (6.2)	0 (0)
Fast reading	8 (4.9)	1 (2.4)
Less-error prone	7 (4.3)	0 (0)
Familiarity with known report	0 (0)	3 (7.1)

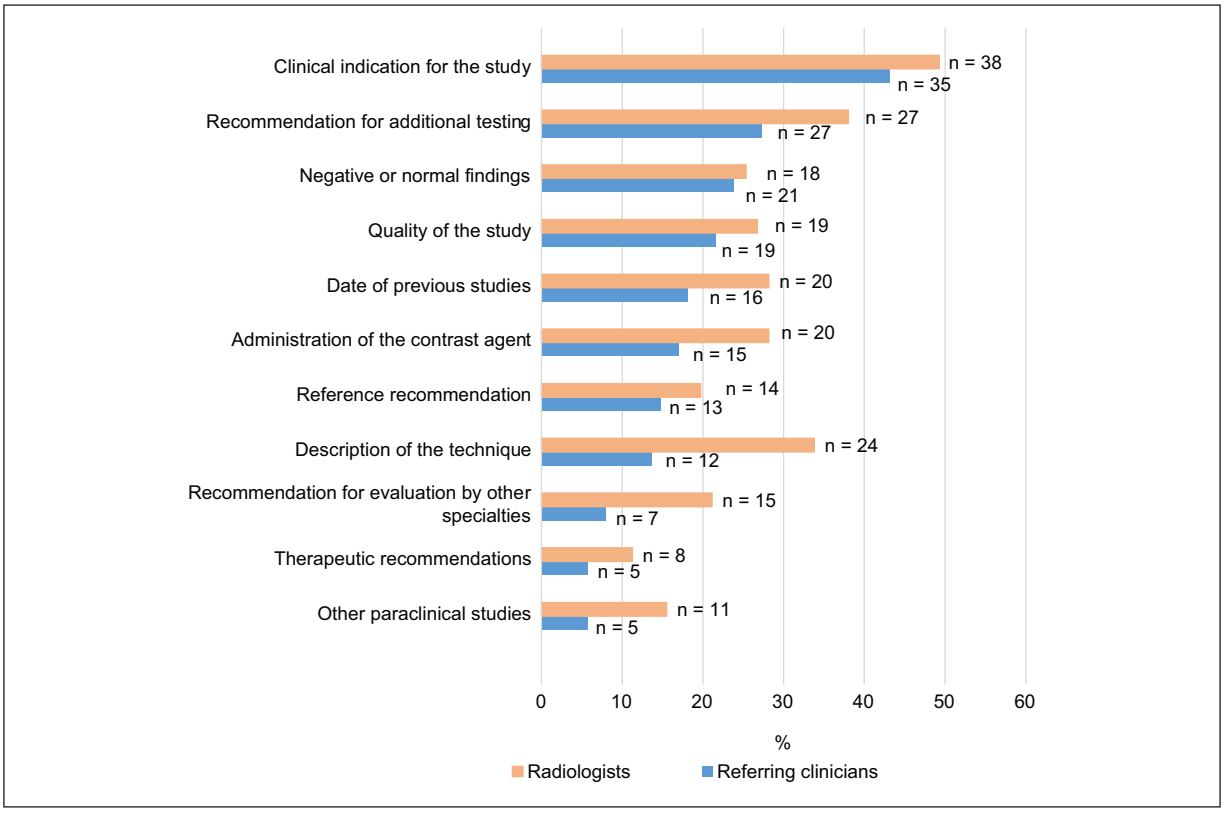

Figure 3. Eleven characteristics from which radiologists and referring clinicians selected those they considered necessary to complete the content in a radiology report. Adapted from: Naik SS et al.[6]

between detailed description and standardization of relevant information to improve the quality of medical care, teaching and to enable its use in research.

There are few reports in the medical literature about the content of the radiology report[12,13]. The standardized structured radiology report needs to improve to achieve optimal communication between radiologists and referring clinicians[11,14]. The major radiological societies in North America and Europe have formed committees to determine what the standardized structured radiology report should contain to improve radiologists' compliance and meet the expectations of referring

clinicians. It was suggested that bibliographic information, differential diagnoses, radiologic follow-up, and important patient responses should be reported[7,12]. In our study, the recommended content of the radiology report by radiologists and referring clinicians were the clinical indication for the study, recommendations for additional testing, negative or normal findings, quality of the study, date of previous studies, administration of a contrast agent, and recommendation for evaluation by other specialties.

The use of templates to promote consistency in radiology reporting is recommended by some and opposed by others[7]. Larson et al.[8] implemented 223 standardized structured reports corresponding to 199 000 departmental studies. They showed that participating radiologists were highly accepting and compliant with these reports, overcoming their previous beliefs about radiology reporting. Our study showed that the radiologists and referring clinicians preferred standardized structured radiology reports regardless of their age, specialty, or years in the profession. This finding suggests that it would be possible to successfully implement templates for standardized structured reports in Mexico by focusing on the organizational and ethical challenges[8].

The strengths of our study are related to the design, which allowed us to identify the preferences of radiologists and referring clinicians in the medical and surgical specialties and subspecialties. In addition, we used questionnaires with standardized structured radiology reports and prose reports of real clinical cases that were specific to each specialty or subspecialty of the participants. The limitation of the study is related to the exclusive use of MRI reports to determine radiologists and referring clinicians' preferences.

CONCLUSION

Our study showed that Mexican radiologists and referring clinicians preferred the standardized structured radiology report, regardless of age, specialty, and years of professional practice. The qualities of the standardized structured report were that it was organized, understandable, concise, easy to read, descriptive, and focused on the clinical setting. In Europe and the United States, the standardized structured radiology report has been long established. In Mexico, however, it is used only in exceptional cases. Some authors have recommended it for specific pathologies, such as tomographic assessment of SARS-CoV2 pneumonia[20], head and neck[21], liver[9], or renal mass[22]. Institutional efforts are needed to introduce a standardized structured radiology report in México. It can be difficult for a large group of radiologists with strongly held beliefs to reach a consensus on a topic as sensitive as radiologic reporting[8].

Acknowledgments

The authors thank Professor Ana M. Contreras-Navarro for her guidance in preparing and writing this scientific paper.

Funding

This research received no external funding.

Conflicts of interest

The authors declare that they have no conflicts of interest.

Ethical disclosures

Protection of human and animal subjects. The authors declare that the procedures followed were in accordance with the regulations of the relevant clinical research ethics committee and with those of the Code of Ethics of the World Medical Association (Declaration of Helsinki).

Confidentiality of data. The authors declare that they have followed the protocols of their work center on the publication of patient data.

Right to privacy and informed consent. The authors have obtained the written informed consent of the patients or subjects mentioned in the article. The corresponding author is in possession of this document.

REFERENCES

1. Armas RR. Letter. Qualities of a good radiology report. AJR Am J Roentgenol. 1998;170(4):1110. doi: 10.2214/ajr.170.4.9530077.
2. Laswad T, Fournier D, Moreau J, Brat H, Deac M, Tancredi T, et al. Structured reports: 10 years experience in private radiology clinics. Poster session presented at: European Congress of Radiology. Annual congress of the European Society of Radiology; 2014 March 6-10; Vienna, AT. doi: 10.1594/ecr2014/C-2028.
3. Reiner BI, Knight N, Siegel EL. Radiology Reporting, Past, Present and Future: The Radiologist's Perspective. J Am Coll Radiol. 2007; 4(5):313 -319. doi:10.1016/j.jacr.2007.01.015.
4. Wallis A, McCoubrie P. The radiology report - Are we getting the message across?. Clin Radiol. 2011;66:1015 - 1022. doi:10.1016/j.crad.2011.05.013.
5. Chen JY. Sippel Schmidt TM, Carr CD, Kahn CE. Enabling the next generation Radiology Report: Description of Two New System Standards. RadioGraphics. 2017;37(7):2106 - 2112. doi:10.1148/rg.2017160106.
6. Naik SS, Hanbidge A, Wilson SR. Radiology Reports: Examining Radiologist and Clinician Preferences Regarding Style and Content. AJR Am J Radiol. 2001;176:591-598. doi:10.2214/ajr.176.3.1760591.

7. Bosmans JML, Peremans L, De Schepper AM, Duyck PO, Parizel PM. How do referring clinicians want radiologists to report? Suggestions from the COVER survey. Insights Imaging. 2011;2:577-584.
8. Larson DB, Towbin AJ, Pryor RM, Donnelly LF. Improving Consistency in Radiology Reporting through the Use of Department-wide Standardized Structured Reporting. Radiology. 2013;267(1): 240-250. doi: 10.1148/radiol.12121502.
9. Illescas-Cárdenas J, Rodríguez-Nava P, Dena-Espinoza E. Evaluation of liver lesions by multiphasic multislice multiphase tomography: a proposal for a structured report. An Radiol Mex. 2017;16(2):87-101.
10. Society of Radiology (ESR). ESR paper on structured reporting in radiology. Insights Imaging. 2018; 9:1-7. doi:10.1007/s13244-017-0588-8.
11. Schwartz LH, Panicek DM, Berk AR, Li Y, Hricak H. Improving communication of diagnostic radiology findings through structured reporting. Radiology. 2011;260(1):174-181. doi: 10.1148/radiol.11101913.
12. Camilo DMR, Tibana TK Adôrno IF, Santos RFT, Klaesener C, Gutierrez Junior W, et al. Radiology report format preferred by requesting physicians: prospective analysis in a population of physicians at a university hospital. Radiol Bras. 2019;52(2):97-103. doi:10.1590/0100-3984.2018.0026.
13. Bosmans JML, Weyler JJ, De Schepper AM, Parizel PM. The Radiology Report as seen by Radiologist and Referring Clinicians: Results of the COVER and ROVER Surveys. Radiology. 2011;259 (1):184-195. doi:10.1148/radiol.10101045.
14. Clinger NJ, Hunter TB, Hillman BJ. Radiology Reporting: Attitudes of Referring Physicians. Radiology. 1988;169(3):825-826. doi: 10.1148/radiology.169.3.3187005.
15. Goldenberg C, Yablok S. Quality improvement through the implementation of structured reports. Clin Imaging. 2020; 67:143-145. doi:10.1016/j.clinimag.2020.06.015.
16. Brady AP. Error and discrepancy in radiology: inevitable or avoidable? Insights Imaging. 2017;8(1):171-182. doi: 10.1007/s13244-016-0534-1.
17. Boland GW, Duszak R Jr. Structured Reporting and Communication. J Am Coll Radiol. 2015;12(12):1286-1288. doi:10.1016/j.jacr.2015.08.001.
18. Mamlouk MD, Chang PC, Saket RR. Contextual Radiology Reporting: A New Approach to Neuroradiology Structured Templates. AJNR Am J Neuroradiol. 2018;39(8):1406-1414. doi: 10.3174/ajnr.A5697.
19. Motta-Ramírez G. Radiological learning based on specific clinical problem: part 2, how is a radiological report elaborated? An Radiol Mex. 2021;20:122-136. doi: 10.24875/ARM.20000119.
20. Murrieta-Peralta E. Chischistz-Condey AP. Ramírez-Landero J. Moctezuma-Velasco CR. Murrieta-González H, Salazar-Segovia J. The radiological report in patients with suspected COVID-19: our experience at the ABC Medical Center. An Radiol Mex. 2020;19(3):276-285. doi: 10.24875/ARM.20000088.
21. Morales-Pérez F, Rodríguez-Nava P, Dena-Espinoza E, Vásquez-Gijón M. Utility of multislice computed tomography in the evaluation of neck tumors. Proposal for a structured report. An Radiol Mex. 2016;15(2):103-110.
22. Vásquez-Guijón M, Rodríguez-Nava P, Dena-Espinoza E, Morales-Pérez F. Characterization of renal tumors by multislice computed tomography and its anatomopathologic concordance. Proposal for a structured report. An Radiol Mex. 2016;15(2):140-147.

JMeXFRI

Journal of the Mexican Federation of Radiology and Imaging

Check for updates

FULL RESEARCH ARTICLE

Diagnostic criteria of ultrasound duplex doppler for venous thoracic outlet syndrome: fifteen years' experience

Mauricio Figueroa-Sanchez[1,2,a] and L. Johanna Montaño-Rodriguez[2]*

[1]*University Center of Health Sciences, Universidad de Guadalajara;* [2]*Radiology and Imaging Department, Antiguo Hospital Civil of Guadalajara "Fray Antonio Alcalde" Guadalajara, Jalisco, Mexico*

[a]*0000-0001-7042-5221*

ABSTRACT

Introduction: *There is no consensus regarding ultrasound (US) duplex Doppler findings for diagnosing vascular thoracic outlet syndrome (TOS). Our aim was to determine the ultrasound findings of the subclavian vein using US duplex Doppler with dynamic maneuvers to diagnose venous TOS.* **Material and methods:** *This retrospective cohort study conducted from May 2005 to December 2020 included patients with a clinical suspicion of vascular TOS examined by US duplex Doppler with dynamic maneuvers in three positions, 0°, 90°, and 180° by a single expert radiologist.* **Results:** *We included 110 US duplex Doppler scans from 97 patients (84 unilateral and 13 bilateral). Nineteen (17.2%) were normal and 91 (82.8%) abnormal; 84 (76.4%) with pure venous TOS and 6 (5.4%) with mixed TOS (venous and arterial); only one case (1%) was pure arterial TOS. In patients with venous TOS, the mean baseline (0°) diameter was 7.42 ± 1.36 mm (pure) and 7.33 + 0.82 mm (mixed); during the dynamic maneuver at 180°, a complete diameter reduction (0 mm) and flow velocity (0 cm/s) were observed ($p < 0.001$). In contrast, normal US duplex Doppler showed a mean diameter reduction of 50% or less from 7.37 ± 0.83 mm at 0° to 3.68 ± 0.48 mm during the dynamic maneuver at 180°. Flow velocity showed no significant change.* **Conclusion:** *We propose complete diameter reduction and absence of flow velocity in the subclavian vein during an ultrasound with a dynamic maneuver at 180° as criteria for diagnosing venous TOS. These diagnostic criteria have not been previously reported.*

Keywords: *Dynamic maneuvers. Subclavian vein. Subclavian vein diameter. Subclavian flow velocity. TOS. Ultrasound findings.*

INTRODUCTION

The diagnosis of thoracic outlet syndrome (TOS) is based on the medical history and physical examination. Imaging methods identify and evaluate normal and abnormal anatomic structures to locate affected sites and confirm or exclude a vascular origin and complications. In more than 90% of cases, TOS is neurogenic. The second most common type is venous TOS, and arterial TOS is uncommon (<3%)[1]. Ultrasound (US) duplex Doppler, a contrasted CT of the chest, or catheter venography of the upper extremity are recommended for the initial diagnosis of venous TOS[2]. US duplex Doppler is a noninvasive procedure that provides dynamic assessment of the subclavian vessels and detects compression and associated complications in the subclavian artery, subclavian vein, or both[2]. The extent of vascular compression may increase during dynamic maneuvers[3], such as arm abduction, which may narrow the thoracic outlet in all three spaces (the scalene triangle, the costoclavicular space, and the retropectoral space). This reduction is evidenced by decreased vessel diameter, increased flow velocities,

Corresponding author:
*Mauricio Figueroa-Sanchez, MD
E-mail: figueroa_sanchez@hotmail.com

Received for publication: 15-10-2021
Approved for publication: 11-11-2021
DOI: 10.24875/JMEXFRI.M21000005

Available online: 31-03-2022
J Mex Fed Radiol Imaging. 2022;1(1):23-31
www.JMeXFRI.com

and/or spectral wave change on US duplex Doppler. These parameters may be observed as physiologic (normal) or abnormal changes in patients with TOS[1,3].

The US duplex Doppler parameters for the diagnosis of venous TOS have not been defined. Longley et al.[4] described significant venous compression with hyperabduction (90°, 135°, 180°) and a complete loss of the spectral waveform in the subclavian vein. The authors reported a US duplex Doppler sensitivity of 92% and a specificity of 95% compared with venography, which is the gold standard for diagnosing venous TOS. Spectral enhancement was not considered sufficient evidence for diagnosis and was associated with mild venous compression and turbulent blood flow. In another report, provocative maneuvers such as arm abduction to 90° and 180° were performed in patients with vascular TOS. It was suggested that a flow velocity reduction of 50% or greater or a complete Doppler signal loss in the subclavian vein confirmed venous TOS[5]. However, the characteristics of the diameter and flow velocity of the subclavian vein in US duplex Doppler in patients with venous TOS have not yet been defined. The aim of this study was to determine the ultrasound findings of the subclavian vein using US duplex Doppler with dynamic maneuvers to diagnose venous TOS.

MATERIAL AND METHODS

This retrospective cohort study was conducted from May 2005 to December 2020 in the Radiology and Imaging Department of the Antiguo Hospital Civil de Guadalajara "Fray Antonio Alcalde" and the Laboratorio Vascular in Guadalajara Jalisco, Mexico. The US duplex Doppler studies of patients consecutively referred by angiologists, neurosurgeons, and orthopedists with a clinical suspicion of vascular TOS were included. Referring clinicians were experts in vascular and neurogenic TOS. Clinical suspicion was based on the medical history and physical examination with specific maneuvers described in the literature. Patients with a functional limitation of the shoulder to perform dynamic US duplex Doppler maneuvers were excluded. The study protocol and retrospective analysis of radiographic data obtained during routine medical care were approved by the institutional ethics and research committees.

The included variables were age, sex, laterality, unilateral or bilateral involvement, occlusion site, and scalene muscle hypertrophy. The ultrasound parameters recorded for the subclavian vein were diameter (mm), patency (absent or present), flow velocity (cm/s), and thrombosis (absent or present); for the subclavian artery, diameter (mm), patency (absent or present), flow velocity (cm/s) and A/B ratio.

Definitions

Normal US duplex Doppler was a reduction in the vessel diameter equal to or less than 50% with variable changes in flow velocity. These findings were considered physiological changes in response to dynamic maneuvers[1,3].

Abnormal US duplex Doppler was defined by a reduction of the subclavian vein and/or artery diameter to 0 mm and absence of flow velocity and during a dynamic assessment at 180°.

A/B ratio in the subclavian artery was performed with the modified measurement, specifically for the study of arterial TOS with the dynamic maneuvers at 0° and 180° as follows: Flow velocity of the subclavian artery at 0°=B. Flow velocity of the subclavian artery at 180°= A (e.g., flow velocity of A= 200 cm/s/flow velocity of B=50; the A/B ratio is 4). An A/B ratio >3 was considered positive.

US duplex Doppler imaging protocol

All studies were performed by a single radiologist with 26 years of experience in vascular US duplex Doppler (MFS). Aloka SSD4000™ devices with 10- and 13-MHz linear transducers (Aloka Co. Tokyo, Japan), a LOGIG E9™ (GE, Wisconsin, USA) with 10- and 16-MHz linear transducers, and an Acuson S2000™ (Siemens, Mountain View, USA) with 9-, 14-, and 18-MHz linear transducers were used. An endocavitary 6-10-MHz transducer was also used. Imaging studies were performed with the patient supine. Transverse and sagittal projections were performed in B-mode, pulsed Doppler, color Doppler, and angio-Doppler with vascular presetting (venous and arterial). The US duplex Doppler technique was the same for all three devices. Resolution and image quality improved as the devices were updated, but ultrasound parameters were comparable.

The venous protocol started with a transverse approach in the proximal inframandibular region of the internal jugular vein and continued caudally along its trajectory with a supraclavicular and infraclavicular approach to the junction with the ipsilateral subclavian vein. The transducer was placed slightly oblique to obtain a true sagittal image of the subclavian vein. These areas correspond to the costoclavicular space

Figure 1. Patient in supine position with the arm at 0°(A); dynamic maneuver with the arm abducted at 90°(B) and 180°(C) with continuous flexion and extension of the fingers of the ipsilateral hand to increase the subclavian vein flow.

in supraclavicular and infraclavicular approaches, where dynamic maneuvers were performed in three positions: 0°, 90°, and 180° (Figure 1). The variables recorded in these positions were diameter, permeability, flow velocity, scalene muscle hypertrophy, thrombosis, and concomitant findings such as tumors. In the 90° and 180° abduction positions, the patient was asked to continuously flex and extend the fingers of the ipsilateral hand to increase venous flow. A true sagittal projection was then continued to assess the subclavian vein in the infraclavicular approach throughout its course to its junction with the axillary vein. At this point, the third minor retropectoral space was assessed, and an image of the axillary vein was obtained in the three positions mentioned before. In addition, the superior vena cava was examined through the suprasternal approach with an endocavitary transducer to determine the diameter, permeability, and flow velocity.

The study protocol of the subclavian artery was performed in a manner similar to that described previously, beginning with a transverse approach in the common carotid artery from its bifurcation to examine the triangle between the anterior, middle, and posterior scalene muscles, continuing along the common carotid artery to its junction with the subclavian artery. This area was examined in the three positions (0°, 90°, and 180°) and diameter, permeability, flow velocity, A/B ratio, and associated findings such as stenosis, aneurysm, and thrombosis were recorded. The infraclavicular approach was continued to the confluence of the subclavian and axillary arteries, where the third minor retropectoral space is located. The same variables were evaluated in the three described positions.

Statistical analysis

The mean, standard deviation, minimum, median, and maximum of quantitative variables were calculated and compared with the one-way ANOVA and the Kruskal-Wallis test. The statistical significance between categories of qualitative variables was determined using the Chi-squared test and Fisher's exact test. A p-value < 0.05 was considered significant. The IBM-SPSS statistical program version 20.0 (IBM Corp., Armonk, NY, USA) was used.

RESULTS

Ninety-seven patients were included, 33 (34%) men and 64 (66%) women with a mean age of 45.07 ± 15.26 years; the age range was wide (9 to 89 years). A total of 110 US duplex Doppler examinations were performed, of which 84 were unilateral and 13 bilateral. Nineteen (17.2%) were normal in 17 patients (bilateral US duplex Doppler was performed in two cases), while 91 (82.7 %) were abnormal, confirming the diagnosis of vascular TOS in 80 (87.9%) of 97 patients; 73 with pure venous TOS (62 unilateral and 11 bilateral US duplex Doppler), 6 with mixed venous TOS (arterial and venous) and one case with arterial TOS. The results of 110 US duplex Doppler are shown in Figure 2. In 19 (17.2%) normal US duplex dopplers, a neurogenic etiology was considered the cause of the symptoms, defined by the clinicians based on the results of magnetic resonance imaging of the brachial plexus and electromyography (not shown).

Ultrasound findings of normal US duplex Doppler, pure venous TOS, and mixed (venous and arterial) TOS are shown in Table 1. Diameter of the subclavian vein with the maneuver at 90° was not reported. The mean basal (0°) diameter of the subclavian vein in pure venous

Table 1. Comparison of subclavian vein findings in normal and abnormal US duplex Doppler in pure and mixed venous TOS

Characteristics	Normal US duplex Doppler (n = 19)	Abnormal US duplex Doppler		p-value
		Pure venous TOS[a] (n = 84)	Mixed TOS[b] (Venous and arterial) (n = 6)	
Age, years	40.47 ± 11.08 (29 – 65)	46.65 ± 15.79 (9 – 89)	53.17 ± 10.03 (43 – 64)	0.093
Basal diameter at 0° (mm)	7.37 ± 0.83 (6 – 8)	7.42 ± 1.36 (5 – 13)	7.33 ± 0.82 (6 – 8)	0.984
Flow velocity at 0° (cm/s)	35.74 ± 17.67 (17 – 81)	29.98 ± 16.14 (0 – 86)	22.83 ± 7.31 (16 – 36)	0.155
Flow velocity at 90° (cm/s)	35.79 ± 12.79 (17 – 57)	27.87 ± 17.28 (0 – 90)	18.83 ± 11.25 (10 – 38)	0.023
Flow velocity at 180° (cm/s)	35.53 ± 10.25 (11 – 48)	0	0	0.001
Diameter at 180° (mm)	3.68 ± 0.48 (3 – 4)	0	0	0.001

US: Ultrasound; TOS: Thoracic Outlet Syndrome; [a]73 patients with 62 unilateral and 11 bilateral US duplex Doppler; [b]6 patients with unilateral US duplex Doppler; Data are mean ± SD (range) unless otherwise specified.

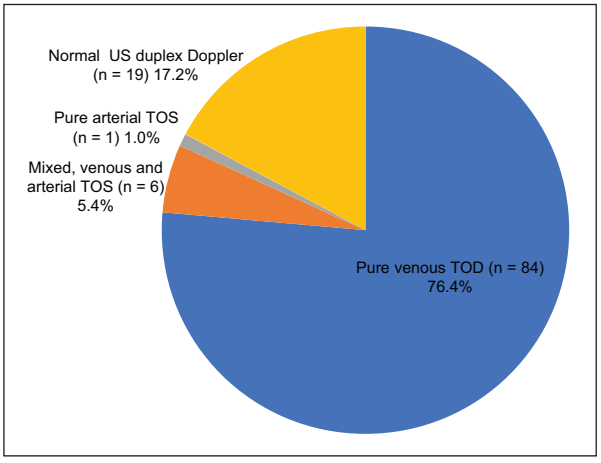

Figure 2. Normal and abnormal US duplex Doppler in patients with clinical suspicion of a vascular TOS. The diagnosis of venous (pure or mixed) and arterial TOS was defined based on ultrasound findings.
US: ultrasound; TOS: thoracic outlet syndrome.

TOS (7.42 ± 1.36 mm) and mixed TOS (7.33 ± 0.82 mm) showed a reduction to 0 mm with the dynamic maneuver at 180° (p<0.001). In contrast, the mean basal (0°) diameter of the subclavian vein in patients with a normal US duplex Doppler showed a reduction of 50% or less with 7.37 ± 0.83 at 0° versus 3.68 ± 0.48 with the dynamic maneuver at 180°. There was no significant difference in the flow velocity of the subclavian vein at 0° between the groups. A lower mean flow velocity was observed at 90° in pure venous TOS (27.87 ± 17.28 cm/s) and mixed venous TOS (18.83 ± 11.25 cm/s) compared with normal US duplex Doppler (35.79 ± 12.79 cm/s). Flow velocity was not absent during the 90° maneuver in any of the venous TOS cases. In contrast, in patients with pure and mixed venous TOS, the flow velocity in the subclavian vein was absent during the dynamic maneuver at 180° (p<0.001); whereas a flow velocity at 0°, 90°, and 180° showed no change in normal US duplex Doppler. A complete diameter reduction and absence of flow velocity in the subclavian vein during the dynamic maneuver at 180° were ultrasound findings of venous TOS.

In pure venous TOS, the costoclavicular space was commonly involved (n=82, 97.6%). Only two (2.4%) cases were in the costoclavicular and retropectoral space. Thrombosis of the subclavian vein (Paget-Schroetter syndrome) was found in 11 patients, seven with complete occlusion and four with partial occlusion. One patient with mixed TOS was found to have non-occlusive thrombosis. In 68 (86.1%) of 79 patients with pure or mixed TOS, we found intermittent subclavian vein compression (McCleery syndrome). On the other hand, hypertrophy of the scalene muscle was found in 13 (14%) of 97 patients. This finding was found in only one case with normal US duplex Doppler. Figure 3 shows a US duplex Doppler of a 31-year-old male patient with normal patency and flow velocity in the subclavian vein during dynamic maneuvers at 0°, 90°, and 180°. A physiological decrease in diameter vein was observed from 6.6 mm to 2.2 mm at 180°. Figure 4 shows a US duplex Doppler of a 31-year-old male patient with normal diameter, patency, flow velocity, and spectrum of the subclavian artery during dynamic maneuvers at 0°, 90°, and 180°. Figure 5 shows a US duplex Doppler of a 34-year-old male patient with venous TOS. The subclavian vein

Table 2. Comparison of subclavian artery findings on normal and abnormal US duplex Doppler in arterial, pure, and mixed TOS

Characteristics	Normal US duplex Doppler (n = 19)	Abnormal US duplex Doppler		p-value
		Pure arterial TOS (n = 1)	Mixed TOS (Venous and arterial) (n = 6)	
Diameter (mm)	6.42 ± 0.77 (5 – 8)	7	7.17 ± 0.41 (7 – 8)	0.069
Flow velocity at 0º (cm/s)	76.11 ± 25.53 (40 –136)	41	70.67 ± 39.19 (40 – 144)	0.231
Flow velocity at 90º (cm/s)	75.95 ± 27.61 (44 – 148)	48	66 ± 40.09 (36 – 142)	0.186
Flow velocity at 180º (cm/s)	71.68 ± 19.27 (42 – 121)	0	0	0.001
Maximum velocity during dynamic maneuvers (cm/s)	80.26 ± 25.80 (45 – 148)	48	66 ± 40.09 (36 – 143)	0.113
A/B ratio	0.91 ± 0.26 (0.18 –1.27)	0.85	1.10 ± 0.11 (1.00 – 1.28)	0.065

US: Ultrasound; TOS: Thoracic Outlet Syndrome; Data are mean ± SD (range) unless otherwise specified.

Table 3. Comparison of superior vena cava findings on normal and abnormal US duplex Doppler in relation to pure venous, mixed, and arterial TOS

Characteristics	Normal US duplex Doppler (n = 19)	Abnormal US duplex Doppler			p-value
		Pure venous TOS[a] (n = 83)	Mixed TOS (Venous and arterial) (n = 6)	Pure arterial TOS (n = 1)	
Diameter (mm)	15.74 ± 2.28 (13 – 21)	15.76 ± 2.01 (12 –21)	16.17 ± 0.41 (16 – 17)	19	0.331
Flow velocity (cm/s)	47.58 ± 8.93 (33 – 36)	44.96 ± 11.77 (20 –76)	44.67 ± 9.58 (37 – 58)	67	0.264

US: Ultrasound; TOS: Thoracic Outlet Syndrome; [a]Patient with mediastinal lymphoma was not included; Data are mean ± SD (range) unless otherwise specified.

diameter, patency, and flow velocity were normal at 0°; the diameter, patency, and flow velocity decreased during dynamic maneuvers at 90°, and a complete reduction in the diameter and flow velocity occurred at 180°.

Table 2 compares the subclavian artery findings in 19 normal US duplex Doppler, one with pure arterial TOS and 6 with mixed arterial and venous TOS. No significant differences in diameter and flow velocity were observed at 0° and 90°. In contrast, an absence of subclavian artery flow velocity was observed in the dynamic maneuver at 180° with pure arterial and mixed TOS ($p<0.001$). In one patient, pure arterial TOS involvement was found in the scalene triangle; in addition, an accessory cervical rib was found on a chest x-ray. In no case was an A/B ratio >3 or hypertrophy of the scalene muscle observed.

The ultrasound findings of the superior vena cava from normal and abnormal US duplex Doppler are shown in table 3. No significant differences in diameter and flow velocity were found between groups. The superior vena cava was not visualized in only one patient because of severe extrinsic compression by a mediastinal mass diagnosed as lymphoma. Figure 6 shows a US duplex Doppler examination of the superior vena cava with normal diameter, patency, and flow velocity. In contrast, in the case of a 42-year-old male patient with mediastinal lymphoma, the superior vena cava could not be visualized. A solid mediastinal mass measuring 6.4 x 5.9 cm was identified. A chest angiotomography (not shown) in this patient showed filiform passage of the contrast agent into the superior vena cava. This finding was due to extrinsic compression by the tumor.

DISCUSSION

In our study, the US duplex Doppler findings of venous TOS were complete reduction of the diameter to 0 mm and the absence of flow velocity in the

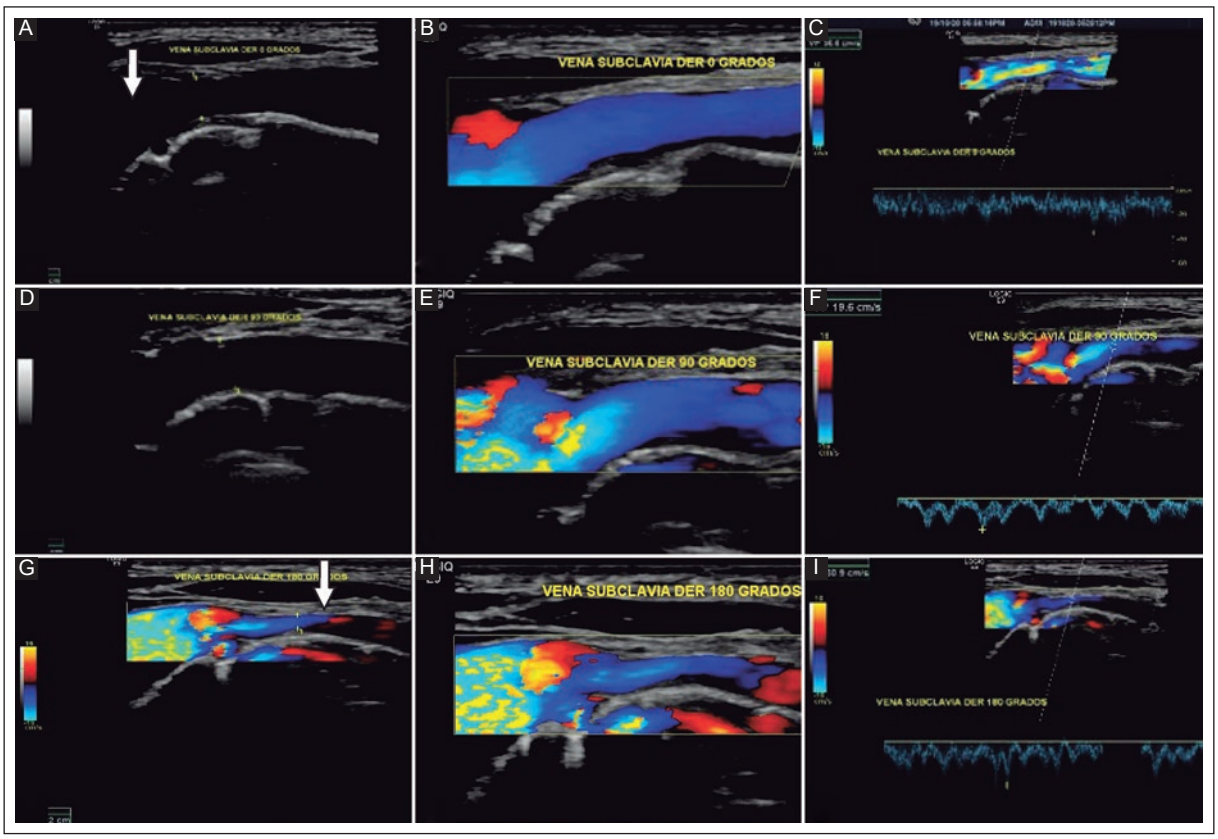

Figure 3. Normal US duplex Doppler of a 31-year-old male patient with dynamic maneuvers showing a normal diameter **(A)**, patency **(B)**, and flow velocity **(C)**, in the subclavian vein at 0° 90° **(D, E, F)**, and 180° **(G, H, I)**, respectively. Physiological decrease in diameter was observed from 6.6 mm at 0° **(A)** (arrow) to 2.2 mm at 180° **(G)** (arrow).
US: Ultrasound.

subclavian vein with the dynamic 180° maneuver. We propose these findings as ultrasound criteria for the diagnosis of venous TOS. These diagnostic criteria have not been previously reported in the literature. US duplex Doppler is suggested as the primary imaging modality for evaluating patients with clinical suspicion of vascular TOS.

There is no consensus on the definition of ultrasound findings for diagnosing venous TOS in patients with clinical suspicion[2,4-8]. In 1992, Longley et al.[4] in a study of 16 patients with clinical manifestations of vascular TOS and 20 healthy controls evaluated with US duplex Doppler, identified a complete loss of the spectral waveform in the subclavian vein as a criterion for significant venous compression during arm hyperabduction (90°, 135°, and 180°) with a sensitivity of 92% and a specificity of 95%, compared with venography for the diagnosis of venous TOS. US duplex Doppler with dynamic arm abduction maneuvers at 90° and 180° is useful for evaluating subclavian vessels[5]. We included 97 patients with a clinical suspicion of vascular TOS, 73 cases with pure venous TOS, and 6 with mixed TOS. The mean basal (0°) diameter of the subclavian vein was comparable in both normal and abnormal US duplex Doppler. In pure venous and mixed TOS, a reduction of 0 mm was found with the dynamic maneuver at 180° ($p < 0.001$). In contrast, the mean basal (0°) diameter of the subclavian vein in patients with normal US duplex Doppler showed a reduction of 50% or less with the dynamic maneuver at 180° (7.37 ± 0.83 and 3.68 ± 0.48, respectively). We propose a complete diameter reduction in the subclavian vein during the 180° dynamic maneuver as a diagnostic ultrasound criterion for venous TOS.

In a healthy population, physiological thoracic outflow changes are detected by variations in the diameter and flow velocity of the subclavian vein, the subclavian artery, or both during dynamic maneuvers in different arm positions[3,5,9]. Our study considered normal US duplex Doppler with physiological changes in response to dynamic maneuvers as a decrease in the vessel diameter of 50% or less with variable changes in flow velocity. There was no significant difference in the flow

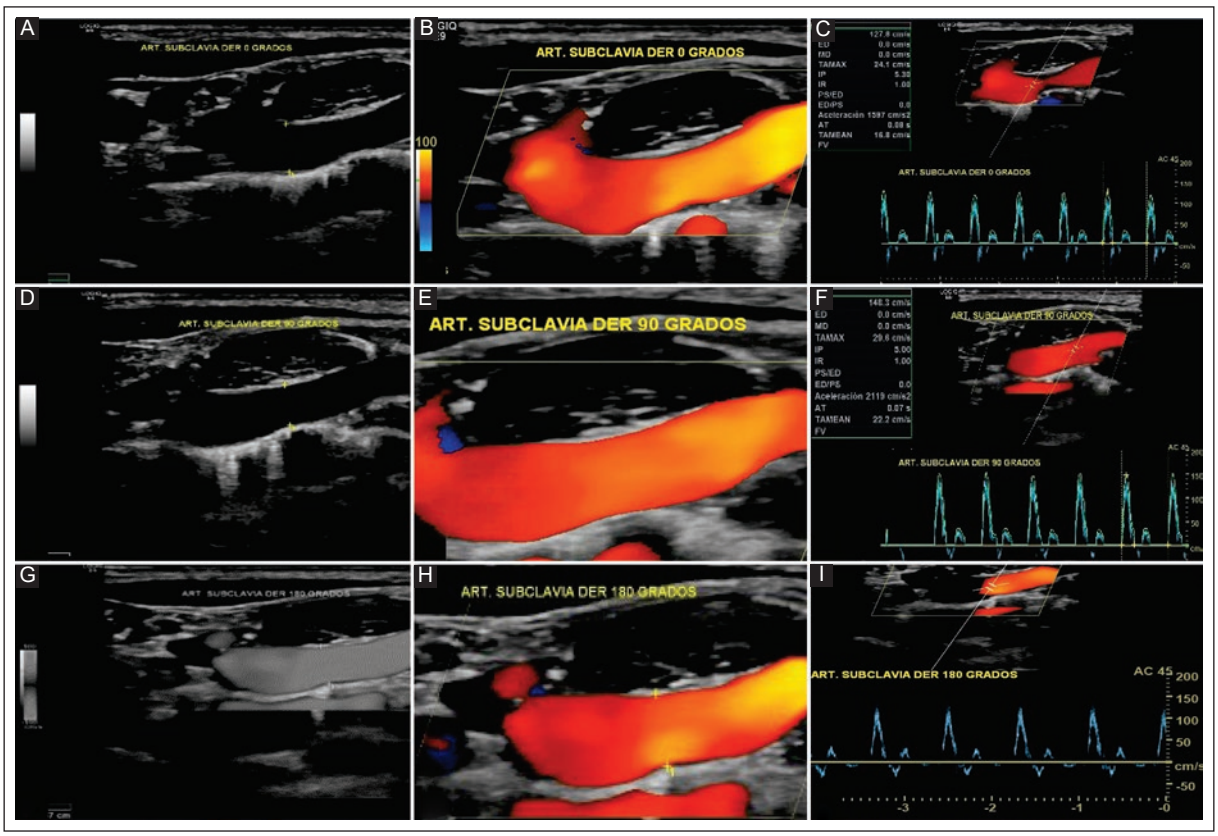

Figure 4. Normal US duplex Doppler of a 31-year-old male patient with dynamic maneuvers showed normal diameter **(A)** patency **(B)**, flow velocity, and spectrum **(C)** in the subclavian artery at 0° **(A, B, C)**, 90° **(D, E, F)**, and 180° **(G, H, I)**, respectively.
US: ultrasound.

velocity of the subclavian vein at 0° between the normal and abnormal US duplex Doppler. Furthermore, the flow velocity at 0°, 90°, and 180° did not change in normal US duplex Doppler. In these cases, symptoms were attributed to neurogenic TOS; in no case was catheter venography recommended. On the other hand, in patients with pure and mixed venous TOS, the flow velocity in the subclavian vein was absent during the dynamic maneuver at 180° ($p < 0.001$). Accordingly, we propose the absence of flow velocity in the subclavian vein with the dynamic 180° maneuver as another diagnostic ultrasound criterion of venous TOS. According to our proposed diagnostic criteria, identification of physiological changes during dynamic US duplex Doppler maneuvers may avoid overestimation of venous TOS.

US duplex Doppler has undergone amazing technological development in the last 30 years. This fact together with a high level of experience of the operator makes US duplex Doppler the primary modality for diagnosing venous TOS. Its limitations are related to a reduced acoustic window that may restrict the acquisition of images in the costoclavicular space in muscular patients or in the presence of abundant adipose tissue[1]. CT with IV contrast or catheter venography are equivalent alternatives for venous TOS diagnosis[2,10]; however, these techniques have disadvantages related to the use of intravenous contrast agents, radiation, and high cost. The latter is a limitation, especially in middle- or low-income countries such as ours. On the other hand, we recommend that catheter venography be performed only in acute thrombosis when fibrinolytic therapy is used. US duplex Doppler is popular because it is a widely available, noninvasive, cost-effective method that does not use ionizing radiation or contrast agents. In our study, US duplex Doppler was used as the primary diagnostic modality in patients with clinical suspicion of vascular TOS. Venous TOS diagnosis based on our proposed ultrasound criteria was established in 79 (81.4%) of 97 cases. In our study population, the diagnosis of pure or mixed venous TOS was confirmed in 4 of 5 cases, which represents a high diagnostic accuracy of US duplex Doppler.

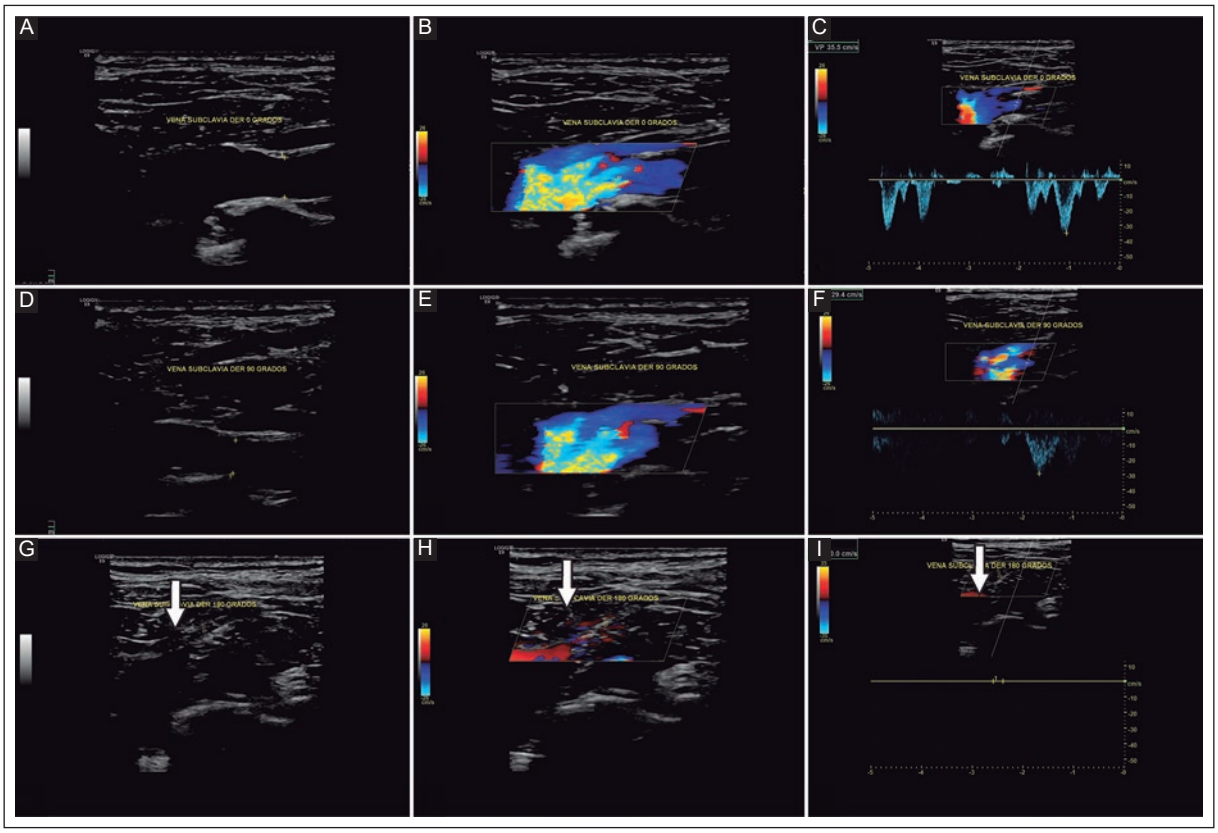

Figure 5. Abnormal US duplex Doppler in a 34-year-old male patient with venous TOS. The subclavian vein was assessed at 0° with a normal diameter **(A)**, patency **(B)**, and flow velocity **(C)**; with dynamic maneuvers at 90°, a decreased diameter **(D)**, patency **(E)**, and flow velocity **(F)** were observed, and at 180° a complete reduction in diameter **(G)** (arrow) absent patency **(H)** (arrow) and flow velocity **(I)** (arrow) were observed.

US: Ultrasound; TOS: thoracic outlet syndrome.

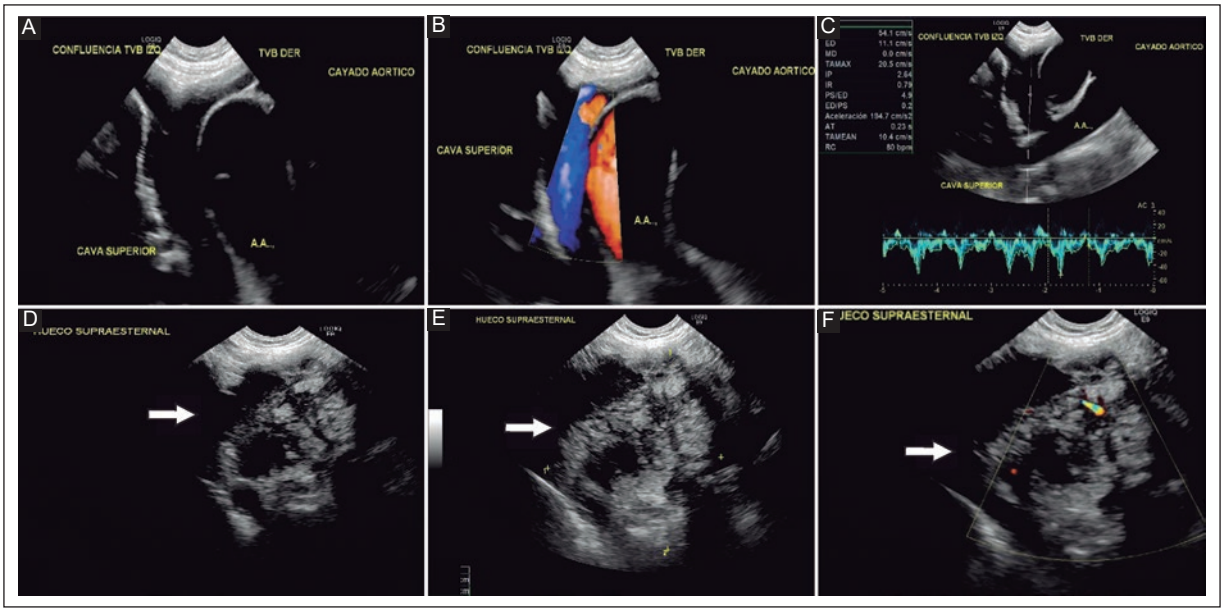

Figure 6. Normal US duplex Doppler in a 36-year-old female patient with a normal diameter **(A)**, patency **(B)**, and flow velocity **(C)** of the superior vena cava with a suprasternal approach. Abnormal Doppler US in a 42-year-old male patient with a solid mass (lymphoma) **(D)** (arrow) of 6.4 cm x 5.9 cm **(E)** (arrow) with intralesional vascularity in the mediastinum **(F)** (arrow) that did not allow identification of the superior vena cava.

US: Ultrasound.

Traditionally, US duplex Doppler examination of the thoracic outlet does not include a description of the superior vena cava diameter, permeability, and flow velocity. Its evaluation in our study, was performed with an endocavitary transducer that provided adequate visualization of the superior vena cava in 96 (99%) of 97 patients. A mean diameter of 15.74 ± 2.28 mm and a mean flow velocity of 45.72 ± 11.32 cm/s were found. No differences were observed between patients with normal and abnormal US duplex Doppler. The superior vena cava was not visualized in only one patient because of severe extrinsic compression by a mediastinal mass diagnosed as lymphoma. We suggest that superior vena cava assessment should be included in the US duplex Doppler of patients with a clinical suspicion of vascular TOS.

Our study has several strengths. The sample size was the largest of patients diagnosed with venous TOS in any study. In addition, the US duplex Doppler examination was performed by the same radiologist in all cases. On the other hand, there were some limitations. The study design was retrospective, and catheter venography, the gold standard, was not performed. The ultrasound criteria proposed for the diagnosis of venous TOS could have limited applicability with less experienced vascular ultrasound operators.

CONCLUSION

We propose two ultrasonographic criteria for diagnosing venous TOS: a complete reduction in the subclavian vein diameter to 0 mm and the absence of flow velocity during a dynamic maneuver at 180°. The accuracy of US duplex Doppler for the diagnosis of venous TOS requires an experienced operator in vascular imaging and a systematic protocol of the thoracic outlet, and time (between 60 and 90 minutes for each thoracic limb). It is possible that, in the coming years, the diagnosis of venous TOS in young adults will increase due to sports activities that cause hypertrophy of the scalene muscle. Other imaging modalities such as CT with IV contrast and catheter venography may be used as equivalent alternatives to US duplex Doppler[2]. Research studies with a prospective design in other populations are needed to apply and validate the proposed US duplex Doppler criteria for diagnosing venous TOS.

Acknowledgments

The authors thank Professor Ana M. Contreras-Navarro for her guidance in preparing and writing this scientific paper.

Funding

Supported with funds from the National Quality Postgraduate Program of the Consejo Nacional of Ciencia and Tecnología of México (Conacyt).

Conflicts of interest

The authors declare that they have no conflicts of interest.

Ethical disclosures

Protection of human and animal subjects. The authors declare that the procedures followed were in accordance with the regulations of the relevant clinical research ethics committee and with those of the Code of Ethics of the World Medical Association (Declaration of Helsinki).

Confidentiality of data. The authors declare that they have followed the protocols of their work center on the publication of patient data.

Right to privacy and informed consent. Approval for analysis of routinely acquired clinical data was obtained from the Ethics Committee and informed consent was not required for this retrospective observational study of information collected during routine clinical care.

REFERENCES

1. Raptis CA, Sridhar S, Thompson RW, Fowler KJ, Bhalla S. Imaging of the Patient with Thoracic Outlet Syndrome. RadioGraphics. 2016;36 (4): 984-1000. doi.org/10.1148/rg.2016150221.
2. Expert Panels on Vascular Imaging, Thoracic Imaging, and Neurological Imaging, Zurkiya O, Ganguli S, Kalva SP, Chung JH, Shah LM, Majdalany BS, et al. ACR Appropriateness Criteria® Thoracic Outlet Syndrome. J Am Coll Radiol. 2020;17(5S): S323-S334. doi: 10.1016/j.jacr.2020.01.029.
3. Chen H, Doornbos N, Williams K, Criado E. Physiologic variations in venous and arterial hemodynamics in response to postural changes at the thoracic outlet in normal volunteers. Ann Vasc Surg. 2014; 28(7):1583-1588. doi.org/10.1016/j.avsg.2014.05.003.
4. Longley DG, Yedlicka J W, Molina EJ, Schwabacher S, Hunter DW, Letourneau JG. Thoracic outlet syndrome: evaluation of the subclavian vessels by color duplex sonography. AJR Am J Radiol. 1992;158 (3):623-630. doi/10.2214/ajr.158.3.1739007.
5. Hamby BA, Ronningen EL, Humphries MD, Freischlag JA. Role of the Noninvasive Vascular Laboratory in Thoracic Outlet Syndrome. In Abu-Rahma AF, Noninvasive Vascular Diagnosis. A Practical Textbook for Clinicians. 4th Edition. West Virginia (USA). © Springer International Publishing AG; 2017:569-577.
6. Gillard J, Pérez-Cousin M, Hachulla É, Remy J, Hurtevent J-F, Vinckier LA, et al. Diagnosing Thoracic Outlet Syndrome: Contribution of Provocative Tests, Ultrasonography, Electrophysiology, and Helical Computed Tomography in 48 Patients. Joint Bone Spine. 2001; 68 (5): 416-424. doi.org/10.1016/s1297-319x (01)00298-6.
7. Li N, Dierks G, Vervaeke HE, Jumonville A, Kaye AD, Myrcik D, et al. Thoracic Outlet Syndrome: A Narrative Review. J Clin Med. 2021;10: 962. doi.org/10.3390/jcm10050962.
8. Baz AA. An overview of the findings of dynamic upper limbs' arterial and venous duplex in cases of vascular thoracic outlet syndrome. Egypt J Radiol Nucl Med. 2019; 50 (76):1-11. doi.org/10.1186/s43055-019-0100-1.
9. Moore R, Lum YW. Venous thoracic outlet syndrome. Vasc Med. 2015; 20(2):182-189. doi.org/10.1177/1358863X14568704.
10. Butros SR, Liu R, Oliveira GR, Ganguli S, Kalva S. Venous compression syndromes: clinical features, imaging findings and management. Br J Radiol. 2013;86:1-11. doi.org/10.1259/bjr.20130284.

JMeXFRI

Journal of the Mexican Federation of Radiology and Imaging

Check for updates

FULL RESEARCH ARTICLE

Image optimization of abdominal and pelvic multislice computed tomography with oral mannitol contrast

Araceli Cue-Castro[1,a], Luis A. Concha-Rebollar[2], Dante R. Casale-Menier[3], and Rosa M. Alanis-Salazar[4]*

[1]Head of Computed Tomography Department "Dr. Enrique Cabrera" General Hospital, Secretaría de Salud de la Ciudad de México (SEDESA), Mexico City; [2]Magnetic Resonance Imaging Department, Angeles Lomas Hospital, Huixquilucan, State of Mexico; [3]Department of Diagnostic and Therapeutic Imaging, Angeles Hospital, Ciudad Juarez, Chihuahua; [4]Department of Radiology, Clínica de Medicina Familiar Guadalupe, Instituto de Seguridad y Servicios Sociales de los Trabajadores del Estado (ISSSTE), Monterrey, Nuevo Leon. Mexico

[a]0000-0003-2935-7305

ABSTRACT

Introduction: *Oral mannitol has been used as gastrontestinal (GI) tract contrast mainly for enterography. There is no report on which oral contrast agent is more suitable to optimize multiplanar reconstruction in abdominal and pelvic multislice computed tomography (MSCT), considering that GI tract distension is critical for image analysis. The aims of this study were to (1) evaluate the qualitative and quantitative luminal distension of the entire GI tract in abdominal and pelvic (MSCT) with oral mannitol contrast in patients with related and unrelated GI pathologies, and (2) define the usefulness of oral mannitol in tomographic reconstructions.* **Material and methods:** *This retrospective cohort study included patients with related and unrelated GI tract pathologies. Oral mannitol (2.5%), 100 ml in 900 ml of water, was administered with 30- or 120-minutes waiting period before performing the MSCT scan in a 16-slice CT scanner. Qualitative luminal distension was classified as fair, adequate, or excellent. Multiplanar (MPR), maximum intensity projection (MIP), and volume rendering (3D) reconstructions were obtained.* **Results:** *Ninety-one patients with an MSCT of the abdomen and pelvis with oral mannitol were included. GI distension was fair in 17 (18.6%) cases, adequate in 24 (26.3%) and excellent in 50 (54.8%). Optimized tomographic reconstructions without artifacts allowed integral evaluation of the GI tract and viscera and revealed incidental findings.* **Conclusion:** *We found adequate to excellent luminal distension in 80% of cases using oral mannitol as a contrast agent in MSCT with reconstructions of diagnostic quality of the abdomen, pelvis, and retroperitoneum. This study is the first in Mexico to consider distension in the context of optimized imaging.*

Keywords: *Mannitol. Oral contrast agent. Multislice computed tomography. Qualitative assessment. Quantitative assessment. Gastrointestinal tract. Multiplanar reconstruction.*

INTRODUCTION

Oral contrast is a critical factor to accurately detect abdominal and pelvic pathology on multislice computed tomography (MSCT). It allows assessment of intestinal distension and visibility of the gastrointestinal (GI) wall. An oral contrast agent can be positive (iodine or barium), negative (air), or neutral (water, milk, polyethylene glycol, meglumine, sorbitol, lactulose, xanthine gum, or mannitol)[1-7]. Conventional iodine or barium preparations have the disadvantages of artifacts and decreased or absent detection of the intrinsic wall, vascular, and calcic lesions[1,2]. Neutral oral contrast agents allow assessment of the intestine and its vessels for accurate diagnosis of vascular, inflammatory, or neoplastic pathologies. There is a commercial preparation on the market that combines sorbitol and barium (VoLumen™)

Corresponding author:
*Araceli Cue-Castro
E-mail: arabicho@hotmail.com

Received for publication: 29-10-2021
Approved for publication: 06-12-2021
DOI: 10.24875/JMEXFRI.M21000003

Available online: 31-03-2022
J Mex Fed Radiol Imaging. 2022;1(1):32-41
www.JMeXFRI.com

and another that contains sorbitol, mannitol, and xanthine gum (Breeza™). These products have limited availability in Latin America and cost more than 7 USD per unit.

Several studies have suggested mannitol as an optimal oral contrast agent for adequate imaging with small and large bowel distention, and wall delimitation[1-4,7,8]. Mannitol is inexpensive and well-tolerated with minimal side effects[1,2,6]. Advanced tomography systems and modern workstations mainly used for enterography allow multiplanar (MPR), maximum intensity projection (MIP), and volume rendering (3D) reconstructions. Optimized images are defined as high multiplanar resolution, artifact-free with adequate or excellent GI distension. Oral positive contrast agents interfere or these reconstructions whereas oral mannitol does not produce artifacts with image degradation[2-4,7,9].

There is no consensus regarding mannitol as an oral contrast agent in abdominal and pelvic MSCT scans. Considering that GI tract distention is critical for image analysis in multiplanar reconstruction, this study aimed to (1) evaluate the qualitative and quantitative distention of the entire GI tract on abdominal and pelvic MSCT scan with oral mannitol as a contrast agent in patients with related and unrelated GI pathologies, and (2) define the usefulness of oral mannitol as contrast agent in MPR, MIP, and volume rendering reconstructions to optimize images.

MATERIAL AND METHODS

This retrospective cohort study was conducted from January to June 2017 in the Computed Tomography Department of the "Dr. Enrique Cabrera" General Hospital in Mexico City, Mexico. Patients with related and unrelated GI pathologies consecutively referred by different clinical-surgical services for MSCT of the abdomen and pelvis were included. Medical requests with insufficient information or intolerance to oral administration were non-inclusion criteria. Lack of cooperation for the MSCT scan, and technically inadequate imaging studies were elimination criteria. The study protocol and retrospective analysis of radiographic data obtained during routine medical care were approved by the institutional ethics and research committees

Age, sex, and clinical diagnoses were recorded. The latter were classified as pancreas pathology (inflammation, sequelae, or neoplasia), stomach, liver, gallbladder, biliary tract, and pelvic or retroperitoneal pathologies such as a tumor, uterine fibroids, and other causes (cervical cancer, inflammatory or traumatic processes). Tomographic findings were described by anatomic region and pathology related to the clinical diagnosis or detected incidentally. Tolerability of the oral mannitol preparation and side effects such as diarrhea, nausea, and/or vomiting were also recorded.

Preparation and administration of mannitol

Upper abdominal MSCT was performed in patients with a clinical diagnosis related to the upper GI tract, biliary tract, or biliary-pancreatic junction and full-length abdominal and pelvic MSCT was performed in patients with a clinical diagnosis of lower GI tract, retroperitoneum, or pelvis pathology. Mannitol 2.5% (100 ml) was diluted in 900 ml of water, it was administered during a period of 40-60 minutes. For upper abdominal exploration, the transit period before acquiring tomographic images was 30 minutes (30-min) and for the full-length abdomen and pelvis MSCT was 120 minutes (120-min). With the patient lying on the CT examination table, 100 ml of the same solution was administered orally.

MSCT image acquisition protocol

All MSCT scans were performed using a 16-slice Neusoft ™ tomograph (Neusoft Medical Systems Co, Ltd., Shenyang, China) with a Stellant ™ dual-head automatic injector (Medrad Inc., Warrendale, PA. USA). An average of 80 ml of the intravenous contrast agent, Optiray™ 350 (organically bound iodine 350 mg/mL/ioversol injection 74%. Mallinckrodt, Damastown, Ireland), was administered at an injection rate of 99 milliliters/second with a 3.5 caudal in a 15-second period. MPR reconstructions were performed in all cases, and MIP and volume rendering reconstructions were performed when the radiologist identified incidental findings, vascular lesions, or anatomic localization of structures was difficult. Images were sent to a PACS (Picture Archiving and Communication System) (Carestream™, Rochester, NY, USA).

Qualitative assessment of distension

A radiologist (ACC) with 20 years of experience who knew the period of administration and transit of the oral mannitol preparation performed the assessment. Three categories of distension were defined: fair when the GI tract segments were collapsed; adequate, when there was distension that allowed the segment to be

distinguished from other structures; and excellent, when, in addition to the maximum physiological intraluminal distance, it was possible to identify the intestinal wall anatomy. The quality of the images acquired lacked artifacts or blacked out calcifications.

Quantitative assessment of wall thickness and distension

Measurements were made at the points of maximum physiological distension of the different segments of the digestive tract: from the *incisura angularis* to the greater curvature of the stomach; in the duodenum, in the second portion that corresponds to the anatomical region of the ampulla of Vater; in the jejunum, in the upper left quadrant; in the ileum, in the lower right quadrant; and in the colon, in the cecum and splenic angle. All measurements were made in the axial axis. The physiologic distension of the stomach is variable; for the small intestine, it is 30 mm, the cecum is 90 mm, and for the rest of the colon, 60 mm. The wall thickness of each segment was measured in millimeters from the inner to the outer edge.

Statistical analysis

The qualitative evaluation of the distension of the different segments of the GI tract was analyzed using the Chi-square test and Fisher's exact test. Quantitative assessment of distension and wall thickness was analyzed with Student's *t*-test and the Mann-Whitney U test. The mean, standard deviation, minimum, median, and maximum of the quantitative variables were calculated, and the statistical significance between the categories of qualitative variables was a p-value <0.05. The IBM-SPSS statistical program (version 20.0, IBM Corp., Armonk, NY, USA) was used.

Table 1. Clinical diagnoses of related and unrelated GI tract pathologies referred for abdominal and pelvic MSCT scan with the oral mannitol contrast agent

Description	Related GI tract pathologies[a] (n = 61)
Pancreatic pathology (inflammation, sequelae, or neoplasia), n	23
Gallbladder and bile duct pathology, n	12
Hepatic pathology, n	7
Gastric pathology, n	5
Other, n	14
Description	**Unrelated GI tract pathologies[b] (n = 30)**
Pelvic tumor, n	2
Adrenal Tumor, n	6
Uterine fibroids, n	3
Retroperitoneal pathology , n	11
Other causes (CC, inflammatory or traumatic processes), n	8

GI: Gastrointestinal; MSCT: Multislice computed tomography; CC: Cervical cancer. [a]Upper and lower GI pathologies; [b]Pelvic, vascular, or retroperitoneal pathologies.

Table 2. Transit period between oral mannitol contrast agent intake and acquisition of abdominal and pelvic MSCT scan in related and unrelated GI tract pathologies

Transit period	Related GI tract pathologies[a]	Unrelated GI tract pathologies[b]	Total
	(n = 60)	(n = 31)	(n = 91)
30-min, n (%)	37 (61.7)	2 (6.5)	39 (42.9)
120-min, n (%)	23 (38.3)	29 (93.5)	52 (57.1)

MSCT: Multislice computed tomography; GI; Gastrointestinal; min: minutes; [a]Upper and lower GI pathologies; [b]Pelvic, vascular, or retroperitoneal pathologies.

RESULTS

Ninety-five abdominal and pelvic MSCT scans were performed with oral mannitol and intravenous iodinated contrast medium. Ninety-one patients with a mean age of 44.2 ± 18.8 years (range, 6 to 88) were included; 56 were women and 35 men. Four patients were excluded because of diarrhea without an electrolyte imbalance (n = 2), rejection of the mannitol preparation (n = 1), and lack of cooperation (n = 1). The tolerability of oral mannitol was adequate. Some patients reported intestinal cramps without the need for an antispasmodic. The related (n = 61, 67%) and unrelated (n = 30, 33%) GI tract pathologies based on clinical diagnoses are shown in Table 1. The 30-min or 120-min transit period between oral mannitol contrast agent intake and the abdominal and pelvic MSCT scan in related and unrelated GI tract pathologies are shown on Table 2.

Qualitative evaluation of distension

The distension of the different GI tract segments on abdominal and pelvic MSCT with the oral mannitol contrast agent was adequate in 24 (26.3%) and excellent

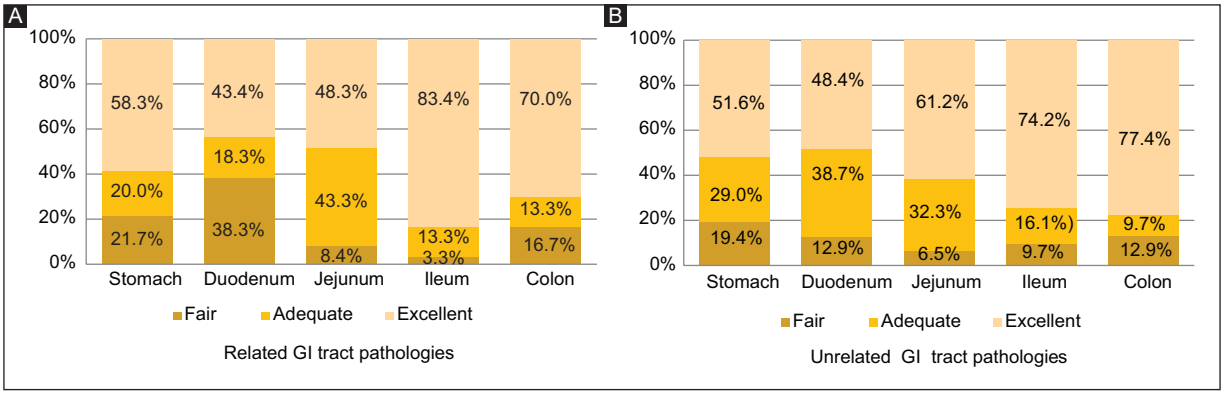

Figure 1. Qualitative evaluation of distension in different GI tract segments in MSCT of the abdomen and pelvis with oral mannitol contrast; **(A)** pathologies related to the GI tract (upper and lower). **(B)** pathologies not related to the GI tract (pelvic, vascular, or retroperitoneal pathologies).

GI: Gastrointestinal; MSCT: Multislice computed tomography.

in 50 (54.8%) of 91 patients. In contrast, in 17 (18.6%) cases, it was fair. The adequate to excellent distension of the different segments was comparable between related (Figure 1A) and unrelated GI tract conditions (Figure 1B): the stomach (78.3% and 80.6%), duodenum (61.6% and 87.1%), jejunum (91.6% and 93.6%), ileum (96.6% and 90.3%) and colon (83.3% and 87.1%), respectively.

Abdominal CT scan with oral mannitol and intravenous contrast is shown in Figure 2 with normal gastric wall with distension in all segments, distended jejunum with normal folds, MIP reconstruction of omental vascularity, and the arterial image of the mesentery irrigation with multiplanar resolution and artifact-free.

In the various segments of the small intestine and up to the splenic angle of the colon, adequate or excellent distension was observed with oral mannitol in the MSCT scan at 30- and 120-min (Figure 3); in 15 (28.8%) of 52 cases, distension was observed up to the sigmoid. Figure 4 images, from another facility, shows abdomen and pelvis MSCT scans referred as an appendicular plastron in the right iliac fossa. The same patient on a second MSCT with oral mannitol contrast shows bowel loops with normal features in the right iliac fossa; thus, the appendicular pathology was excluded.

Optimized images with an oral mannitol contrast agent allowed the assessment of vascular structures and the detection of incidental findings in MPR, MIP, and volume rendering reconstructions. Axial and coronal sections of the MSCT scan with the oral mannitol and intravenous iodine contrast agents showed altered

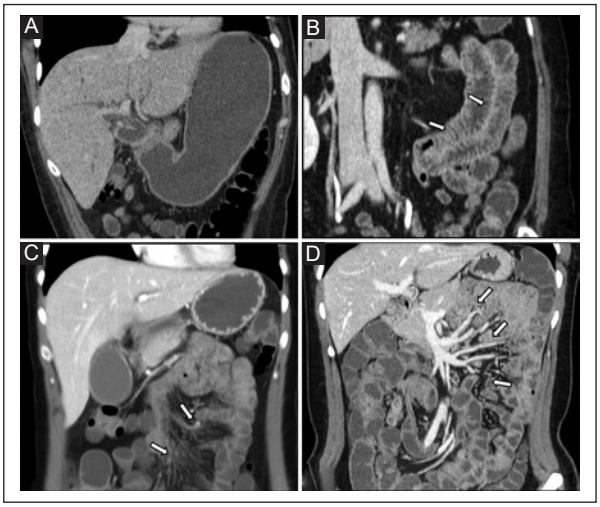

Figure 2. Abdominal MSCT with oral mannitol contrast and intravenous iodine contrast; coronal MPR reconstructions showing upper GI tract distension. **(A)** normal stomach with mannitol, distended in all segments. **(B)** distended jejunum with normal folds (arrows). **(C)** MIP reconstruction of omental vascularity (arrows) and **(D)** arterial image of mesenteric irrigation (arrows).

GI: Gastrointestinal; MSCT: Multislice computed tomography; MPR: Multiparametric reconstruction; MIP: Maximum intensity projection.

vascular structures, collateral circulation, and the presence of hemorrhage. Figure 5 shows an iliac aneurysm, abnormal irrigation of a pelvic tumor, and intraperitoneal hemorrhage of uterine origin. Figure 6 shows reconstructions demonstrating distended duodenum and hypodense lithiasis in the ampulla of Vater with dilatation of the bile ducts.

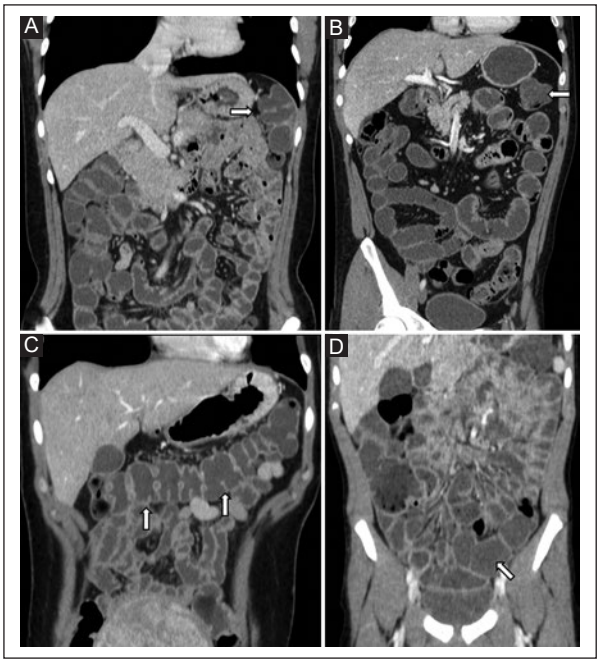

Figure 3. Abdominal MSCT with oral mannitol contrast and intravenous iodine contrast with coronal MPR reconstructions with imaging at 30 **(A)** and 120 minutes **(B, C, D)** showing distension in the different segments **(A, B)**, transit to the splenic angle (arrows); **(C)** transverse mesocolon (arrows), and **(D)** sigmoid in a pediatric patient (arrow).

MSCT: Multislice computed tomography; MPR: Multiparametric reconstruction.

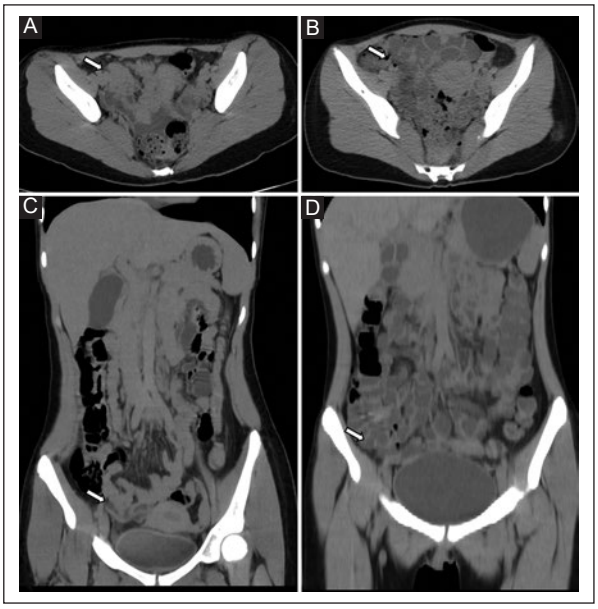

Figure 4. Simple abdominal MSCT with axial sections and coronal MPR reconstructions in simple phase **(A, C)** without oral mannitol contrast; **(B, D)** with oral mannitol contrast; **(A, C)** images show a previous study referred from another facility as a plastron "in the right iliac fossa" (arrow); **(B, D)** a control study with distended intestinal loops shows normal features.

MSCT: Multislice computed tomography; MPR: Multiparametric reconstruction.

Quantitative evaluation of distension and wall thickness

The distension and wall thickness of the different segments of the GI tract on MSCT of the abdomen and pelvis with oral mannitol are shown in Table 3 with comparable mean and median values. Distension was observed within physiological parameters; a mean value of 53.03 mm (± 2.65 SD) in the stomach, 19.61 mm (± 0.87 SD) in the duodenum, 18.62 mm (± 0.59 SD) in the jejunum, 17.25 mm (± 059 SD) in the ileum, and 32.09 mm (± 1.12 SD) in the colon, which allowed delineation of the different segments according to their characteristics and anatomic course (Table 3)(Figure 7A). The mean wall thickness for each segment was within normal anatomical parameters: 5.83 mm (± 0.52 SD) in the stomach, 2.89 mm (± 0.12 SD) in the duodenum, 2.84 mm (+ 0.15 SD) in the jejunum, 2.04 mm (± 0.06 SD) in the ileum and 2.09 (± 0.09 SD) in the colon (Table 3) (Figure 7B). Abnormal values of gastric wall thickness (Figure 8) were observed in various pathologies of the stomach (n = 5), extrahepatic bile ducts (n = 5), pancreas (n = 4), intraabdominal abscesses (n = 3), and causes unrelated to the upper abdomen (n = 4). Acquiring a simple tomographic phase with the oral mannitol contrast also allowed us to identify lithiasis and hemorrhage.

DISCUSSION

The use of mannitol as a neutral oral contrast agent in MSCT of the abdomen and pelvis demonstrated adequate to excellent distension of the GI tract in 80% of cases in our study. Optimized MPR, MIP, and volume rendering reconstructions were obtained artifact-free without image degradation to diagnose abdominopelvic and retroperitoneal pathology and identify incidental findings. This study is the first in Mexico that consider distension in the context of optimized imaging.

Better image quality and distention of the GI tract have been reported using oral mannitol compared to a positive oral contrast agent in MSCT enterography scans[1-4,7-10]. Elamparidhi et al.[4] in a quasi-experimental study of 75 patients, divided into three groups receiving oral contrast with mannitol (n = 25), iodine (n = 25), or water (n = 25), showed excellent distension in 13 (52%)

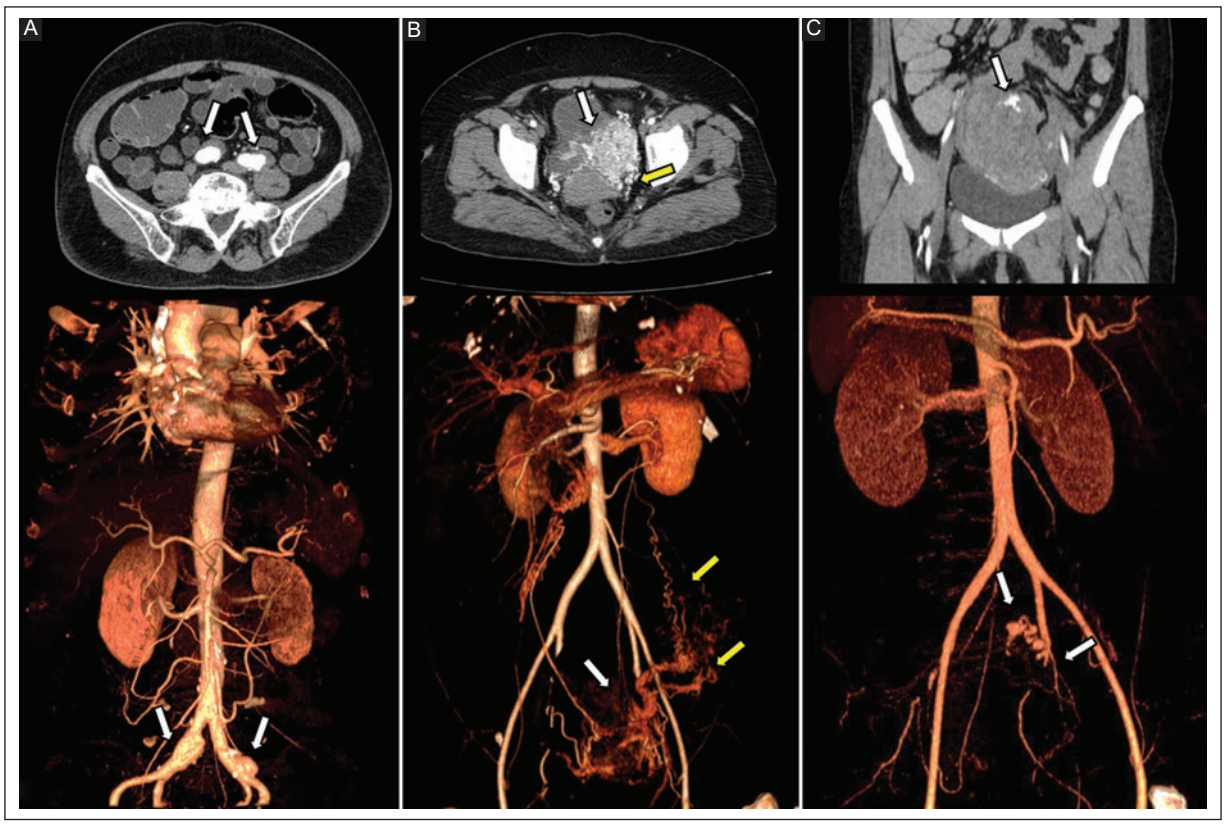

Figure 5. Abdominal and pelvic MSCT scan with intravenous (iodine) and oral mannitol contrast with axial **(A, B)** and sagittal **(C)** MPR views with corresponding volumetric reconstructions showing distension of the digestive tract that does not affect the quality of the vascular volumetric reconstruction; **(A)** Bilateral iliac aneurysm (arrows); **(B)** highly vascularized left parametrial tumor (arrow) with evidence of irrigation of the tumor by anomalous vessels (yellow arrows); **(C)** active subserosal hemorrhage after instrumented uterine curettage (arrows).

MSCT: Multislice computed tomography; MPR: Multiparametric reconstruction.

of 25 abdominal CT scans with oral mannitol, whereas only one case (4%) with iodine and none with water. In the evaluation by segments, except for the third portion of the duodenum, distension was better in the mannitol group than with iodine or water. Berther et al.[3] studied 200 patients with oncologic diseases, medical emergencies, and surgical evaluations (preoperative and postoperative) randomized into two groups that received mannitol (n = 100) or iodine (n = 100) as an oral contrast agent for MSCT enterography. Image quality and distension of the various segments of the GI tract, except the stomach, were significantly better in the oral mannitol group; however, assessment of the colon was not included. In our study, which included 91 patients with related and unrelated pathologies of the GI tract with MSCT of the abdomen and pelvis with an oral mannitol contrast agent, adequate distension was observed in 24 (26.3%) cases and excellent distension in 50 (54.8%) in the different GI tract segments. The use of oral mannitol in abdominal MSCT resulted in image optimization.

Abdominal and pelvic MSCT with a 120-min waiting period between oral mannitol administration and image acquisition allows complete assessment of the colon segments, pelvic and retroperitoneal structures without additional rectal contrast administration. In an experimental study by Prakashini et al.[2] of 300 patients randomly divided into three groups receiving oral mannitol (n = 100), iodine (n = 100), or water (n = 100) and evaluated with MSCT of the abdomen and pelvis, adequate distension and visualization of the haustrum of the various colon segments were observed in 61% of cases in the mannitol group without additional rectal contrast administration. This finding was not observed in the water or iodine groups. In our study with an oral mannitol contrast agent, distension of the different colonic segments was adequate to excellent in 49 (80%) of 61 patients with related GI pathologies and 22 (73.3%)

Table 3. Distension and wall thickness of GI tract segments in MSCT of the abdomen and pelvis with an oral mannitol contrast agent

Segment	Distension (mm), mean ± SD (min, median, max)	Wall thickness (mm), mean ± SD (min, median, max)
Stomach	53.03 ± 2.65 (5.60, 55.77, 98.00)	5.83 ± 0.52 (0.68, 3.42, 20.90)
Duodenum	19.61 ± 0.87 (2.00, 18.68, 38.40)	2.89 ± 0.12 (1.30, 2.66, 6.60)
Jejunum	18.62 ± 0.59 (3.80, 18.16, 33.00)	2.84 ± 0.15 (0.66, 2.50, 8.20)
Ileum	17.25 ± 0.59 (2.60, 16.64, 48.00)	2.04 ± 0.06 (0.70, 2.00, 4.00)
Colon	32.09 ± 1.12 (2.00, 32.10, 50.70)	2.09 ± 0.09 (0.90, 1.92, 5.40)

GI: Gastrointestinal; MSCT: Multislice computed tomography.

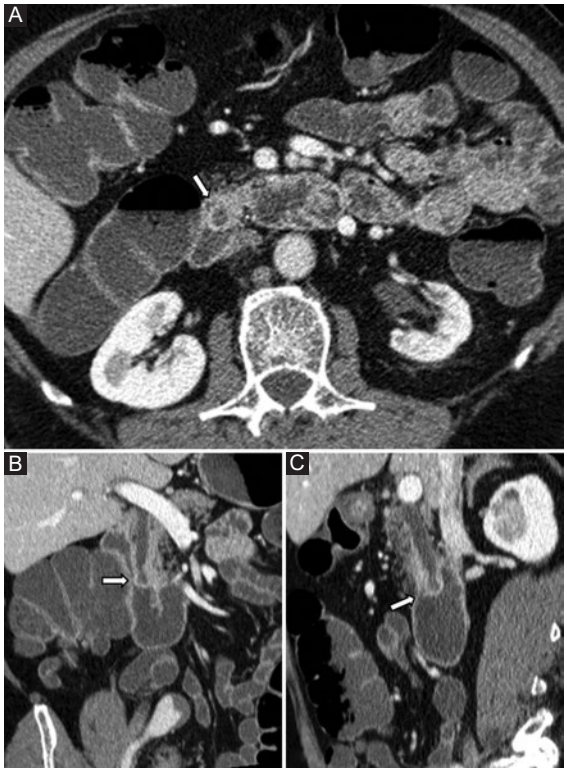

Figure 6. Abdominal MSCT scan with intravenous iodine and oral mannitol contrast. It shows an axial view **(A)**, a coronal curved MPR reconstruction **(B)**, and a sagittal image **(C)** showing distension of the duodenum, allowing detection of choledochal ectasia by the presence of fat-rich density lithiasis in the ampulla of Vater (arrows).

MSCT: Multislice computed tomography; MPR: Multiparametric reconstruction.

of 30 cases with unrelated GI pathologies in the group with a 120-min waiting period between mannitol intake and image acquisition. The high osmolarity of mannitol prevents its absorption in the GI tract; thus, visualization of distal segments is achieved. Water absorption in the proximal segments limits distal distension[3,11]. On the other hand, iodine causes heterogeneous dilution in the distal segments and artifacts, so adequate distension is not achieved, and visualization of the vascular structures is impaired. In our study, the previous clinical diagnosis knowledge allowed us to adequately indicate a 30-min waiting period for the upper abdomen or a 120-min transit period for the abdomen and pelvis, between the intake of oral mannitol and the acquisition of images of the MSCT in related and unrelated GI tract pathologies.

Several studies have shown that oral mannitol in abdominal and pelvic MSCT scans has advantages over oral positive contrast (iodine) in evaluating abdominal and pelvic pathologies[2,3,4]. Oral positive contrast is not useful in acute GI bleeding, characterization of folds, vascular reconstruction, urinary lithiasis,[12] choledochal lithiasis, or tumors of the ampulla of Vater. It also interferes with MPR, MIP, and volume rendering reconstructions, which may be necessary for better surgical planning[1]. Due to its similar attenuation to GI secretions, mannitol does not interfere with any type of reconstruction and does not produce artifacts.[3] We found optimal visualization of vascular structures with distension of all GI tract segments, including the colon. The use of oral mannitol in abdominal and pelvic MSCT scans allowed detection of incidental findings such as altered vascular structures, collateral circulation, hemorrhage, iliac aneurysms, abnormal irrigation of pelvic tumors, and intraperitoneal hemorrhage of uterine origin, as well as lithiasis of the ampulla of Vater. MPR reconstructions of MSCT images of the abdomen and pelvis with oral mannitol allow assessment of the course of the segment of interest and areas that are difficult to diagnose in the absence of distension (the duodenum and ileocecal

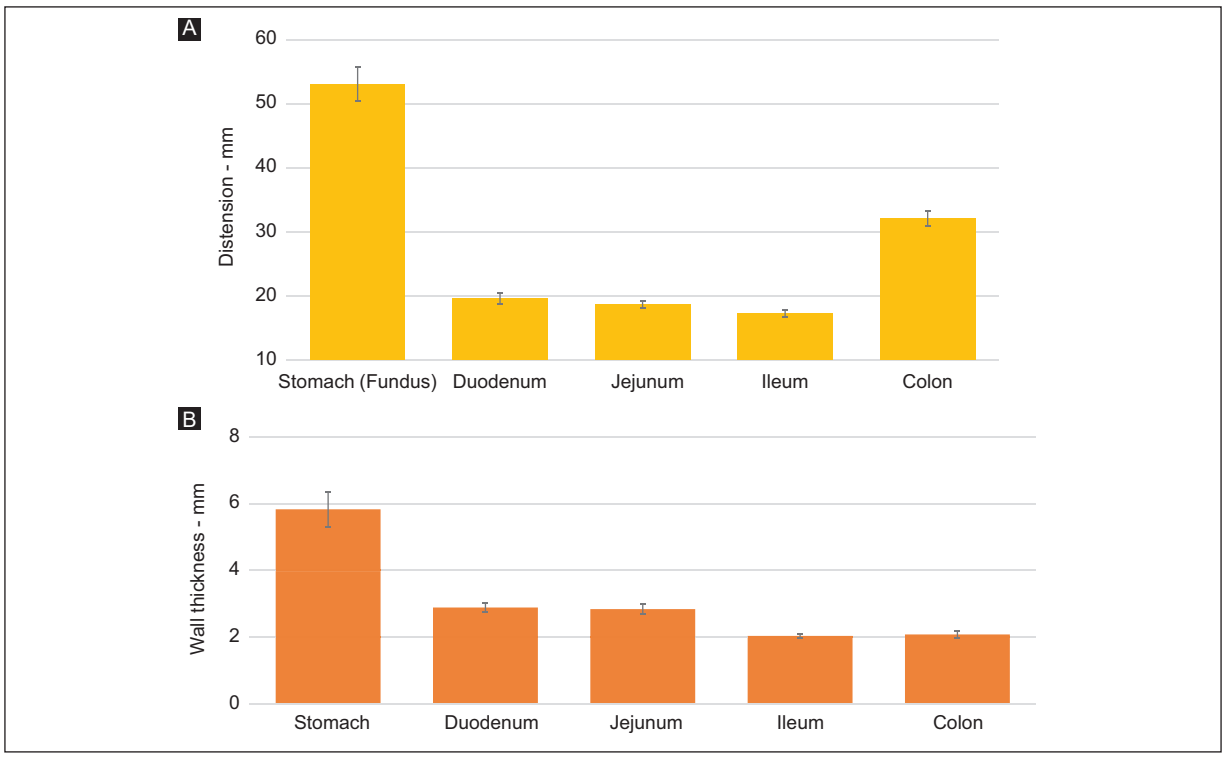

Figure 7. Quantitative evaluation of the different segments of the digestive tract in the abdomen and pelvis MSCT with oral mannitol; **A)** distension (mm) of the segment. **B)** thickness (mm) of the intestinal wall.

MSCT: Multislice computed tomography.

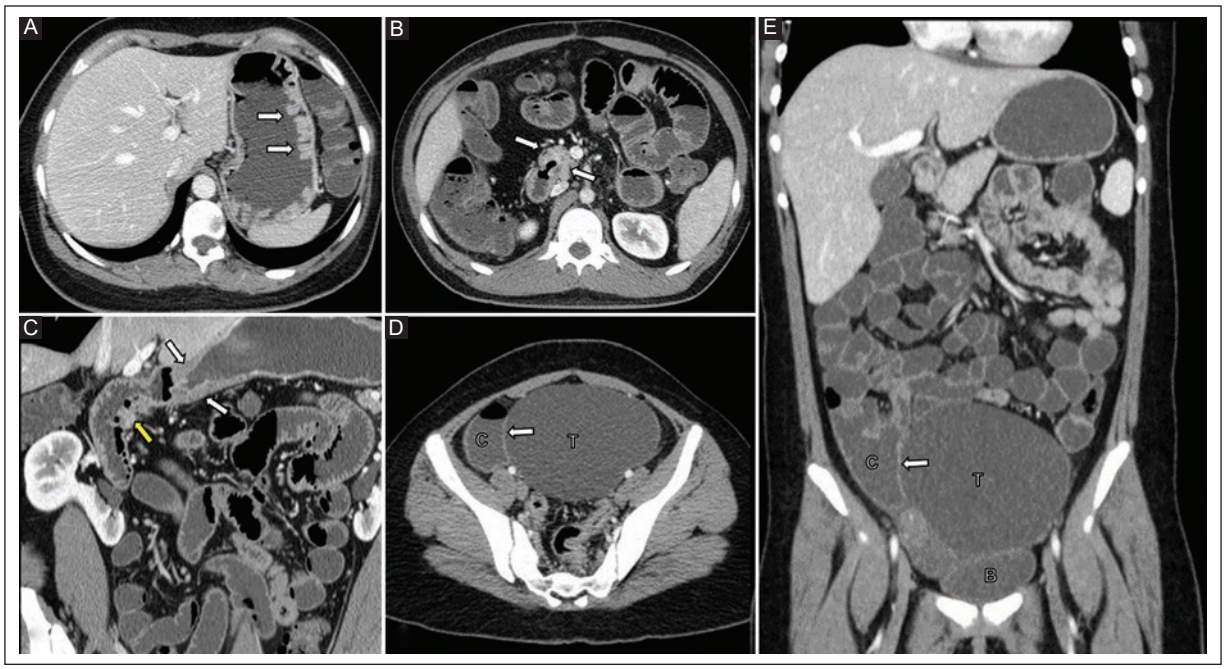

Figure 8. Abdominal MSCT with intravenous iodine contrast and oral mannitol contrast with axial sections **(A, B)** and coronal curved MPR reconstruction **(C)**; axial and coronal sections **(D, E)**; **(A)** distended stomach with abnormal thickening of the folds (arrows); **(B)** second portion of the duodenum with asymmetric concentric thickening of the wall (arrows); **(C)** thickened antral wall (arrows) and thickening of the duodenal folds (yellow arrow); **(D, E)** completely distended GI tract and cystic tumor of the right adnexa (T). The wall of the tumor (arrow) is differentiated from the cecum **(C)** and bladder **(B)**.

GI: Gastrointestinal; MSCT: Multislice computed tomography; MPR: Multiparametric reconstruction.

valve)[2,4,7]. In our study, the curved MPR reconstructions of the gastric antrum and duodenal arch were of optimal quality. Choledochal dilatation was detected secondary to the presence of lithiasis in the ampulla of Vater. We also found incidental iliac aneurysms in a 71-year-old man and an aortic aneurysm in another 76-year-old man. In patients with a 120-min waiting period, image acquisition was performed in the arterial or equilibrium phase, and it was possible to distinguish normal loops from adnexal cystic lesions. The use of oral mannitol in abdominal and pelvic CT scans allows obtaining optimized diagnostic images without artifacts. In addition, oral mannitol improves the definition of abdominal, pelvic, and retroperitoneal structures and the detection of incidental findings.

The study has several strengths. Patients with a wide range of ages with related and unrelated GI pathologies were included; the oral mannitol contrast preparation was well tolerated by patients. Furthermore, in cases with incidental findings, it was possible to perform additional MPR, MIP, and volume rendering reconstructions of the abdomen and pelvis focused on specific pathologies. A limitation was the study design, which did not include a comparison group with positive oral contrast or water. Also, the evaluation of tomographic findings was not blinded, and interobserver agreement of tomographic findings was not assessed.

CONCLUSION

In our study, oral mannitol as a neutral contrast agent in abdominal and pelvic MSCT showed adequate to excellent distension of the GI tract in four of five cases. Differentiation of the GI tract wall to the lumen, adjacent and vascular structures were observed in related and unrelated GI pathologies and pelvic or retroperitoneal pathologies. The use of oral mannitol as a contrast agent in MSCT resulted in image optimization with diagnostic quality. A longer waiting period before image acquisition, including oral mannitol intake and a transit period of 30-min to 120-min, should be considered to achieve adequate passage of the oral contrast agent into the rectal ampulla and to avoid the administration of an additional rectal contrast agent. To achieve proper cooperation, the patient should know the length of the preparation and imaging acquisition times in advance. Currently, a clinical trial is being developed with a 30- to 60-min transit period for MSCT images of the abdomen and pelvis. Preliminary results have shown that oral mannitol adequately reaches the distal portions of the colon. We recommend using oral mannitol as a contrast agent for abdominal and pelvic MSCT scans in related and unrelated GI pathologies with a clinical radiology approach that is part of the Mexican School of Radiology profile. Clinical trials with larger study populations with blinded assessment and interobserver concordance of abdominal and pelvic MSCT scans with oral mannitol contrast agent are needed.

Acknowledgments

The authors thank Professor Ana M. Contreras-Navarro for her guidance in the preparation and writing of this scientific article; Engineer Rogelio Troyo Sanroman for his data analysis, Dulce Ruby López-Trujano R.T. and J. Osvaldo Alvarado-Mondragon R.T for their dedicated work in the acquisition of the MSCT scans, Yenny A. Lopez-Paulino R.N. for her care in the preparation of patients and monitoring during the MSCT scans and Rocio Velazco-Martinez for her diligent data gathering, organizing and storing.

Funding

This research received no external funding.

Conflicts of interest

The authors declare no conflicts of interest.

Ethical disclosures

Protection of human and animal subjects. The authors declare that the procedures followed were in accordance with the regulations of the relevant clinical research ethics committee and with those of the Code of Ethics of the World Medical Association (Declaration of Helsinki).

Confidentiality of data. The authors declare that they have followed the protocols of their work center on the publication of patient data.

Right to privacy and informed consent. Informed consent was not required for this retrospective study of information collected during routine clinical care and ethics approval for analysis was obtained from the Ethics Committee.

REFERENCES

1. Vikram N, Rahalkar AM, Rahalkar M, Halkude A, Rana P, Khopade P. Comparison of mannitol and meglumine diatrizoate for stomach and small bowel wall study by computed tomography, a prospective study. Int J Contemp Med Surg Radiol. 2019;4(3): C162-C167. doi.org/10.21276/ijcmsr.2019.4.3.35.

2. Prakashini K, Kakkar C, Sambhaji C, Shetty CM, Rao VR. Quantitative and qualitative bowel analysis using mannitol, water and iodine-based endoluminal contrast agent on 64-row detector CT. Indian J Radiol Imaging. 2013;23(4):373-378. doi.org/10.4103/0971-3026.125594.
3. Berther R, Patak MA, Eckhardt B, Ertuk SM, Zollikofer CL. Comparison of neutral oral contrast versus positive oral contrast medium in abdominal multidetector CT. Eur Radiol. 2008;18 (9):1902-1909. doi.org/10.1007/s00330-008-0958-1.
4. Elamparidhi P, Sivaranjanie S, Kumar R, Sibhithran R, Kumar A. Comparison of water, Mannitol and Positive Oral Contrast for Evaluation of Bowel by Computed Tomography. Int J Anat Radiol Surg. 2017;6 (4): RO13-RO17. doi.org/10.7860/IJARS/2017/29481:2316.
5. Badawood A, Alsioufi N, Fathuddin S, Mishah N, Jastaniah S. Utilization of milk as an oral contrast agent in CT scan of the abdomen. Adv Comput Tomogr. 2015;4(3):33-41. doi.org/10.4236/act.2015.43005.
6. Koo CW, Shah-Patel LR, Baer JW, Frager DH. Cost-effectiveness and patient tolerance of low-attenuation oral contrast material: milk versus VoLumen. AJR. 2008;190(5):1307-1313. doi.org/10.2214/AJR.07.3193.
7. Wong J, Moore H, Roger M, McKee C. CT enterography: Mannitol versus VoLumen. J Med Imaging Radiat Oncol. 2016;60(5):593-598. doi.org/10.1111/1754-9485.12486.
8. Deepak P, Pundi KN, Bruining DH, Fidler JL, Barlow JM, Hansel SL, et al. Multiphase computed tomographic enterography: diagnostic yield and efficacy in patients with suspected small bowel bleeding. Mayo Clin Proc Innov Qual Out. 2019;3(4):438-447. https://doi.org/10.1016/j.mayocpiqo.2019.09.001
9. Ilangovan R, Burling D, George A, Gupta A, Marshall M, Taylor SA. CT enterography: review of technique and practical tips. Br J Radiol. 2012; 85: 876-886. doi.org/10.1259/bjr/27973476.
10. Zhang LH, Zhang SZ, Hu HJ, Gao M, Zhang M, Cao Q, et al. Multi-detector CT enterography with iso-osmotic mannitol as oral contrast for detecting small bowel disease. World J Gastroenterol. 2005;11(15):2324-2232. doi.org/10.3748/wjg.v11.i15.2324.
11. Wang YR, Yu XL, Peng ZY. Evaluation of different small bowel contrast agents by multi-detector row CT. Int J Clin Exp Med. 2015;8(9):16175-16182.
12. Costello CH Cook CKL. Intravenous urography and imaging of the urinary tract. Hosp Med. 2004;65(7):426-430. doi.org/10.12968/hosp.2004.65.7.15479.

JMeXFRI

Journal of the Mexican Federation of Radiology and Imaging

Check for updates

FULL RESEARCH ARTICLE

Ultrafast brain magnetic resonance imaging in hyperacute and acute ischemic stroke: Diagnostic accuracy and interobserver concordance

Azalea Garza-Baez[a], Rebeca D. Pichardo-Palacios, Ilse C. Frias-Molina, Margarita Ramirez-De Aguilar, and Miguel A. Carrillo-Martinez*

Department of Radiology and Imaging, Escuela de Medicina y Ciencias de la Salud, Tecnologico de Monterrey, Monterrey, Nuevo Leon, Mexico

[a]0000-0002-1304-2352

ABSTRACT

Introduction: *New ultrafast magnetic resonance imaging (MRI) protocols with shorter acquisition times have advantages over the conventional protocols. This study aimed to (1) evaluate the quality of the conventional and ultrafast MRI protocols for hyperacute and acute ischemic stroke and (2) compare the diagnostic accuracy of both protocols and interobserver agreement.* **Material and methods:** *This diagnostic test study was performed in patients with suspected hyperacute or acute ischemic stroke. The duration of the conventional MRI protocol was up to 10:22 minutes and that of the ultrafast protocol 5:13 minutes. Four radiologists and two radiology residents evaluated the images. The diagnosis was validated by two neuroimaging experts. Image quality was classified as poor, moderate, or good. Sensitivity, specificity, positive and negative predictive values, and interobserver agreement were calculated.* **Results:** *Ninety MRI scans were evaluated, 45 with the conventional protocol and 45 with ultrafast. Both protocols demonstrated an overall adequate diagnostic quality. The sensitivity for hyperacute or acute stroke diagnosis with the ultrafast protocol was 90.9% (95% CI, 75.7-98.1) compared with 85.7% (95% CI, 63.7-97.0) (p=0.55) with the conventional protocol. The diagnostic accuracy of the observers was comparable with the two experts.* **Conclusion:** *The new ultrafast MRI protocol (5:13 minutes) showed high diagnostic sensitivity and specificity with good interobserver agreement for detecting hyperacute and acute ischemic stroke in images of adequate quality compared with the conventional protocol. This study is the first in Mexico to propose a time-reduced MRI protocol for stroke detection.*

Keywords: *Ultrafast MRI. Stroke. Ischemic. Susceptibility weighted imaging. Diagnostic accuracy. Image quality.*

INTRODUCTION

The ideal imaging modality for evaluating stroke patients should accurately detect brain ischemia and intracranial hemorrhage and distinguish them from other nonvascular pathologies. Magnetic resonance imaging (MRI) has higher sensitivity in detecting ischemic vascular events and excludes hemorrhage with the same accuracy as computed tomography (CT)[1]. The major disadvantage of MRI is acquisition time, as the conventional MRI protocols take 10 to 20 minutes[2-7]. Advances in resonator tesla strength, brain antenna design, echoplanar and parallel imaging techniques such as SiMultaneous Acquisition of Spatial Harmonics (SMASH), SENSitivity Encoding (SENSE), and GeneRalized Autocalibrating Partial Parallel Acquisition (GRAPPA) have enabled the development of ultrafast protocols with shorter acquisition times compared with conventional protocols with minimal signal-to-noise ratio reduction[3,6,8].

The conventional and ultrafast protocol sequences are similar, including mainly diffusion-weighted imaging (DWI)

Corresponding author:
*Azalea Garza-Baez
E-mail: azalea.garza@medicos.tecsalud.mx

Received for publication: 03-12-2021
Approved for publication: 23-12-2021
DOI: 10.24875/JMEXFRI.M21000008

Available online: 31-03-2022
J Mex Fed Radiol Imaging. 2022;1(1):42-51
www.JMeXFRI.com

and fluid attenuation inversion recovery imaging (FLAIR), combined with other alternatives such as T1, T2[2], T2*, 3D TOF, and Perfusion[3,4]. DWI is the most important sequence because it is the only one that can detect ischemic stroke with a development time of less than 6 hours (hyperacute) with increased sensitivity and interobserver agreement for early ischemic lesions[3]. On the other hand, the FLAIR sequence defines temporality by identifying cytotoxic edema characteristic of an ischemic stroke with a development time of more than 6 hours (acute). In contrast, T2* is commonly used in the conventional protocol to identify hemorrhage, but this sequence has the disadvantage of not differentiating between microbleeds and calcifications.

In MRI interpretation, a greater agreement than CT has been noted between observers[1], radiologists, and other specialists with less experience[6]. Studies that compare conventional protocols with new ultrafast MRI acquisition modalities are needed. This study aimed to (1) evaluate the image quality of conventional and ultrafast MR imaging protocols for hyperacute and acute ischemic stroke and (2) compare the diagnostic accuracy of both protocols and the interobserver agreement of evaluators with different years of experience.

MATERIAL AND METHODS

This comparative, ambispective cohort diagnostic test study was conducted in the Department of Radiology and Imaging of the Hospital Zambrano Hellion and the Hospital San José of the Escuela de Medicina y Ciencias de la Salud del Tecnologico de Monterrey (TecSalud) in Monterrey, Nuevo Leon, Mexico. MRI brain scans with conventional or ultrafast protocols performed in suspected hyperacute or acute stroke patients were included. Incomplete or technically deficient MRI scans were excluded. The ethics committee approved the analysis of MRI scans performed as part of routine clinical care. Institutional ethics and research committees approved the protocol.

Definitions

Hyperacute stroke (0 to 6 hours of clinical evolution): MRI with DWI restriction without visual representation in FLAIR sequence[9].

Acute stroke (6 to 24 hours of clinical evolution): MRI with DWI restriction visible in FLAIR sequence[9].

Subacute stroke: early subacute stroke (24 hours to one week of clinical evolution), MRI with restriction in DWI visible in FLAIR sequence; late subacute (one week to 4 weeks of clinical evolution), MRI with T2 shine-through effect in DWI, visible in FLAIR sequence[9].

Figure 1. Schematic view of the ultrafast MRI protocol for suspected hyperacute and acute stroke showing sequences and time.

DWI: Diffusion-weighted imaging; FLAIR: Fluid attenuation inversion recovery imaging; MRI: Magnetic Resonance Imaging; SWI: Susceptibility weighted imaging.

Chronic stroke: more than four weeks of clinical evolution. The MRI shows encephalomalacia and gliosis, hypointense in DWI, hyperintense in apparent diffusion coefficient (ADC) sequence[9].

Hemorrhagic transformation: microbleeds or hemorrhage within the ischemic stroke area[10].

Microbleed: a round or oval hypointense lesion with a blooming artifact in T2* or SWI sequences up to 10 mm in diameter[11].

Hemorrhagic stroke: intracranial hemorrhage (intracerebral or subarachnoid)[12].

Traumatic hemorrhage: located subdural, epidural, subarachnoid, ventricular, or parenchymal[13].

MRI protocol

MRI scans were selected from the Picture Archiving and Communication System (PACS) (Carestream™ Rochester, NY. US) according to the following protocols:

Conventional MRI Protocol: acquired from May 2017 to March 2018. Conventional protocol MRI scans with a duration of up to 10:22 minutes with the following sequences were retrospectively included: sagittal and axial T1, axial T2*, axial and coronal T2, axial FLAIR, and axial DWI. In addition, localizer sequences of 19 to 26 seconds were performed.

Ultrafast MRI Protocol (Figure 1): acquired from September 2018 to August 2019. MRI studies with an ultrafast protocol duration of 5:13 minutes (Table 1) performed with the following sequences were prospectively included: DWI, FLAIR, and SWI in axial axis (Figure 2) with optimization of the individual sequence parameters and the use of the parallel imaging technique GRAPPA with higher acceleration factors (Table 1). In addition, a T2* sequence was performed

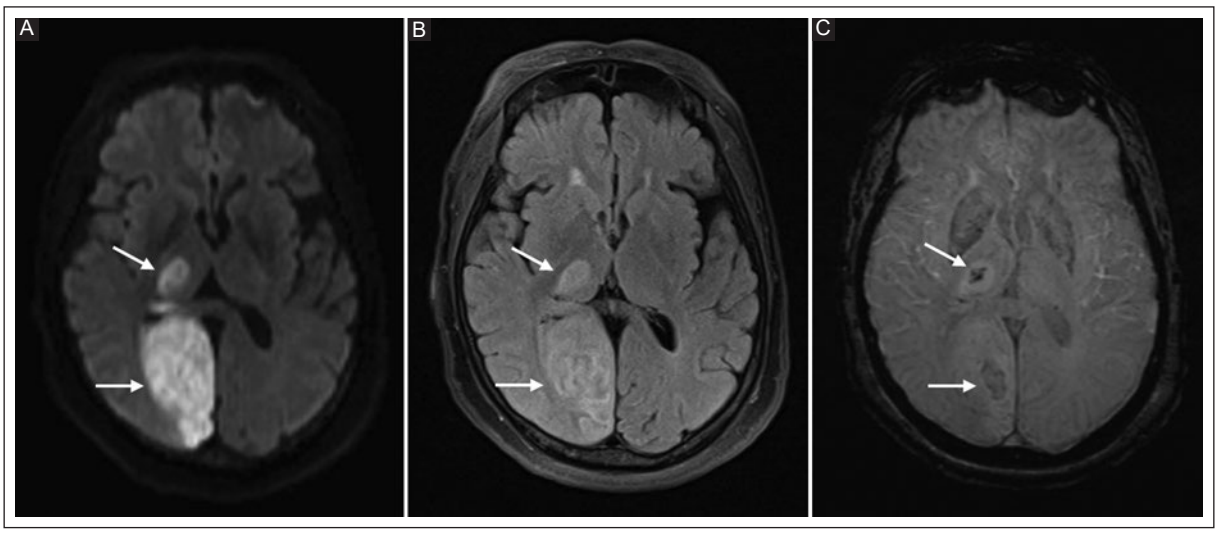

Figure 2. Ultrafast MRI protocol for stroke in axial view in a 69-year-old woman. DWI sequence **A:** shows an area of restricted diffusion in the distribution of the right posterior cerebral artery territory, visible as a hyperintensity on FLAIR **B:** consistent with an acute ischemic stroke (arrows). **C:** SWI sequence shows hypointense foci that represent hemorrhagic transformation within the ischemic stroke area (arrows). The ADC map was calculated from the DWI sequence; the filtered phase and MIP are derived from SWI (not shown).

ADC: Apparent Diffusion Coefficient; DWI: Diffusion-weighted imaging; FLAIR: Fluid attenuation inversion recovery imaging; MIP: Minimum intensity projection; MRI: Magnetic Resonance Imaging; SWI: Susceptibility weighted imaging.

during data acquisition for comparison with SWI and 19-second localizer sequences.

The ultrafast MRI protocol was the only study in prospectively enrolled patients. The conventional protocol was not performed for comparison in these patients to not delay immediate therapeutic decision-making.

Image acquisition and analysis

Images were acquired on a 1.5 T Magnetom Espree™ and Magnetom Aera™ resonators (Siemens Healthineers, Erlangen, Germany) with a 12-channel brain antenna at Hospital San José and a 16-channel antenna at Hospital Zambrano Hellion. A copy of each imaging study was made with a number to maintain anonymity. A folder named "STROKE" was created in PACS to store all studies for later analysis. Six observers were included in the analysis: four board-certified radiologists, two with more than 10 years of experience (fifteen and eleven years each), two with 5 years of experience, and two diagnostic and therapeutic imaging residents who were in their fourth and first year of specialty. The observers were double-blinded (clinical and imaging information) to stroke diagnosis. The reference standard was the diagnosis made by a radiologist dedicated to neuroimaging (MRA) with 18 years of experience and a board-certified neuroradiologist (AGB) with two years of experience. A modified questionnaire was given to each participant to assess image quality and diagnostic accuracy[4] (Annex). Image quality was assessed for Diffusion, FLAIR, and SWI sequences using a scale with three categories: poor, moderate, or good quality in terms of distortion, noise, motion, and delineation of major structures. A score of moderate or good was considered as overall adequate diagnostic image quality. T2* was not considered for image quality evaluation. The observers' diagnostic accuracy compared with experts' diagnosis was determined by the

Table 1. Sequence parameters of the ultrafast MRI protocol for hyperacute and acute stroke

Parameters	DWI	FLAIR	SWI	T2*
TR/TE	6200/113	6000/84	49/40	712/25
FOV (mm)	240	230	230	240
Slice thickness (mm)	5	5	4	5
Slice number	28	23	32	23
GRAPPA	2	3	2	3
Acquisition time (min)	1:35	1:38	2:00	1:08

DWI: Diffusion-weighted imaging; FLAIR: Fluid attenuation inversion recovery imaging; FOV: Field of view; GRAPPA: GeneRalized Autocalibrating Partial Parallel Acquisition; MRI: Magnetic Resonance Imaging; SWI - Susceptibility weighted imaging; TE: Time Echo; TR: Time Repetition. Included only for comparison with SWI.

Table 2. MRI findings with the conventional and ultrafast protocols in patients with suspected hyperacute and acute stroke

Description	Conventional MRI Protocol (n = 45) (%)	Ultrafast MRI Protocol (n = 45) (%)	Total (n = 90) (%)
Ischemic Stroke			
Hyperacute	5 (11.1)	13 (28.8)	18 (20)
Acute	16 (35.5)	18 (40)	34 (37.7)
Subacute	1 (2.2)	1 (2.2)	2 (2.2)
Chronic	11 (24.4)	10 (22.2)	21 (23.3)
Hemorrhagic transformation	2 (4.4)	8 (17.7)[a]	10 (11.1)
Hemorrhagic Stroke			
Intracerebral	2 (4.4)	4 (8.8)[b]	6 (6.6)
Subarachnoid	1 (2.2)	1 (2.2)[b]	2 (2.2)
Traumatic hemorrhage	2 (4.4)	0 (0)	2 (2.2)
Chronic microbleeds	5 (11.1)	10 (22.2)	15 (16.6)

MRI: Magnetic Resonance Imaging; [a]Two patients with the ultrafast protocol had chronic infarcts with hemosiderin deposition indicative of past hemorrhagic transformation; [b]One patient with the ultrafast protocol had both intracerebral and subarachnoid hemorrhage.

presence of restriction areas in the DWI sequence consistent with a diagnosis of ischemia, its timeline (hyperacute, acute, subacute, or chronic), and hemorrhagic transformation. In patients with hemorrhagic stroke, the hemorrhage site was classified as intracerebral and/or subarachnoid. In addition, the presence of traumatic hemorrhage and/or chronic microbleeding in the brain parenchyma, brainstem, and cerebellum was recorded when relevant.

Statistical analysis

For continuous variables, the mean, standard deviation, minimum and maximum were calculated. The median with interquartile range (Shapiro-Wilks test) was calculated for variables of non-normal distribution. Categorical variables were presented as frequencies and percentages. Statistical significance between categories was determined using the chi-square test or Fisher's exact test with 95% confidence intervals. Quantitative variables were analyzed using the Student's *t*-test or the Mann-Whitney U test (parametric and nonparametric data, respectively). Sensitivity, specificity, positive LR, negative LR, positive predictive value (PPV), and negative predictive value (NPV) with 95% confidence intervals were determined for each observer in relation to the final diagnosis validated by the experts. Interobserver agreement between the participants and the experts' diagnosis was determined using the kappa coefficient with 95% confidence intervals. A p-value ≤0.05 was considered statistically significant; all p-values were bilateral. Jamovi Project™ software (version 1.6, Jamovi Co. Sydney, Australia) and SPSS™ (version 26, IBM Corp., Armonk, NY, USA) were used.

RESULTS

Ninety MRI scans of patients with a probable hyperacute or acute stroke diagnosis were included: 45 with the conventional protocol and 45 with the ultrafast protocol. The mean age was 65 ± 13 years; 46 were men, and 44 were women. Hyperacute ischemic stroke was identified in 5 (11.1%) and 13 (28.8%) conventional and ultrafast protocols, respectively, whereas acute ischemic stroke was detected in 16 (35.5%) and 18 (40%), respectively. The findings of hemorrhagic transformation, hemorrhagic stroke, hemorrhage of traumatic origin, and chronic microbleeds detected with both protocols are described in Table 2.

Image quality

DWI images were rated as having adequate diagnostic image quality in 43 (95.5%) of 45 and 44 (97.8%) of 45 MRIs with the conventional and ultrafast protocols, respectively (Figure 3). A higher number of cases with good image quality (n = 32, 71.1%) was observed in the DWI sequence of the ultrafast protocol than with the conventional protocol (n = 20, 44.4%) (p = 0.038). On the other hand, a higher number of good quality images were observed in the FLAIR sequence of the conventional protocol (n = 32, 71.1%) than with the ultrafast protocol (n = 21, 46.7%) (p = 0.026). The SWI sequence

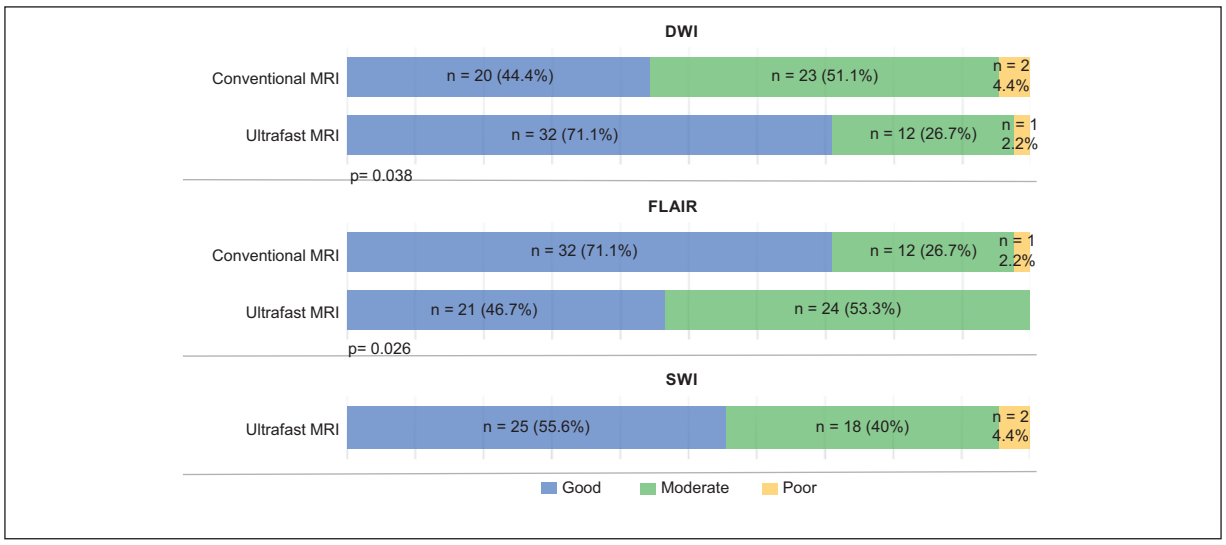

Figure 3. Image quality comparison of conventional and ultrafast brain MRI protocols. DWI and FLAIR sequences for the conventional and ultrafast protocols, SWI for the ultrafast protocol. For DWI, adequate quality (good and moderate) was observed in 95.5% and 97.8% of the studies with the conventional and ultrafast protocols, respectively; 97.8% and 100% with FLAIR. SWI was included only in the ultrafast protocol and had adequate diagnostic quality in 95.6% of studies.

DWI: Diffusion-weighted imaging; FLAIR: Fluid attenuation inversion recovery imaging; MRI: Magnetic Resonance Imaging; SWI - Susceptibility weighted imaging

was only included in the ultrafast protocol and showed adequate diagnostic quality in 43 (95.6%) of 45 MRI studies.

Diagnostic accuracy and interobserver agreement

Expert accuracy in diagnosing hyperacute or acute ischemic stroke was comparable in both protocols (Table 3). Sensitivity was 90.9% (95% CI, 75.7-98.1) with the ultrafast protocol, compared with 85.7% (95% CI, 63.7-97.0) with the conventional protocol (p = 0.55); specificity, on the other hand, was similar with both protocols. The mean accuracy of the six observers in diagnosing hyperacute or acute stroke compared to the two experts was 89.3% (95% CI, 70.8-97.6) and 89.6% (95% CI, 51.9-95.7) with the conventional and ultrafast protocols, respectively (p = 0.95) (Figure 4). Interobserver agreement on ischemia detection between the six evaluators was excellent compared to the experts' diagnosis and comparable between the conventional and ultrafast protocols (κ 0.79, 95% CI, 0.77-0.88) (κ 0.78, 95% CI, 0.67-0.86) (Table 4). The first-year radiology resident agreement (observer 6) was good in both protocols.

SWI versus T2 for the diagnosis of hemorrhage*

The ultrafast protocol included T2* and SWI sequences that identified acute or chronic hemorrhage in 22 (48.8%) of 45 cases, including ischemic stroke with hemorrhagic transformation, hemorrhagic stroke, and chronic microbleeds (Table 2). Hemorrhagic transformation was observed in 6 (19.3%) of 31 cases of hyperacute and acute stroke. The sensitivity for the diagnosis of hemorrhage was higher with SWI (87.5%, 95% CI, 61.7-98.4) than with T2* (81.3%, 95% CI, 54.4-96.0) (p = 0.62) (Table 5). Three false negatives were found at T2*. The observers detected one additional case of hemorrhage with SWI, which corresponded to a false negative result at T2* (Figure 5). There were two false negatives at SWI, while one false positive was detected at both sequences. SWI also identified five patients with intravascular thrombi and two cases with prominent cerebral veins that were not detected in the T2* sequence. The six observers reported that they preferred the SWI sequence to diagnose hemorrhage and/or microbleeds in 263 (97.4%) of 270 evaluations in 45 patients evaluated with the ultrafast MRI protocol.

Table 3. Expert accuracy in diagnosing hyperacute and acute ischemic stroke comparing conventional and ultrafast MRI protocols

Parameters	Conventional MRI Protocol (CI 95%)	Ultrafast MRI Protocol (CI 95%)
Sensitivity, %	85.7 (63.7-97.0)	90.9 (75.7-98.1)
Specificity, %	100 (85.8-100)	100 (73.5-100)
Accuracy, %	93.3 (81.7-98.6)	93.3 (81.7-98.6)
Positive predictive value, %	100 (81.5-100)	100 (88.4-100)
Negative predictive value, %	88.9 (70.8-97.6)	80 (51.9-95.7)
Positive likelihood ratio	∞	∞
Negative likelihood ratio	0.14 (0.05-0.40)	0.09 (0.03-0.26)

CI: Confidence interval; MRI: Magnetic Resonance Imaging.

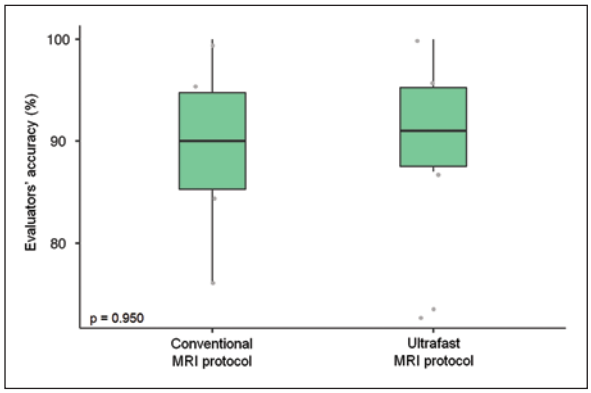

Figure 4. A box-and-whisker figure of evaluators' accuracy in diagnosing hyperacute and acute ischemic stroke compared with the experts' evaluation: a mean of 89.3% with conventional MRI protocol and 89.6% with the ultrafast MRI protocol. The horizontal line within each box represents the median, and the top and bottom of each box represent the 25th and 75th percentiles, respectively. The bars represent the 2.5th and 97.5th percentiles. The circles represent outliers.
MRI: Magnetic Resonance Imaging.

DISCUSSION

In our study, a new ultrafast MRI protocol (5:13 minutes) showed high diagnostic sensitivity and specificity with good interobserver agreement for detecting hyperacute and acute ischemic stroke with adequate image quality compared with the conventional protocol. This study is the first in Mexico to propose a time-reduced MRI protocol to detect hyperacute and acute stroke.

MRI provides more information than a CT scan in the evaluation of patients with suspected stroke. However, the duration of conventional MRI with its longer acquisition time has limited its routine use as an initial examination. Consequently, new accelerated protocols have been developed. Reports in the literature state that the acquisition time of ultrafast protocols varies from 4:33 to up to 6 minutes[2-7], whereas conventional protocols are 10:22 to up to 20 minutes[2-7]. In a prospective diagnostic test study, Kazmierczak et al.[2] compared a conventional 15-minute protocol with an ultrafast protocol of 4:33 minutes in 60 patients with acute nontraumatic neurologic symptoms, including ischemic and hemorrhagic stroke. The ultrafast protocol had elevated diagnostic accuracy with a sensitivity of 93.9% (95% CI, 88.1-97.2) and a specificity of 100% (95% CI, 89.5-100). The authors concluded that the ultrafast protocol provides a time-optimized diagnostic approach to neurologic emergencies that directly impacts patient management. The results of this report are similar to those of our study comparing 45 conventional MRI protocols with 45 ultrafast MRI protocols in patients with suspected hyperacute and acute ischemic stroke. The sensitivity of the ultrafast protocol was comparable to that of the conventional protocol (90.9%, 95% CI, 75.7-98.1, and 85.7%, 95% CI, 63.7-97.0, respectively). Our proposed ultrafast MRI protocol (5:13 minutes) showed comparable diagnostic accuracy with the conventional MRI protocol with a shorter acquisition time, which is advantageous in evaluating patients with hyperacute and acute ischemic stroke.

Agreement in interpreting a diagnostic test is important in determining its reproducibility and usefulness in confirming the suspected pathology. Therefore, the most experienced and knowledgeable radiologists are the reviewers who usually decide whether an imaging protocol is appropriate. Interestingly, recent studies have included a variety of evaluators (radiologists and other specialists) with different levels of professional

Table 4. Interobserver concordance of the reviewers compared with the experts' opinion for the diagnosis of hyperacute and acute stroke with the conventional and ultrafast MRI protocols

Evaluators	Conventional MRI protocol		Ultrafast MRI protocol	
	Agreement, %	Concordance correlation (95% CI)	Agreement, %	Concordance correlation (95% CI)
1[a]	91.1	0.82 (0.69-0.89)	84.4	0.64 (0.44-0.78)
2[a]	100.0	1.00	95.6	0.89 (0.81-0.93)
3[b]	88.9	0.77 (0.62-0.86)	93.3	0.83 (0.71-0.90)
4[b]	95.6	0.91 (0.84-0.95)	95.6	0.88 (0.79-0.93)
5[c]	88.9	0.77 (0.62-0.87)	88.9	0.73 (0.57-0.84)
6[c]	77.8	0.54 (0.32-0.70)	71.1	0.45 (0.22-0.62)
Median	90.0	0.79 (0.77-0.88)	91.1	0.78 (0.67-0.86)

CI: Confidence interval; MRI: Magnetic Resonance Imaging; [a]Radiologists with > 10 years of experience (fifteen years and eleven years, respectively); [b]Radiologists with five years of experience; [c]Radiology residents: fourth and first year, respectively.

Table 5. Diagnostic test accuracy of the ultrafast MRI protocol for cerebral hemorrhage in patients with suspected hyperacute and acute stroke

Parameter	T2* -weighted (95% CI)	SWI (95% CI)
Sensitivity, %	81.3 (54.4-96.0)	87.5 (61.7-98.4)
Specificity, %	96.6 (82.2-99.9)	96.6 (82.2-99.9)
Accuracy, %	91.1 (78.8-97-5)	93.3 (81.7-98.6)
Positive predictive value, %	92.9 (66.1-99.8)	93.3 (68.1-99.8)
Negative predictive value, %	90.3 (74.2-98.0)	93.3 (77.9-99.2)
Positive likelihood ratio	23.6 (3.38-163.99)	25.4 (3.66-175.65)
Negative likelihood ratio	0.19 (0.07-0.54)	0.12 (0.03-0.47)

CI: Confidence interval; MRI: Magnetic Resonance Imaging; SWI: Susceptibility weighted imaging; T2*: "T2-star".

experience[2,4-7,14]. In a prospective diagnostic test study of 23 adult patients with suspected acute or subacute stroke evaluated with a conventional and ultrafast MRI protocol, the interobserver agreement between a neuroradiologist and a stroke neurologist was determined[6]. Interobserver agreement of the DWI sequence was 100% for both protocols. In our study, the reviewers were four radiologists with different levels of experience (between 5 and 15 years) and two residents (in the first and last year of residency training). The interobserver agreement of the six evaluators for the diagnosis of hyperacute or acute ischemic stroke was excellent with respect to the expert radiologists' diagnosis in the conventional MRI protocol (κ 0.79, 95%CI 0.77-0.88) and in the ultrafast MRI protocol (κ 0.78, 95%CI 0.67-0.86). The first-year resident had good agreement. We demonstrated that less experienced radiologists could easily interpret the ultrafast MRI protocol evaluated in our study.

Various scales have been used to evaluate the quality of MRI images, resolution, signal-to-noise ratio, and acquisition time as the most important aspects[2,4-7]. Advanced techniques, such as parallel imaging within the ultrafast MRI protocol, allow adequate image definition in patients with suspected stroke with reduced acquisition time and quality comparable to the conventional protocol. Nael et al.[4], in a prospective study including 62 patients with suspected acute stroke, demonstrated that it is possible to perform a 6-minute ultrafast MRI protocol with high diagnostic quality (≥ 90%) with good to excellent interobserver agreement. The authors concluded that the ultrafast MRI protocol competes with the duration of multimodal CT, with a significant decrease in scanning time. In our study, the time reduction with the ultrafast protocol was possible using a parallel acquisition technique such as GRAPPA. The proposed ultrafast MRI protocol, which included DWI, FLAIR, and SWI sequences, demonstrated adequate diagnostic quality with a minimal reduction in the signal-to-noise ratio. It is also easily interpreted by radiologists with different levels of experience, including residents.

MRI sequences included in the ultrafast protocol vary depending on the needs or approach of the hospital center. The most commonly used sequences are DWI, T1,

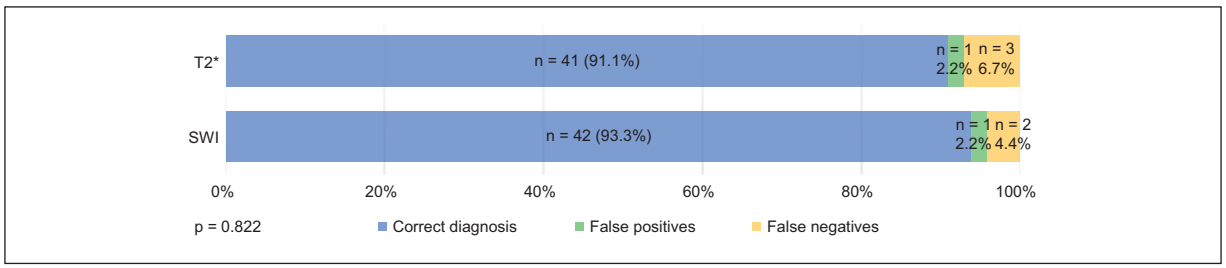

Figure 5. Diagnostic accuracy in detecting hemorrhage and microbleeds in T2*-weighted and SWI sequences of the ultrafast MRI protocol. Most of the hemorrhages and microbleeds were detected in both sequences. There were three false-negative results in T2* and two false-negative results in SWI, indicating that one additional case of microbleeds was detected in SWI. In addition, one false-positive result was detected in both sequences.

T2*: "T2-star" MRI: Magnetic Resonance Imaging; SWI - Susceptibility weighted imaging.

T2, FLAIR, and T2*[2,4-7,14]. In our ultrafast MRI protocol, DWI, FLAIR, and SWI sequences were included. The SWI sequence identifies microbleeds that are not detected by CT, which have a potential impact on treatment decisions (> 5 microbleeds have a higher risk of hemorrhagic transformation in patients undergoing thrombolysis)[11]. The SWI sequence requires a longer acquisition time than the T2* sequence (included in the conventional protocol) but has higher accuracy in detecting microbleeds, thrombi, or cerebral flow asymmetry[3]. In our study, the SWI sequence detected hemorrhages, intravascular thrombi, and prominent cerebral veins that were not detected with T2*. Even though the SWI sequence has been used in conventional MRI protocols to detect stroke, to our knowledge, this is the first time it was included in a protocol of ultrafast MRI in patients with suspected hyperacute or acute stroke.

The strengths of our study are the following: A 1.5-T resonator was used, which is available in most hospitals, making our ultrafast protocol reproducible. In addition, inclusion of the SWI sequence increased the sensitivity of MRI for the diagnosis of microbleeds, the detection of intravascular thrombi, and prominent cerebral veins. Finally, our ultrafast protocol is easily interpreted even by radiology residents. On the other hand, our study has several limitations. First, the sample size was small; second, because of the diagnostic suspicion of hyperacute or acute stroke in patients studied with the ultrafast protocol, the conventional protocol was not performed simultaneously so as not to delay treatment; thus, false-negative results were not obtained with the ultrafast MRI protocol; third, only the SWI and T2* sequences were performed in the ultrafast MRI protocol, so it is possible that blinding was lost when observers identified these sequences.

CONCLUSION

The diagnostic performance of our ultrafast MRI protocol and the quality of the images were comparable with the conventional protocol; therefore, it could be an alternative to the conventional protocol for the diagnosis of hyperacute and acute ischemic stroke. There was good interobserver agreement, and the ultrafast MRI protocol was easy to interpret by less experienced radiologists. Our ultrafast protocol is currently complemented by MR angiography to assess the integrity of the Willis polygon and the vertebrobasilar system, which may influence therapeutic decisions (thrombolysis vs. endovascular therapy). Prospective randomized trials with larger numbers of patients and application of new technologies such as artificial intelligence to improve imaging quality, speed and reduce stroke imaging evaluation[15], are needed to establish the recommendation of the ultrafast brain MRI protocol as the initial imaging study for diagnosing hyperacute and acute ischemic stroke.

Acknowledgments

The authors thank professor Ana M. Contreras-Navarro for her guidance in preparing and writing this scientific paper. We thank doctor Everardo Garcia-Estrada, for his support in the statistical analysis.

Funding

Supported with funds from Programa Nacional de Posgrado de Calidad of the Consejo Nacional de Ciencia y Tecnología de México.

Conflicts of interest

The authors declare that they have no conflicts of interest.

Ethical disclosures

Protection of human and animal subjects. The authors declare that the procedures followed were in accordance with the regulations of the relevant clinical research ethics committee and with those of the Code of Ethics of the World Medical Association (Declaration of Helsinki).

Confidentiality of data. The authors declare that they have followed the protocols of their work center on the publication of patient data.

Right to privacy and informed consent. Ethics approval for analysis of routinely acquired clinical data was obtained from the Ethics Committee and informed consent was not required for the retrospective part of the study of information collected during routine clinical care.

REFERENCES

1. Chalela JA, Kidwell CS, Nentwich LM, Luby M, Butman JA, Demchuk AM, et al. Magnetic resonance imaging and computed tomography in emergency assessment of patients with suspected acute stroke: a prospective comparison. Lancet. 2007; 27;369(9558):293-298. doi: 10.1016/S0140-6736(07)60151-2.
2. Kazmierczak PM, Dührsen M, Forbrig R, Patzig M, Klein M, Pomschar A, et al. Ultrafast Brain Magnetic Resonance Imaging in Acute Neurological Emergencies: Diagnostic Accuracy and Impact on Patient Management. Invest Radiol. 2020;55(3):181-189. doi: 10.1097/RLI.0000000000000625.
3. Graves MJ, U-King-Im J, Howarth S, Gillard JH. Ultrafast magnetic resonance imaging protocols in stroke. Expert Rev Neurother. 2006;6(6):921-930. doi: 10.1586/14737175.6.6.921.
4. Nael K, Khan R, Choudhary G, Meshksar A, Villablanca P, Tay, J et al. Six-minute magnetic resonance imaging protocol for evaluation of acute ischemic stroke: pushing the boundaries. Stroke. 2014;45(7):1985-91. doi: 10.1161/STROKEAHA.114.005305.
5. Prakkamakul S, Witzel T, Huang S, Boulter D, Borja MJ, Schaefer P, et al.Ultrafast Brain MRI: Clinical Deployment and Comparison to Conventional Brain MRI at 3T. J Neuroimaging. 2016;26(5):503-510. doi: 10.1111/jon.12365.
6. U-King-Im JM, Trivedi RA, Graves MJ, Harkness K, Eales H, Joubert I, et al. Utility of an ultrafast magnetic resonance imaging protocol in recent and semi-recent strokes. J Neurol Neurosurg Psychiatry. 2005;76(7):1002-1005. doi: 10.1136/jnnp.2004.046201.
7. Sindhura M, Rangasami R, Chandrasekharan A. Role of Ultrafast MR Imaging in Stroke Patients. J Neurosci Rural Pract. 2020;11(3):436-441. doi: 10.1055/s-0040-1712716.
8. Hamilton J, Franson D, Seiberlich N. Recent advances in parallel imaging for MRI. Prog Nucl Magn Reson Spectrosc. 2017;101:71-95. doi:10.1016/j.pnmrs.2017.04.002.
9. Vachha BA, Schaefer PW. Imaging Patterns and Management Algorithms in Acute Stroke: An Update for the Emergency Radiologist. Radiol Clin North Am. 2015;53(4):801-826, ix. doi: 10.1016/j.rcl.2015.02.012.
10. Choi PMC, Ly JV, Srikanth V, Ma H, Chong W, Holt M, et al. Differentiating between Hemorrhagic Infarct and Parenchymal Intracerebral Hemorrhage. Radiol Res Pract. 2012;2012:475497. doi: 10.1155/2012/475497.
11. Dannenberg S, Scheitz JF, Rozanski M, Erdur H, Brunecker P, Werring DJ, et al. Number of cerebral microbleeds and risk of intracerebral hemorrhage after intravenous thrombolysis. Stroke. 2014;45(10):2900-2905. doi: 10.1161/STROKEAHA.114.006448.
12. Unnithan AKA, Mehta P. Hemorrhagic Stroke. 2021 Aug 11. In: StatPearls [Internet]. Treasure Island (FL): StatPearls Publishing; 2021 Jan-.
13. Schweitzer AD, Niogi SN, Whitlow CT, Tsiouris AJ. Traumatic Brain Injury: Imaging Patterns and Complications. RadioGraphics. 2019;39(6):1571-1595. doi: 10.1148/rg.2019190076.
14. Singh RK, Smith JT, Wilkinson ID, Griffiths PD. Ultrafast MR imaging in pediatric neuroradiology. Acta Radiol. 2003;44(5):550-557. doi: 10.1034/j.1600-0455.2003.00118.x.
15. Mouridsen K, Thurner P, Zaharchuk G. Artificial Intelligence Applications in Stroke. Stroke. 2020;51(8):2573-2579. doi: 10.1161/STROKEAHA.119.027479.

ANNEX

Evaluation of MRI Quality and Diagnostic Accuracy in Patients with Suspected Hyperacute and Acute Stroke
Stroke ID Patient #

IMAGE QUALITY

Select one of the options to rate the following sequences:

DIFFUSION

1) Poor (non-diagnostic imaging)
2) Moderate (non-perfect, but diagnostic)
3) Good (diagnostic)

FLAIR

1) Poor (non-diagnostic imaging)
2) Moderate (non-perfect, but diagnostic)
3) Good (diagnostic)

SWI

1) Poor (non-diagnostic imaging)
2) Moderate (non-perfect, but diagnostic)
3) Good (diagnostic)

DIAGNOSTIC ACCURACY

1. Is a restriction zone observed in the diffusion sequence?
   Yes ( ) No ( )
2. If you detected a restriction zone, is it represented in the FLAIR sequence?
   Yes ( ) No ( )
3. If a lesion is present, are there bleeding foci within the lesion?
   Yes ( ) No ( )
4. If a lesion is present, are there foci of parenchymal hemorrhage outside the lesion?
   Yes ( ) No ( )
5. If hemorrhage(s) and/or microbleed(s) were present, which of the two sequences (T2* or SWI) was most useful for detecting hemorrhage(s) and/or microbleed(s)?
   T2* ( ) SWI ( )

JMeXFRI

Journal of the Mexican Federation of Radiology and Imaging

Check for updates

BRIEF RESEARCH ARTICLE

Decreased ^{18}F-FDG PET/CT uptake in the gastrointestinal tract with oral hyoscine-N-butyl bromide

*Hugo E. Solis-Lara[1,a], Ernesto Herrera-Garza[1], Marcos A. Rosas-Rodriguez[2], Miguel A. Olarte-Casas[2], and Belen Rivera-Bravo[2,b]**

[1]Centro Universitario de Imagen Diagnóstica, School of Medicine, "Hospital Universitario Dr. Jose Eleuterio Gonzalez" Universidad Autónoma de Nuevo Leon, Monterrey, Nuevo Leon; [2]School of Medicine, Universidad Nacional Autonoma de Mexico, Mexico City

[a]0000-0002-4510-0166; [b]0000-0002-6439-2686

ABSTRACT

Various protocols have been proposed to reduce the gastrointestinal uptake of ^{18}F-FDG in PET/CT for the accurate detection of malignant neoplasms. The aim of this study was to evaluate the effect of hyoscine-N-butyl bromide in ^{18}F-FDG PET/CT in different gastrointestinal tract segments. This quasi-experimental study included patients with extraintestinal malignancies assigned to a control group and an intervention group. The intervention group received 10 mg of hyoscine-N-butyl bromide orally before ^{18}F-FDG administration. A semiquantitative evaluation was based on the SUVmean of the ^{18}F-FDG PET/CT scan in different gastrointestinal tract segments. Statistical significance was defined as a p-value < 0.05. Twenty patients were included in the control group and 10 in the intervention group. The mean SUVmean of all gastrointestinal regions was 1.15 in the intervention group compared to 1.56 in the control group (p < 0.05). A significant reduction in radiotracer uptake was observed in the transverse colon (0.76 ± 0.30, p < 0.001), the descending colon (0.77 ± 0.40, p = 0.002), the sigmoid (1.17 ± 0.39, p < 0.001), the rectum (1.25 ± 0.48, p < 0.001), and the anus (1.72 ± 0.52, p = 0.01). We found that oral hyoscine-N-butyl bromide decreased the uptake of ^{18}F-FDG PET/CT in different gastrointestinal tract segments with a focus on the colon.

Keywords: *PET/CT scan. ^{18}F-FDG. Hyoscine-N-butyl bromide. Intestine. Colon. Large intestine.*

INTRODUCTION

Positron emission tomography/computed tomography (PET/CT) is a diagnostic technique that combines both techniques to provide a functional image at the cellular level. Fluorine-18-fluorodeoxyglucose (^{18}F-FDG) is the most commonly used radiotracer in a PET/CT scan. Its uptake in the gastric wall is common, and it can be intense in the colon, especially in the cecum and sigmoid colon[1]. Peristaltic movements in these segments range from 2 to 6/min[2], resulting in an increased physiologic uptake of ^{18}F-FDG at these sites. Interpretation of PET/CT images is difficult because variable biodistribution and uptake may be indistinguishable between benign and malignant abdominopelvic pathology[3]. Tumor cells have a high glucose uptake and concentrate a greater proportion of this tracer, allowing accurate detection of malignant neoplasms. On the other hand, the physiologic uptake areas of the gastrointestinal tract on PET/CT with ^{18}F-FDG are highly variable, both in biodistribution and intensity from the esophagus to the anus. This effect limits adequate interpretation to distinguish physiologic and non-neoplastic pathologic patterns of radiopharmaceutical uptake with low specificity for detecting malignant tumors.

Corresponding author:
*Belen Rivera-Bravo
E-mail: belen13@yahoo.com

Received for publication: 11-10-2021
Approved for publication: 28-10-2021
DOI: 10.24875/JMEXFRI.M21000002

Available online: 31-03-2022
J Mex Fed Radiol Imaging. 2022;1(1):52-57
www.JMeXFRI.com

Various ^{18}F-FDG PET/CT protocols have been proposed to decrease uptake by administering drugs such as hyoscine-N-butyl bromide[4] or scopolamine[5,6] to reduce the frequency of false-positive and false-negative results. The effect of hyoscine-N-butyl bromide on the different gastrointestinal tract segments to reduce physiological ^{18}F-FDG uptake and achieve an optimal tumor-to-background ratio has not been adequately studied. The aim of this study was to evaluate the effect of hyoscine-N-butyl bromide on ^{18}F-FDG PET/CT uptake in different gastrointestinal tract segments.

MATERIAL AND METHODS

A quasi-experimental study was conducted from April 2015 to January 2016 at the PET/CT unit of the School of Medicine of the Universidad Nacional Autonoma de Mexico. Patients with a diagnosis of thyroid or renal cancer were included. The exclusion criterion was the presence of clinical manifestations of a known gastrointestinal pathology and the use of metformin. Eligible patients were invited to participate and provided written informed consent. The study was approved by the institutional research ethics and research committees.

The age and sex of all participants were recorded, and they were assigned to two groups: a control group and an intervention group where 10 mg oral hyoscine-N-butyl bromide was administered 60 minutes before ^{18}F-FDG administration. Patients were consecutively selected in a 2:1 ratio during the study period (control and intervention groups).

Imaging protocol

The ^{18}F-FDG PET/CT scan was performed according to international recommendations[7,8]. No iodine-containing, oral or intravenous contrast agent was administered during the scan acquisition. The technical specifications were: tube potential 120 Kv, the mA was automatically calculated using the Siemens Care 2® application based on the patient's weight and height with a pitch of 0.75, rotation time of 0.5 s, a slice thickness of 3 mm, a slice distance of 3 mm and a FOV of 500 mm. PET images were obtained using integrated whole-body 3D PET/CT systems with 4 iterative reconstructions and 14 subsets, two minutes per bed position. The image size was 168 x 168, Gaussian type filter, zoom with a value of 1, with attenuation and dispersion correction by CT. PET/CT images were subsequently acquired 60 minutes after ^{18}F-FDG injection.

Semiquantitative analysis of the ^{18}F-FDG uptake

The PET/CT images from both groups were evaluated without blinding by a nuclear medicine physician with four years of experience in PET/CT. The mean standard uptake value (SUVmean) was determined using 2D regions of interest (ROI), adjusted according to the size of the anatomic segment evaluated and the greatest uptake visual area: esophagus, stomach, duodenum, jejunum, ileum, ileocecal valve, cecum, ascending, transverse and descending colon, sigmoid, rectum, and anus. Images were analyzed in the coronal, sagittal, and axial planes.

Statistical analysis

Continuous variables were described with means and standard deviation, categorical variables with medians, interquartile range, and percentages. The normality of variables was determined with the Kolmogorov-Smirnov test. Differences between groups were analyzed using Student's *t*-test or the Mann-Whitney U test for continuous variables and the chi-square test for categorical variables. Statistical significance was defined as a p-value < 0.05. SPSS software, version 23.0 (IBM Corp., Armonk, NY, USA) was used.

RESULTS

Twenty patients were included in the control group and 10 in the intervention group (Table 1). The mean ages were 48.75 ± 16.08 (24 to 87) years and 56.1 ± 12.5 (42 to 68) years, respectively. There were 6 men and 14 women in the control group and two men and eight women in the intervention group. None of the patients had an adverse effect to the administration of hyoscine-N-butyl bromide. The intervention group showed a global decrease in ^{18}F-FDG uptake in the gastrointestinal tract, with a SUVmean of 1.15 compared to 1.56 in the control group ($p < 0.05$). The SUVmean of ^{18}F-FDG at the esophagogastric junction was significantly lower in the intervention group than in the control group (1.44, 95% CI 1.1-2.1 vs. 1.98 95% CI 1.5-3.0, $p < 0.001$) (Table 1); radiotracer uptake in the gastric antrum, duodenum, and jejunum also decreased significantly in the intervention group. The behavior of ^{18}F-FDG uptake in the segments of the colon

Table 1. Comparison of ^{18}F-FDG PET/CT uptake in the gastrointestinal segments between the control group and the intervention group: in this group 10 mg oral hyoscine-N-butyl bromide was administered 60 minutes before ^{18}F-FDG

Description	Control group, SUVmean (n = 20)	Intervention group, SUVmean (n = 10)	p-value
Upper esophagus	1.61 ± 0.32 (1.1-2.2)	1.34 ± 0.30 (0.9-1.9)	0.03
Middle esophagus	1.67 ± 0.31 (1.2-2.2)	1.52 ± 0.23 (1.2-1.9)	0.14
Lower esophagus	1.59 ± 0.29 (0.9-2.2)	1.38 ± 0.31 (0.8-1.9)	0.08
Gastroesophageal junction	1.98 ± 0.33 (1.5-3.0)	1.44 ± 0.28 (1.1-2.1)	<0.001
Stomach (body)	0.81 ± 0.32 (0.4-1.5)	0.58 ± 0.21 (0.2-0.9)	0.02
Stomach (fundus)	0.71 ± 0.26 (0.3-1.3)	0.51 ± 0.21 (0.2-0.8)	0.03
Stomach (antrum)	0.83 ± 0.14 (0.4-1.0)	0.28 ± 0.13 (0.1-0.6)	<0.001
Duodenum	1.68 ± 0.39 (1.2-3.0)	0.99 ± 0.24 (0.6-1.3)	<0.001
Jejunum	1.55 ± 0.29 (1.2-2.5)	1.05 ± 0.26 (0.7-1.6)	<0.001
Ileum	1.43 ± 0.25 (1.0-2.0)	1.38 ± 0.78 (0.8-3.5)	0.84
Ileocecal valve	1.92 ± 0.21 (1.5-2.5)	1.92 ± 0.79 (1.0-3.7)	0.98
Cecum	1.5 ± 0.31 (1.0-1.9)	1.62 ± 0.60 (0.9-2)	0.56
Ascending colon	1.35 ± 0.47 (1.0-3.0)	1.06 ± 0.33 (0.6-1.7)	0.06
Transverse colon	1.62 ± 0.26 (1.2-2.0)	0.76 ± 0.30 (0.4-1.1)	<0.001
Descending colon	1.31 ± 0.28 (0.9-1.9)	0.77 ± 0.40 (0.3-1.7)	0.002
Sigmoid	2.15 ± 0.26 (2.0-3.0)	1.17 ± 0.39 (0.8-1.7)	<0.001
Rectum	2.22 ± 0.25 (2.0-2.9)	1.25 ± 0.48 (0.8-2.3)	<0.001
Anus	2.20 ± 0.30 (1.9-3.0)	1.72 ± 0.52 (1.1-3.0)	0.01
Total (mean)	1.56	1.15	<0.05

^{18}F-FDG PET/CT: Fluorine-18-fluorodeoxyglucose positron emission tomography/computed tomography;
^{18}F-FDG: Fluorine-18-fluorodeoxyglucose; SUVmean: Standard uptake value mean. All data are mean ± standard deviation (range) unless otherwise specified.

(transverse, descending, sigmoid, rectum, and anus) was significantly lower in the intervention group than in the control group (Table 1).

Figure 1 is an ^{18}F-FDG PET/CT study in maximum intensity and coronal projection in grayscale (A,B) and fusion (C), showing the physiological distribution of radiotracer in a 59-year-old woman in the control group. A semiquantitative analysis of the ^{18}F-FDG PET/CT scan showed an increase in the SUVmean in different gastrointestinal tract regions. Figure 2 is an ^{18}F-FDG PET/CT image in maximum intensity projection and axial grayscale PET (A,B) and axial fusion (C) showing a SUVmean of 3 in the ascending colon of a 43-year-old male patient from the control group. Figure 3 is the ^{18}F-FDG PET/CT of a 68-year-old woman who received 10 mg oral hyoscine-N-butyl bromide (intervention group) showing an image (3A) in maximum intensity projection with decreased uptake of the radiotracer in the gastrointestinal tract in the segments (3B) small intestine, cecum and descending colon in coronal projection fusion. Axial grayscale PET (3C) and fusion (3D) showed a SUVmean of 1 in the cecum.

DISCUSSION

In our study, oral administration of hyoscine-N-butyl bromide significantly decreased the SUVmean of ^{18}F-FDG PET/CT in the different gastrointestinal tract segments with predominance in the colon. We hypothesize that the decreased uptake of the radiotracer may lead to an appropriate tumor-to-background ratio in the evaluation of malignant tumors.

Increased uptake of radiotracer occurs in gastrointestinal pathologies, whether benign or malignant. Physiologic uptake of ^{18}F-FDG in the wall of the gastrointestinal tract reflects varying degrees of peristaltic

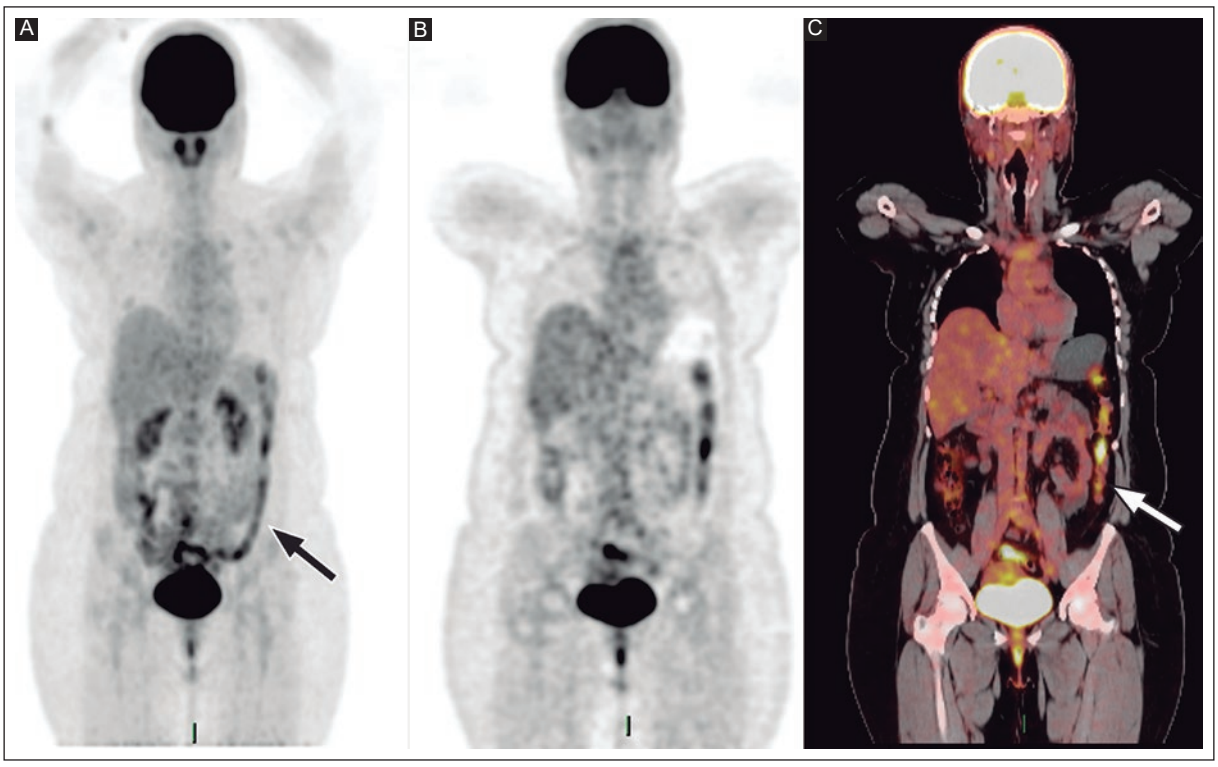

Figure 1. ^{18}F-FDG PET/CT image in maximum intensity and coronal grayscale projection (**A, B**) and fusion (**C**) showing the physiological distribution of radiotracer uptake predominantly in the descending colon (arrows) in a 59-year-old woman from the control group.

^{18}F-FDG PET/CT: Fluorine-18-fluorodeoxyglucose positron emission tomography/computed tomography.

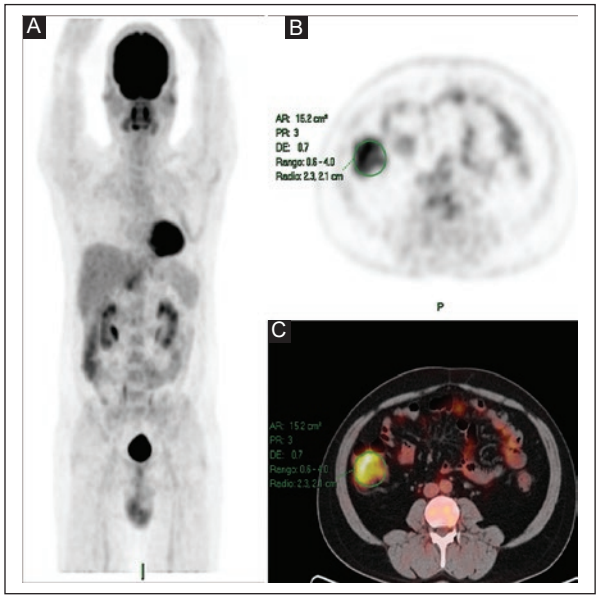

Figure 2. Maximum intensity projection and axial grayscale PET (**A, B**) and axial fusion (**C**) showing a SUVmean of 3 in ascending colon of a 43-year-old male patient from the control group.

PET: Positron emission tomography; SUVmean: Standard uptake value mean.

activity. It is observed in diffuse distribution, whereas incidental focal uptake is of clinical significance in most patients. It has been suggested that the use of spasmolytics before an ^{18}F-FDG PET/CT scan may increase diagnostic accuracy[5,6,9]. In a quasi-experimental study, Emmott et al.[6] evaluated the effects of a single intravenous administration of 20 mg butylscopolamine on ^{18}F-FDG uptake in the gastrointestinal tract of patients with oncologic disease at different extraintestinal sites: 36 control subjects and 36 subjects in the intervention group who received butylscopolamine. Qualitative assessment of radiotracer uptake was based on a scale of 0 to 3: no uptake (0), low uptake (1), moderate uptake (2), and high uptake (3). On average, 1.25 areas of abdominal uptake were identified in the control group, whereas only 0.25 were identified in the intervention group ($p < 0.05$). These results are comparable to our study's results, which included 20 subjects in the control group and 10 in the intervention group. They received a single dose of 10 mg hyoscine-N-butyl bromide orally one hour before the ^{18}F-FDG PET/CT scan. The SUVmean in

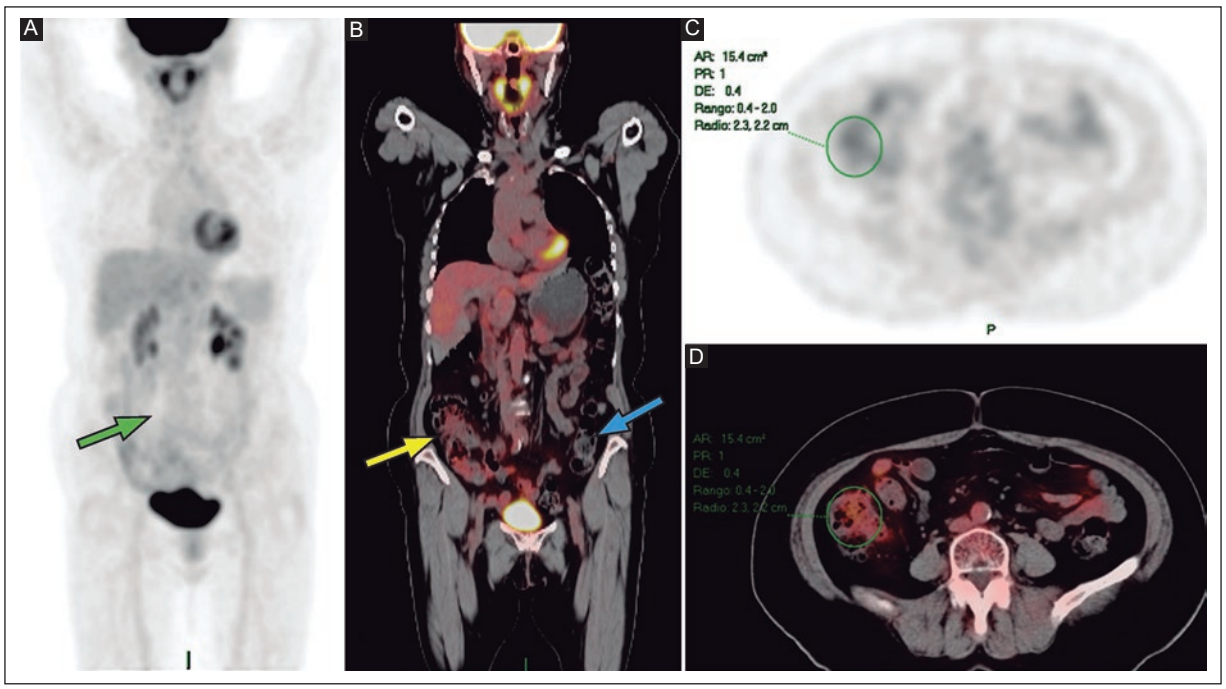

Figure 3. ^{18}F-FDG PET/CT in a 68-year-old woman receiving 10 mg oral hyoscine-N-butyl bromide (intervention group); (**A**) image in maximum intensity projection showing decreased uptake of radiotracer in the gastrointestinal tract segments, small intestine (green arrow) (**B**), cecum (yellow arrow) and descending colon (blue arrow) in coronal projection fusion. Axial grayscale PET (**C**) and fusion (**D**) showed a SUVmean of 1 in the cecum.

^{18}F-FDG PET/CT: Fluorine-18-fluorodeoxyglucose positron emission tomography/computed tomography; PET: Positron emission tomography; SUVmean: Standard uptake value mean.

the different gastrointestinal tract segments was significantly lower in the intervention group compared with the control group. The decrease in ^{18}F-FDG uptake in the gastrointestinal tract may be attributed to the reduction in peristalsis due to the therapeutic effect of hyoscine-N-butyl bromide.

Hyoscine-N-butyl bromide decreases peristalsis in the gastrointestinal tract, and its spasmolytic effect begins 30 to 60 minutes after oral administration and is observed predominantly in the colon. Recently, conflicting results have been reported on the use of spasmolytic drugs in ^{18}F-FDG uptake in PET/CT scans. In a quasi-experimental study, Shukur et al.[4] enrolled 133 patients with lymphoma, colorectal carcinoma, or gynecologic carcinoma; 65 cases were assigned to the control group and 68 to the intervention group. The intervention group received 10 mg hyoscine-N-butyl bromide orally 30 min before ^{18}F-FDG injection. No significant difference in intestinal uptake of the radiotracer was found between the intervention (SUVmean: 1.9) and the control group (SUVmean: 1.6) ($p = 0.215$). Our study showed a semiquantitative reduction in ^{18}F-FDG PET/CT scans in the intervention group receiving oral hyoscine-N-butyl bromide 10 mg, with a SUVmean of 1.15 compared to 1.56 in the control group ($p < 0.05$). In Shukur's study[4], the lack of effect of hyoscine-N-butyl bromide on reducing radiotracer uptake in the intervention group may be related to the abdominopelvic pathologies that were prevalent in this group (n = 32 colorectal carcinomas and n = 13 gynecologic carcinomas, 66%), in contrast to the control group (n = 3 colorectal carcinomas and n = 13 gynecologic carcinomas, 25%). These differences between the study groups may explain the higher SUVmean between the intervention (1.9) and the control group (1.6). In addition, it is likely that due to the lack of ROI standardization and the fact that SUVmean measurement is operator-dependent, no significant difference in ^{18}F-FDG PET/CT uptake was demonstrated between the groups. In another study of 40 patients diagnosed with extra-abdominal lymphoma, the effect of intravenous butylscopolamine administered before ^{18}F-FDG PET/CT scan was evaluated in 20 patients (intervention group) and compared with a control group (n = 20)[5]. A qualitative assessment consisted of visualization of intestinal loops in 5 abdominal regions. In the intervention group, one region was observed, whereas in the control group, 2.5 regions. Moreover, bowel activity influenced the interpretation of PET/CT images in 1 of 20 patients in the

intervention group, in contrast to 6 of 20 in the control group (5% vs. 30% $p < 0.01$). The authors concluded that the use of butylscopolamine decreases ^{18}F-FDG uptake in the gastrointestinal tract, which favors the interpretation of the PET/CT scan. In our study and other reports[5,6], the effect of hyoscine-N-butyl bromide on decreasing radiotracer uptake in ^{18}F-FDG PET/CT scan in patients with extraintestinal malignancies was demonstrated; however, there is insufficient evidence to support this effect in patients with abdominopelvic pathologies.

Our study has several strengths. The quasi-experimental design in patients with extraintestinal neoplastic disease and the timing of drug administration before PET/CT was similar in subjects with homogeneous results to radiotracer uptake. Another strength was the determination of a semiquantitative analysis (ROI) of ^{18}F-FDG uptake in the different gastrointestinal tract segments. The limitations of our study are the small sample size, the fact that participants were not randomly assigned, and there was no blinded observer. Also, the PET/CT images were evaluated by a single observer, so the reproducibility of the results between different observers was not evaluated.

CONCLUSION

Our study demonstrated the effect of oral hyoscine-N-butyl bromide on reducing ^{18}F-FDG PET/CT uptake in the gastrointestinal tract, focusing on the colon. There is not yet sufficient evidence to recommend routine clinical use of oral hyoscine-N-butyl bromide on ^{18}F-FDG PET/CT scan. Randomized, blinded studies are needed to evaluate the effect of hyoscine-N-butyl bromide on 18F-FDG PET/CT uptake in the gastrointestinal tract to achieve an appropriate tumor-to-background ratio in detecting malignancies in the abdomen and pelvis.

Acknowledgments

The authors thank Professor Ana M. Contreras-Navarro for her guidance in preparing and writing this scientific paper. The authors would thank the Facultad de Medicina, “Hospital Universitario Dr. Jose Eleuterio Gonzalez,” and Universidad Autonoma de Nuevo Leon for their support in editing the manuscript.

Funding

This research received no external funding.

Conflicts of interest

The authors declare that they have no conflicts of interest.

Ethical disclosures

Protection of human and animal subjects. The authors declare that the procedures followed were in accordance with the regulations of the relevant clinical research ethics committee and with those of the Code of Ethics of the World Medical Association (Declaration of Helsinki).

Confidentiality of data. The authors declare that they have followed the protocols of their work center on the publication of patient data.

Right to privacy and informed consent. The authors have obtained the written informed consent of the patients or subjects mentioned in the article. The corresponding author is in possession of this document.

REFERENCES

1. Esteves FP, Schuster DM, Halkar RK. Gastrointestinal tract malignancies and positron emission tomography: an overview. Semin Nucl Med. 2006;36(2):169-181. doi: 10.1053/j.semnuclmed.2005.12.002.
2. Barret KE, Barman SM, Boitano S, Brooks HL, Ganong Medical Physiology. 24th ed. McGraw-Hill Professional. Mexico, 2012. 768 p.
3. Kostakoglu L, Hardoff R, Mirtcheva R, Goldsmith SJ. PET-CT fusion imaging in differentiating physiologic from pathologic FDG uptake. RadioGraphics. 2004; 24(5):1411-1431. doi: 10.1148/rg.245035725.
4. Shukur M, Hamzah F, Ahma M. The Effectiveness of Hyoscine-N-Butylbromide (Buscopan) in Reducing Physiological Bowel Uptake in 18 F-FDG. Mal J Med Health Sci. 2018; 14(Supp 1): 58:64.
5. Stahl A, Weber WA, Avril N, Schwaiger M. Effect of N-butylscopolamine on intestinal uptake of fluorine-18-fluorodeoxyglucose in PET imaging of the abdomen. Nuklearmedizin. 2000; 39: 241-245.
6. Emmott J, Sanghera B, Chambers J, Wong WL. The effects of N-butylscopolamine on bowel uptake: an 18F-FDG PET study. Nucl Med Commun. 2008;29(1):11-16. doi: 10.1097/MNM.0b013e3282f1d706.
7. Delbeke D, Coleman RE, Guiberteau MJ, Brown ML, Royal HD, Siegel BA, et al. Procedure Guideline for Tumor Imaging with 18F-FDG PET/CT 1.0, J Nucl Med. 2006; 47(5):885-895. Erratum in: J Nucl Med. 2006;47(6):903.
8. Boellaard R, Delgado-Bolton R, Oyen WJG, Giammarile KT, Eschner W, Verzijlbergen FJ, et al. FDG PET/CT: EANM procedure guidelines for tumour imaging: version 2.0. Eur J Nucl Med Mol Imaging. 2015:42:328–354. doi:10.1007/s00259-014-2961-x
9. Américo MF, Miranda JR, Corá LA, Romeiro FG. Electrical and mechanical effects of hyoscine butylbromide on the human stomach: a non-invasive approach. Physiol Meas. 2009;30(4):363-370. doi: 10.1088/0967-3334/30/4/002.

JMeXFRI

Journal of the Mexican Federation of Radiology and Imaging

Check for updates

CASE REPORT

Usefulness of computed tomography in complicated femoral Littre hernia: case report and literature review

Laura I. Rodriguez-Montoya[a], Carlos A. Calderon-Diaz, Jorge E. Guerrero-Martinez*

Radiology Department, Hospital Regional Monterrey, Instituto de Seguridad y Servicios Sociales de los Trabajadores del Estado (ISSSTE), Monterrey, Nuevo Leon, Mexico

[a]0000-0003-3598-193X

ABSTRACT

The initial diagnostic approach of hernias is usually with ultrasound (US), although cross-sectional imaging studies provide greater accuracy. This case report describes the usefulness of computed tomography (CT) in a patient with an abdominal emergency due to a complicated femoral Littre hernia. The patient was a 59-year-old man with a mass on his right thigh that developed over two years. Before admission, he had persistent pain radiating to the scrotal region. Physical examination revealed a 5-cm painful and non-reducible hernia. Ultrasonography of the right groin and thigh revealed a tubular image with no hernia defect, considering these findings non-specific. Abdominopelvic CT showed a Meckel's diverticulum in a hernial defect dependent on the terminal ileum, characteristic of a femoral Littre hernia. Surgery was performed, and the Meckel's diverticulum with a base dependent on the ileum was identified distal to the incision plane. Color changes of the diverticulum were noted, and it was resected from the base. The patient's evolution was satisfactory. The diagnosis of hernia, its content, and its complications was made by cross-sectional tomography. This case report is the first in Mexico that demonstrated the usefulness of CT in diagnosing complicated Littre hernia.

Keywords: *Littre hernia. Meckel's diverticulum. Femoral hernia. Computed tomography. Case report.*

INTRODUCTION

Meckel's diverticulum has an incidence of 0.3% to 3% in the adult population[1,2]. Littre hernia occurs through the abdominal wall in only 1% of patients with Meckel's diverticulum. The most common site is the right inguinal canal (50%) and the femoral ring (20%), the region where it is most likely to be strangulated[1,2]. Since it is usually asymptomatic, it is underdiagnosed[3,4]. Approximately 5% to 17% of cases of Meckel's diverticulum develop an acute abdomen[5] with bowel obstruction (14%-53%), diverticulitis (12.7%-53%), ulceration (< 4%) or perforation[6].

It is important to characterize masses in the inguinal and femoral regions by imaging studies before surgical treatment to determine the hernia content and the involvement of intestinal components in mixed content hernias. The initial imaging study used for masses in the inguinal and femoral regions is ultrasound (US) because it is inexpensive, easily accessible, and does not require ionizing radiation[2]. The usefulness of computed tomography (CT) in femoral Littre hernia has not been defined. This case report describes the CT diagnostic approach and presents specific findings and complications of femoral Littre hernia in a patient with an abdominal emergency.

CLINICAL CASE DESCRIPTION

The patient was a 59-year-old man with a mass in the right femoral region of two years of evolution

Corresponding author:
*Laura I. Rodriguez-Montoya
E-mail: lauradzm@hotmail.com

Received for publication: 17-11-2021
Approved for publication: 17-12-2021
DOI: 10.24875/JMEXFRI.M21000007

Available online: 31-03-2022
J Mex Fed Radiol Imaging. 2022;1(1):58-62
www.JMeXFRI.com

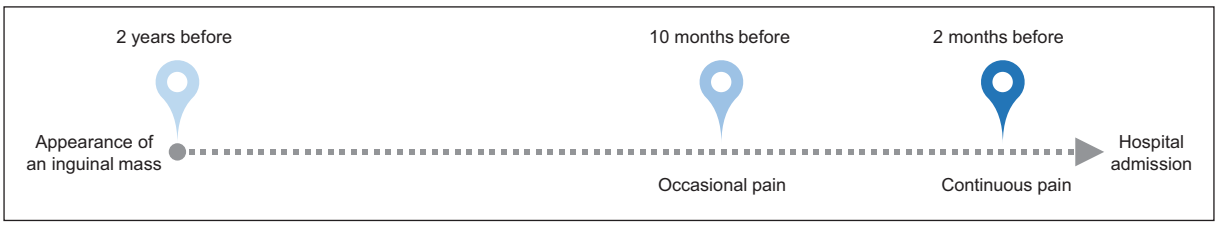

Figure 1. Chronological evolution in a 59-year-old male patient with a mass in the right femoral region of two years of evolution with pain approximately 10 months before hospital admission. He evolved with continuous pain radiating to the scrotal region that limited ambulation two months before hospital admission.

(Figure 1). About ten months before, he had occasional pain; however, two months before hospitalization, it evolved into continuous pain with an intensity of 3/10 on the visual analog scale, radiating to the scrotal region and limiting ambulation. He denied other symptoms, and his family, personal, and medical history was not relevant. Physical examination revealed painful facies and good hydration. A mass was identified below the right inguinal ligament, approximately 5 cm in diameter, with a firm consistency and pain on mobilization, non-reducible (incarcerated), and without skin changes. The abdomen had normal peristalsis with no evidence of associated peritonitis.

Imaging findings

US examination was performed in color Doppler with an exploration focus in the groin and right femoral region with a high-frequency linear probe (9-12 MHz). The exploration was complemented with a convex probe (3-5 MHz) with a Prosound Alpha 6^{TM} Aloka, Tokyo, Japan ultrasound. An anechoic tubular image 3 cm in diameter with posterior acoustic enhancement, increased echogenicity of the adjacent fatty planes, and no hernial defect was identified (Figure 2). Ultrasonography findings were non-specific, so simple and venous contrasted abdominopelvic CT were performed with IV Iodinated contrast and Iodine/300 mg Iodo/ml Omnipaque^{TM} (iohexol) (GE Healthcare, Boston, MA. USA). The tomograph was a 16-slice Brilliance^{TM} Philips Inc., Cleveland, OH, USA.

In Figure 3, venous delay phase in the axial plane CT at the level of the pubic symphysis, a right femoral hernia was observed with the presence of a hernial sac and Meckel´s diverticulum content associated with reactive nodes and effacement of the fatty planes, lateral to the inguinal canal and medial to the common femoral artery and vein. In the axial plane at the level of the acetabular roof, Meckel´s diverticulum was seen, lateral and inferior to the epigastric artery and vein. In Figure 4, an oblique reconstruction of the abdomino-pelvic CT scan in the simple phase shows a femoral hernia with ileum and Meckel´s diverticula union dependent on the anti-mesenteric border with a downward path inferior to the inguinal ligament into the hernia sac. The diagnosis of a true Littre´s hernia was made.

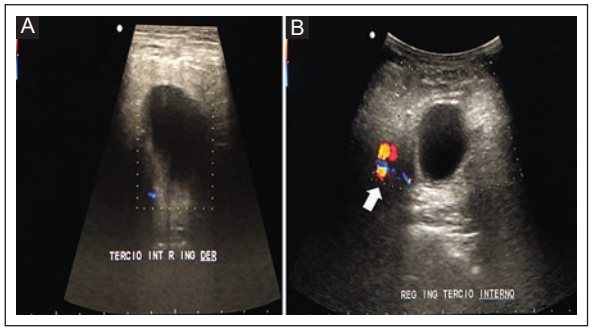

Figure 2. Color Doppler US in the groin and right femoral region of a 59-year-old male patient. **A:** anechoic tubular image was identified with a linear probe, posterior acoustic reinforcement 3 cm in diameter with increased echogenicity of adjacent fatty planes; no vascular alteration or hernial defect was observed. **B:** a convex probe in the transverse plane demonstrated its medial and anterior location to the right iliac vessels (arrow).

US: Ultrasound.

Clinical outcome

The patient underwent surgical management. A small bowel loop was identified proximal to the hernia site. The origin of Meckel's diverticulum was at the anti-mesenteric border, one meter from the ileocecal valve. The distal end of the blind loop was within the hernial defect and had color changes suggestive of ischemia secondary to strangulation. It was resected and repaired from the base with peritoneum and surgical site closure. The patient had a good clinical evolution and was discharged on the third postoperative day.

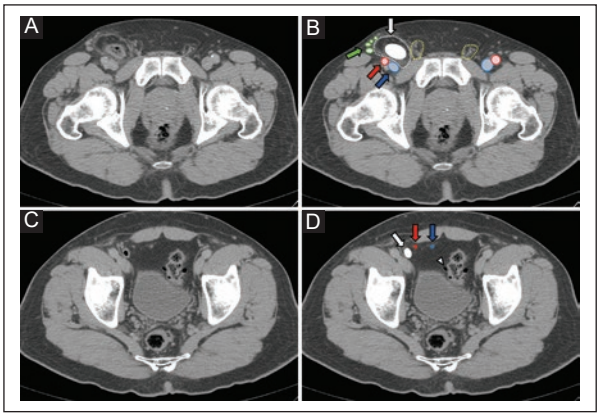

Figure 3. Simple and venous delay phase abdominopelvic CT scan of a 59-year-old male patient. **A-B:** venous delay phase in the axial plane at the level of the pubic symphysis, a right femoral hernia is observed (white arrow) with the presence of a hernia sac (white dotted line) and Meckel´s diverticulum content (white oval), in association with reactive nodes (green arrow and circles) and effacement of the fatty planes, lateral to the inguinal canal (yellow dotted line) and medial to the common femoral artery and vein (red, blue arrow and circle, respectively). **C-D:** in the axial plane at the level of the acetabular roof, Meckel´s diverticulum (white arrow and circle) is seen lateral and inferior to the epigastric artery and vein (red and blue arrow and circle respectively); sigmoid diverticulosis is shown as an incidental finding (white arrowhead).
CT: Computed tomography

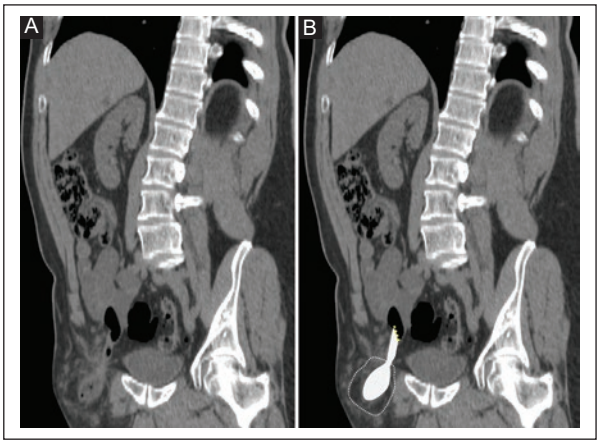

Figure 4. Oblique reconstruction of an abdomino pelvic CT image in simple phase of a 59-year-old male patient. **A-B:** femoral hernia that showing union of ileum and Meckel´s diverticulum (yellow dotted line) depending on the anti-mesenteric border with a downward path inferior to the inguinal ligament into the hernia sac (white dotted circle). The diagnosis of a true Littre´s hernia was made.
CT: Computed tomography.

DISCUSSION

In this case, the abdominopelvic CT was useful to show specific findings for diagnosing and recognizing complications in femoral Littre hernia. This case is the first in Mexico in which computed tomography has been used as a diagnostic method to characterize a femoral hernia associated with Meckel's diverticulum.

Imaging studies are important in rare pathologies such as Littre hernia for accurate diagnosis. In the literature reviewed, eleven femoral Littre hernia cases were found. These cases had acute abdominal complications and were investigated with imaging studies: abdominal radiography, ultrasonography, and/or computed tomography (Table 1)[1,3,7-15]. Plain abdominal radiography is commonly used, but its usefulness is limited because it provides non-specific data. There are only two case reports with CT (Table 1)[1,7]. Our case report is the first to present the results of both imaging studies, pelvic US with color Doppler and CT of the abdomen and pelvis with IV contrast. The CT scan showed the dimensions of the hernia defect, its relationship to vascular structures and ligaments and directly visualized Meckel's diverticulum, which was not associated with other intra-abdominal structures, allowing the diagnosis and classification of a true Littre hernia. In addition, the CT scan accurately identified the contents of the diverticulum and femoral topography because of its relationship to the inferior epigastric vessels, which are located in a plane below the inguinal ligament and parallel to the homonymous canal. The CT scan, with a higher imaging capacity than ultrasound, is a cross-sectional examination that demonstrated accuracy in diagnosing femoral Littre hernia.

Meckel's diverticulum is typically discovered within a hernia sac during surgery. Schizas et al.[2] reported in a systematic review that the diagnosis of Meckel's diverticulum within the hernia sac was made in most cases by direct visualization of the diverticulum during surgery. In our case, detection of Meckel's diverticulum was done with CT, which led to the preoperative diagnosis of Littre hernia. Abdominal and pelvic images CT with a IV contrast agent allowed direct visualization of the dependence of the mesenteric border of the diverticulum and optimal visualization of the inferior epigastric vessels, which are the main feature for the classification of inguinal and femoral hernias. CT provides a multiplanar image and shows the dimensions of the hernia defect, which can be useful for surgical planning.

Table 1. Literature review of case reports of femoral Littre hernia and current case report

Author (year)	Country	Age, years	Sex	Type of Littre´s Hernia	Imaging study	Incarcerated	Strangulated	Perforated	Intestinal obstruction
Payson (1956)[8]	US	43	F	T	Rx	Yes	Yes	No	Yes
Kanazawa (1972)[9]	JP	75	M	T	Rx	Yes	No	Yes	Yes
Mirza (2007)[10]	GB	49	F	T	Rx, US	Yes	No	No	No
Zacharakis (2008)[11]	GB	65	F	T	Rx	Yes	Yes	No	No
Phillips (2012)[1]	GB	73	F	M	CT	Yes	Yes	Yes	Yes
Racy (2013)[12]	GB	71	F	M	Rx	Yes	Yes	No	No
Yagmur (2014)[3]	TR	73	F	M	Rx	Yes	No	Yes	Yes
Misiak (2014)[13]	PL	71	F	M	RX	Yes	Yes	No	No
Malling (2017)[14]	DK	52	F	M	US	Yes	No	No	No
Ioannidis (2018)[15]	GR	82	M	M	Rx	Yes	Yes	No	No
Bains (2019)[7]	AU	63	M	M	CT	Yes	No	No	No
Current case	MX	59	M	T	US, CT	Yes	Yes	No	No

F: Female; M: Male; T: True; M: Mix; Rx: Abdominal radiography; US: Ultrasound; CT: Computer tomography.

In conclusion, in this case report of a complicated femoral Littre hernia, a CT scan provided objective visualization of the contents of a hernia defect and accurate classification of the type of inguinal hernia according to vascular anatomic references, determining the segment of the digestive tract located proximal to the defect, which is less common than Meckel's diverticulum. We recommend abdominal and pelvic CT with IV contrast as part of the initial approach in patients with a right lower quadrant abdominal pain associated with a palpable mass in the groin, except in women of childbearing age because of the possibility of pregnancy. This case report demonstrates the usefulness of CT in diagnosing a complicated femoral Littre hernia and characterizing it before surgical treatment.

Acknowledgments

The authors thank Professor Ana M. Contreras-Navarro for her noble and invaluable work as our mentor in writing scientific research papers and stimulating and promoting radiology research in our country.

Funding

This research received no external funding.

Conflicts of interest

The authors declare that they have no conflicts of interest.

Ethical disclosures

Protection of human and animal subjects. The authors declare that the procedures followed were in accordance with the regulations of the relevant clinical research ethics committee and with those of the Code of Ethics of the World Medical Association (Declaration of Helsinki).

Confidentiality of data. The authors declare that they have followed the protocols of their work center on the publication of patient data.

Right to privacy and informed consent. The authors have obtained the written informed consent of the patient mentioned in the article. The corresponding author is in possession of this document.

REFERENCES

1. Phillips AW, Aspinall SR Appendicitis and Meckel's diverticulum in a femoral hernia: simultaneous De Garengeot and Littre's hernia. Hernia. 2012; 16(6):727-729. doi: 10.1007/s10029-011-0812-2.
2. Schizas D, Katsaros I, Tsapralis D, Moris D, Michalinos A, Tsilimigras DI, et al. Littre's hernia: a systematic review of the literature. Hernia. 2018;23(1):125-130. doi: 10.1007/s10029-018-1867-0.
3. Yagmur Y, Akbulut S, Can MA. Gastrointestinal perforation due to incarcerated Meckel's diverticulum in right femoral canal. World J Clin Cases. 2014; 2(6):232-234. doi:10.12998/wjcc.v2.i6.232.

4. Levy AD, Hobbs CM. From the archives of the AFIP. Meckel diverticulum: radiologic features with pathologic correlation. RadioGraphics. 2004;24 (2):565-587. doi:10.1148/rg.242035187.
5. Tas İ, Culcu S, Duzkoylu Y, Eryilmaz S, Deniz MM, Yilmaz D. A Rare Cause of Acute Abdomen: Perforation of Double Meckel's Diverticulum. Case Rep Gastrointest Med. 2015; 648417. doi:10.1155/2015/648417.
6. Sagar J, Kumar V, Shah DK. Meckel's diverticulum: a systematic review. J R Soc Med. 2006; 99(10): 501-505. doi: 10.1258/jrsm.99.10.501.
7. Bains HK, Agostinho N, Hamilton AE, Byrne C. What is in the sac? Littré hernia. ANZ J Surg. 2020; 90(5): 896-898. doi:10.1111/ans.15353.
8. Payson BA, Schneider KM, Victor MB. Strangulation of a Meckel's diverticulum in a femoral hernia (Littre's). Ann Surg. 1956; 144(2), 277-281. doi:10.1097/00000658-195608000-00024.
9. Kanazawa K, Ishikawa K, Shoji R, Okamoto A. Littré's femoral hernia causing intestinal fistula. Jpn J Surg. 1972; 2(1), 37-46. doi:10.1007/BF02468905.
10. Mirza MS Incarcerated Littre's femoral hernia: case report and review of the literature. J Ayub Med Coll Abbottabad. 2007; 19(2), 60-61.
11. Zacharakis E, Papadopoulos V, Athanasiou T, Ziprin P, Zacharakis E. An unusual presentation of Meckel diverticulum as strangulated femoral hernia. South Med J. 2008; 101(1): 96-98. doi:0.1097/SMJ.0b013e31815d3c83.
12. Racy M, Ramesh S. Littre meets de Garengeot: Meckel's diverticulum and appendix in a femoral hernia. Ann R Coll Surg Engl. 2013; 95(6): e97-e98. doi: 10.1308/003588413X13629960047399.
13. Misiak P, Piskorz Ł, Kutwin L, Jabłoński S, Kordiak J, Brocki M. Strangulation of a Meckel's diverticulum in a femoral hernia (Littre's hernia). Prz Gastroenterol. 2014;9(3):172-174. doi: 10.5114/pg.2014.43580.
14. Malling B, Karlsen AA, Hern J. Littre hernia: A Rare Case of an Incarcerated Meckel's diverticulum. Ultrasound Int Open. 2017; 3(2): E91-E92. doi: 10.1055/s-0043-102179.
15. Ioannidis A, Karanikas I, Koutserimpas C, Velimezis G. Combined Littre and Richter's femoral hernia: an extremely rare intra-operative finding. G Chir. 2018; 39(3): 177-180.

JMeXFRI

Journal of the Mexican Federation of Radiology and Imaging

Check for updates

IMAGES IN RADIOLOGY

Ultrasound and computed tomography: epiploic appendagitis

Gerardo E. Ornelas-Cortinas[a], Ana K. Luna-Marroquin, and Alberto Montemayor-Martinez,*

Centro Universitario de Imagen Diagnóstica, School Medicine,"Hospital Universitario Dr. Jose Eleuterio Gonzalez", Universidad Autonoma de Nuevo Leon, Monterrey, Nuevo Leon, Mexico

[a]0000-0003-2927-7700

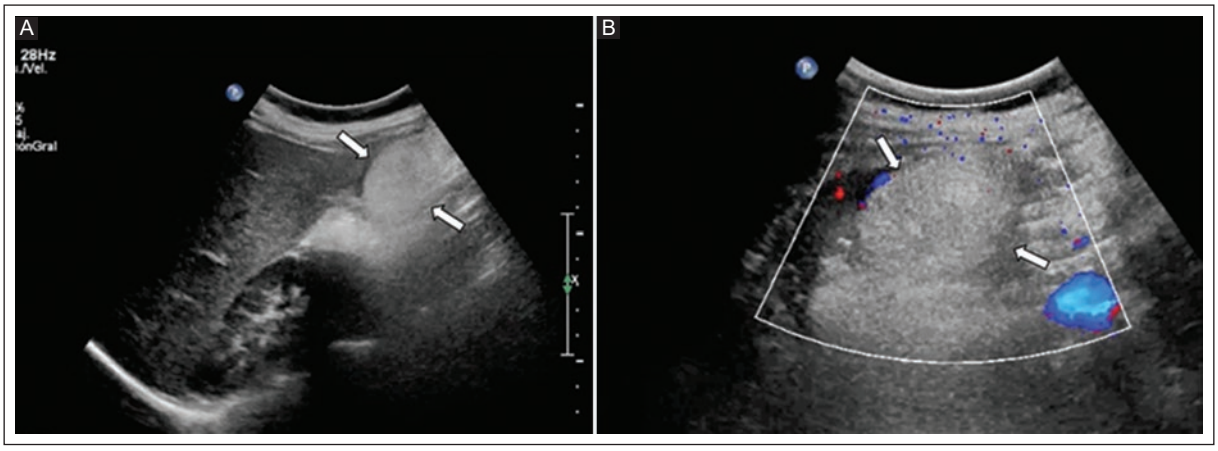

Figure 1. A: gray scale ultrasound shows a solid, ovoid, hyperechoic, non-compressible mass in the hepatorenal fossa with right-sided abdominal pain (white arrows). **B:** magnification of the hepatorenal fossa showing no blood flow with color Doppler ultrasound, suggestive of appendagitis (arrows).

A 10-year-old male patient with a one-day history of right-sided abdominal pain was referred for an abdominal ultrasound because of a clinical suspicion of appendicitis. Ultrasound showed a solid, ovoid, non-compressible mass in the hepatorenal fossa with a hypoechoic rim, obliteration of the adjacent fat planes (Figure 1A, Supplementary video 1), and no flow detected with color Doppler (Figure 1B, Supplementary video 2). Therefore, appendagitis was diagnosed. An enhanced CT, as a complementary study, demonstrated an oval structure with a thin, high-density ring, the "hyperattenuating ring" sign. In addition, a hyperdense central dot and obliteration of the fat planes adjacent to the colon (Figure 2, Supplementary video 3). After 5 days of conservative treatment, the boy was discharged with resolution of his symptoms.

Appendagitis is a rare and benign inflammatory process of vascular etiology due to torsion of the epiploic appendix of the colon or spontaneous venous thrombosis that results in ischemia and necrosis[1,2]. It usually manifests in the fourth to fifth decades of life[3]. Pediatric cases are rare[4]. Imaging tools, such as ultrasound and computed tomography, can be used for diagnosis. The

Corresponding author:
*Gerardo E. Ornelas-Cortinas
E-mail: ornelasge@yahoo.com.mx

Received for publication: 20-12-2021
Approved for publication: 23-12-2021
DOI: 10.24875/JMEXFRI.M21000009

Available online: 31-03-2022
J Mex Fed Radiol Imaging. 2022;1(1):63-64
www.JMeXFRI.com

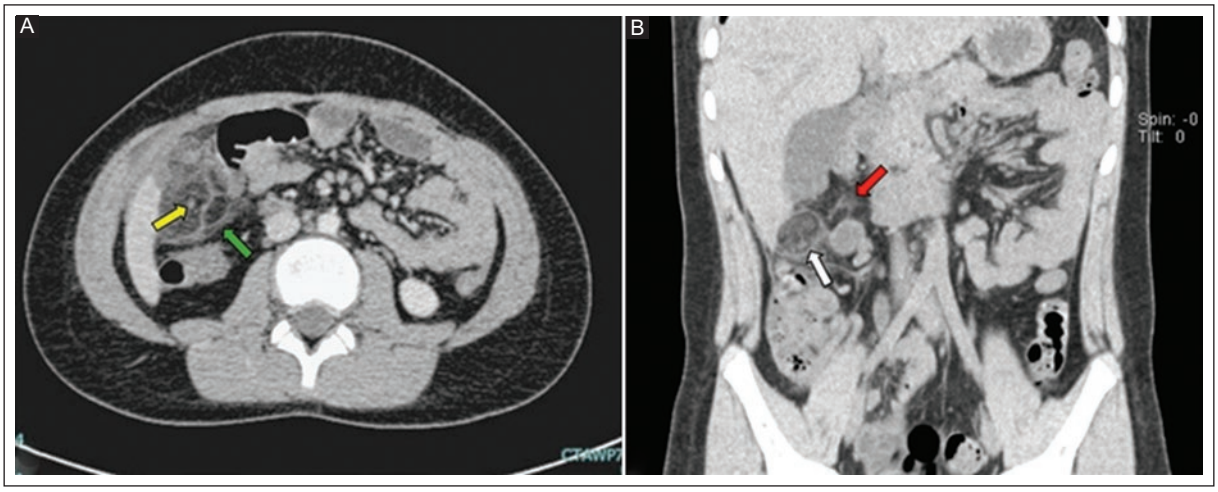

Figure 2. Axial abdominal contrast-enhanced CT. **A:** showing a hyperdense central dot (yellow arrow) associated with inflammation of the epiploic appendix (green arrow). **B:** coronal plane view showing fat tissue obliteration (red arrow) with a peripheral hyperdense area, the "hyperattenuating ring" sign (white arrow).
CT: computed tomography.

importance of this case lies in the characteristic ultrasound images that support the diagnosis of appendagitis.

Acknowledgments

The authors thank Professor Ana M. Contreras-Navarro for her guidance in preparing and writing this scientific paper.

Funding

This paper received no external funding.

Conflicts of Interest

The authors declare that they have no conflicts of interest.

Ethical disclosures

Protection of human and animal subjects. The authors declare that the procedures followed were in accordance with the regulations of the relevant clinical research ethics committee and with those of the Code of Ethics of the World Medical Association (Declaration of Helsinki).

Confidentiality of data. The authors declare that they have followed the protocols of their work center on the publication of patient data.

Right to privacy and informed consent. Informed consent was not required to analyze and publish routinely acquired clinical data. Similarly, informed consent is not required for the publication of imaging data.

Supplementary material

Supplementary material is available online in the Journal of the Mexican Federation of Radiology and Imaging (www.jmexfri.com).

REFERENCES

1. Rioux M, Langis P. Primary Epiploic Appendagitis: Clinical, US, and CT Findings in 14 Cases. Radiology. 1994;191(2):523-526. doi: 10.1148/radiology.191.2.8153333.
2. González Vega A, García Pérez I, Alvarez Alvarez D, Rizzo Ramos A, García Muñiz JL, Pérez Ricarte P. Apendagitis epiploica como etiología de dolor abdominal agudo [Epiploic appendagitis as a cause of acute abdominal pain]. Rev Esp Enferm Dig. 2008;100(11):800-801. Spanish.
3. Singh AK, Gervais DA, Hahn PF, Sagar P, Mueller PR, Novelline RA. Acute epiploic appendagitis and its mimics. Radiographics. 2005; 25(6):1521-1534. doi: 10.1148/rg.256055030.
4. Ozturk M, Aslan S, Saglam D, Bekci T, Bilgici MC. Epiploic Appendagitis as a Rare Cause of Acute Abdomen in the Pediatric Population: Report of Three Cases. Eurasian J Med. 2018; 50(1):56-58. doi: 10.5152/eurasianjmed.2018.17247.